Feasibility assessment of a grass cover dike in a coastal wetland setting

Towards a design tool

M. C. Horstman

UNIVERSITY OF TWENTE.

Photo cover image: Living dikes project

Feasibility assessment of a grass cover dike in a coastal wetland setting

Towards a design tool

by

M. C. Horstman

to obtain the degree of Master of Science
at the University of Twente,
to be defended online on Friday September 18, 2020 at 15:00 AM.

Student number:	1489607	
Project duration:	February 17, 2020 – September 18, 2020	
Thesis committee:	Prof. dr. K. M. Wijnberg,	University of Twente, chair supervisor
	Dr. ir. B. W. Borsje,	University of Twente, daily supervisor
	Ir. S. Post,	Royal HaskoningDHV, daily supervisor

UNIVERSITY OF TWENTE.

Royal HaskoningDHV
Enhancing Society Together

Preface

This research is the final work of my MSc Civil Engineering and Management at the Water Engineering and Management department at the University of Twente. The thesis subject was exciting to work on due to the applicability and the broad scope from coastal wetlands to the hydraulic engineering of a coastal structure. I worked on this project from February 2020 till September 2020 under the supervision of Sander Post, Bas Borsje and Kathelijne Wijnberg.

This thesis was carried out in collaboration with the Rivers & Coasts Department at Royal HaskoningDHV. I would like to thank Royal HaskoningDHV for the provided opportunity, resources and internal knowledge to perform this thesis at their offices in Ammersfoort and Rotterdam. I would also like to thank the Wetterskyp Friesland, who commissioned my thesis on the Koehool-Lauwesmeer dike trajectory. I take this opportunity to express my gratitude to all the persons who had an impact on this final work.

My special thanks go to Sander Post for his constant and valuable guidance. His input at every meeting and availability for discussion have substantially increased the quality of this research. The knowledge of Stef Broersen on the OpenFOAM numerical modelling was essential and highly appreciated. The calls with Leslie Mooyaart showing his interest in the project and giving new insights certainly helped during the corona virus period.

I would also like to express deep gratitude to Bas Borsje in providing me the opportunity to do my thesis at Royal HaskoningDHV. Furthermore, I would like to thank Bas Borsje and Kathelijne Wijnberg for their supervision during this research. Over the course of this research they helped me to focus the research and scope, which was a challenge given the size of the project and the many potential study directions.

Lastly, I would like to thank my family and friends for their personal support during these months. Without their encouragement it would not have been an enjoyable and instructive journey.

M. C. Horstman
Utrecht, September 2020

Abstract

Recently new Dutch flood safety standards came into effect. These new safety standards require dike reinforcements for a large part of the Netherlands. Therefore, high investments and the urge for innovative, sustainable solutions are needed. Accordingly, flood protection projects in the Netherlands have shown interest in adopting nature, biodiversity and climate change into their design solutions. Within these solutions, coastal wetlands are considered to have high potential to reduce wave loads on conventional coastal structures such as dikes and dams. Additionally, dikes that are entirely covered in grass on the waterside slope add to the biodiversity, compared to conventional hard revetments. The aim of this study is to assess the feasibility of a grass cover dike in combination with a coastal wetland in front of it. Herein, the feasibility depends on two factors, namely the erosion depth of the grass and clay layers as well as the required costs for construction and maintenance. The research is divided into two parts. The first part is a numerical analysis (OpenFOAM) extending the current knowledge on the effect of the slope angle on the wave impact load. The second part combines the gained knowledge on the erosion of grass and clay with an assessment on geometric wetland configurations, presented in a design tool. Using this tool, the following three dike design scenarios for the Koehool-Lauwersmeer dike trajectory at the Wadden sea are tested on their feasibility as a case study: (*i*) gentle grass cover dike with a large vegetated foreshore, (*ii*) traditional dike versus a grass cover dike with a small vegetated foreshore and (*iii*) traditional dike versus a grass cover dike with foreshore construction by brushwood dams. The result of the first part of the study confirms a linear trend between the slope angle and the wave impact load. The second part shows the potential of a grass cover dike with a wetland in front of it, whereby important wetland conditions appear to be the inundation depth and critical orbital velocity for stem breaking. The results of the first scenario in the case study do not reject the grass cover dike, considering a gentle dike slope of 1/8 with a vegetated foreshore. For the second scenario, a grass cover dike solution is more cost-effective than the traditional dike design. Considering foreshore construction for the last scenario, a minimal vegetated foreshore width of 350m would have evident impact on the wave height reduction allowing for a grass cover dike. However, continuous maintenance costs make the brushwood construction relatively expensive compared to the traditional dike design. To conclude, the feasibility assessment in the form of a design tool, demonstrates for the Koehool-Lauwersmeer dikes that a grass cover dike in a wetland setting is possible and more cost-effective than conventional hard solutions. It is recommended to consider the design tool in the preliminary design phase of a dike. Furthermore, a first step was taken towards the practical implementation of coastal wetland research in the form of a design tool. Reducing the uncertainty in the long-term morphological development together with integrating plant specific stability will extend and improve the design tool.

List of Figures

1.1 Failure of grass revetment and clay layer (adapted from Breteler (2017)) 2
1.2 Flowchart of research steps in order to answer the main research question 4
1.3 Location of dike trajectory Koehool Lauwersmeer, with three specified dike locations. . . 5

2.1 Definition of impact pressure and quasi-static component for breaking wave impact load 9
2.2 Graph of wave impact experiments on hard revetment (adopted from Peters (2017)) . . 9
2.3 Definition sketch of grass cover Muijs (1999) 11
2.4 Resistance duration curve (adapted from Ministerie van Infrastructuur en Milieu (2016)) 12
2.5 Erosion profile for the approach of Breteler (2012) 13
2.6 Relation between significant pressure head and the slope angle (adopted from Mourik (2015)) 14
2.7 Example of a breaking wave on a dike slope showing the total pressure of a CoastalFOAM simulation 14

3.1 Methodology 16
3.2 An example of the mesh dimensions and wave gauge spacing 18
3.3 Grid spacing of the different meshes. (a) Coarse grid $dx = dy = 0.1$, (b) Fine gird $dx = dy = 0.05$, (c) Multi grading grid $dx_1 = dy_1 = 0.1; dx_2 = dy_2 = 0.05$, (d) Snappy hex mesh $dx_1 = dy_1 = 0.1; dx_2 = dy_2 = 0.05; dx_3 = dy_3 = 0.025$. 19
3.4 Design tool framework 21
3.5 Hydraulic input conditions for the erosion model 22
3.6 Percentage wave attenuation due to vegetation in relation to the inundation depth and foreshore width. This figure adopted from Steetzel et al. (2018) shows the result of a SWAN analysis done on Wadden Sea wetlands with long vegetation and a roughness height of $k_N = 0.09m$ 23
3.7 Hydraulic conditions during the storm surge which is input for the erosion model. 24
3.8 Percentage wave attenuation due to vegetation and depth induced wave breaking in relation to the inundation depth and foreshore width. This figure adopted from Vuik et al. (2016) shows the result of a SWAN analysis done on Zeeland wetlands. 25
3.9 Dike location scenarios 27
3.10 Current cross-section waterside slope of the dike locations 28

4.1 Results sensitivity analysis: (a) Reflection coefficients of the different grids compared to Equation (3.4) on page 19, (b) This figure shows the distribution of the highest 33% of the waves for different grid resolutions 30
4.2 Maximum pressure distribution $P_{2\%}$(top), $P_{10\%}$(middle) and P_s(bottom) over the slope elevation 31
4.3 Wave impact experiment data adopted from Peters (2017) together with the the simulation data 31
4.4 Linear relation between the geometry and design parameters, where the most left describes the relation for $P_{2\%}$, the middle $P_{10\%}$ and the right graph depicts the P_s data. . . . 32
4.5 Maximum pressure distribution $P_{2\%}$(top), $P_{10\%}$(middle) and P_s(bottom) over the erosion profile in the x direction. 33
4.6 Linear relation between the original slope angle and design parameters, where the most left describes the relation for $P_{2\%}$, the middle $P_{10\%}$ and the right graph depicts the P_s data. 34
4.7 Interpolated Hydra-NL hydraulic conditions for the different dike locations: (a) loc. 32.2km has a foreshore of 1850m foreshore, (b) loc. 22.2km has a foreshore of 700m and (c) loc. 17.4km has no foreshore. 35

4.8 Percentage wave attenuation per foreshore width and inundation depth (adopted from Steetzel et al. (2018). . . . 36
4.9 Depth induced wave breaking adjusted from Vuik et al. (2016) . . . 36
4.10 Sensitivity of vegetation attenuation with u_c and $z_f s$ and a foreshore width of 900m. . . 37
4.11 Extention of the WBI model, dike location 32.2km . . . 38
4.12 Example of the calculation output on the erosion depth for alternative 4 with crest height reduction. . . . 39
4.13 Final output of the design tool, giving a cost comparison of the different alternatives at location 22.2km. . . . 40
4.14 Final output of the design tool, giving a cost comparison of the different alternatives at location 17.4km . . . 41

A.1 Erosion profile for gentle slopes. . . . 59
A.2 Geometries of flat profile and the erosion profile . . . 60
A.3 Geometries of flat profile and the erosion profile . . . 61
A.4 Wave spectra of the numerical analysis . . . 63
A.5 Probe spacing for (a) Snapped grid, (b) unsnapped grid . . . 64

B.1 Definition of the schematised erosion profile (adopted from (Kaste and Breteler, 2015)) . 68
B.2 Example of the dike split up into sections (adopted from (Kaste and Breteler, 2015)) . . 69
B.3 Example for the iteration steps to determine the loaded zone (adopted from (Kaste and Breteler, 2015)) . . . 70
B.4 Example of the correction of the erosion volume due to the parallel movement of the slope (adopted from (Kaste and Breteler, 2015)) . . . 71
B.5 percentage of wave attenuation by long vegetation ($k_N = 0.090m$) adopted from Vuik et al. (2016) . . . 72

List of Tables

2.1 Breaker types (adopted from Peters (2017)) 8

3.1 Hydraulic conditions and geometric settings 17
3.2 Gridsizes mesh sensitivity analysis 18
3.3 Overview of geometry relation on wave impact pressure 20
3.4 Summary of the vegetation characteristics 23
3.5 Unit costs of dike reinforcement 26
3.6 Parameter settings for the erosion model 26

4.1 Sensitivity analysis results 29
4.2 summary of the hydraulic conditions and pressure results 30
4.3 Summary of the design conditions 34
4.4 Different design alternatives for dike location 22.2km 38
4.5 Different design alternatives for dike location 17.4km 39

5.1 Cost reduction by lowering gentle slope crest height 46

Contents

Abstract v

List of Figures vii

List of Tables ix

1 Introduction 1
- 1.1 Relevance of this research 1
- 1.2 Grass cover dikes and coastal wetlands 1
- 1.3 Problem definition 3
- 1.4 Research objective 4
- 1.5 Case description 5
- 1.6 Report outline 5

2 Background 7
- 2.1 Introduction 7
- 2.2 Wave breaking 7
- 2.3 Wave loads 8
- 2.4 Wetlands in flood-risk management 10
- 2.5 GEBU assessment 11
  - 2.5.1 WBI-2017 model 12
  - 2.5.2 Clay erosion models 13
- 2.6 Numerical model 14

3 Methodology 15
- 3.1 Methodology outline 15
- 3.2 Numerical analysis 15
  - 3.2.1 Geometry settings 15
  - 3.2.2 Hydraulic conditions 16
  - 3.2.3 Mesh properties 17
- 3.3 Mesh sensitivity analysis 18
  - 3.3.1 Reflection 19
  - 3.3.2 Pressure head 19
- 3.4 Relation between geometry and pressure 20
  - 3.4.1 Validation on empirical relations 20
- 3.5 Design tool 21
  - 3.5.1 Hydraulic input conditions 21
  - 3.5.2 Wetland input strategies 22
  - 3.5.3 Geometry input 25
  - 3.5.4 Costs input 25
  - 3.5.5 Erosion model 26
- 3.6 Case study 27

4 Results 29
- 4.1 Mesh sensitivity analysis 29
- 4.2 Relation between geometry and pressure 30
  - 4.2.1 Flat profile simulations 30
  - 4.2.2 Erosion profile simulations 33
- 4.3 Design tool 34
  - 4.3.1 Hydraulic input conditions 34
  - 4.3.2 Wetland model performance 36
  - 4.3.3 Erosion model 37

4.4 Alternative designs . . . 37
4.4.1 Traditional dike vs green dike (Loc. 22.2km) . . . 38
4.4.2 Traditional dike vs green dike + wetland construction (Loc. 17.4km) . . . 39

5 Discussion **43**
5.1 Insights and limitations of this study . . . 43
5.1.1 Seaward slope angle relation . . . 43
5.1.2 Geometric wetland settings . . . 45
5.1.3 Design Tool . . . 45
5.1.4 Case study . . . 46
5.2 Applicability of this research . . . 47

6 Conclusion and Recommendations **49**
6.1 Conclusion . . . 49
6.2 Recommendations . . . 51
6.2.1 Further research . . . 51
6.2.2 Safety assessment . . . 52

Bibliography **53**

A Numerical analysis **59**
A.1 Geometry profiles. . . . 59
A.2 Wave spectra . . . 62
A.3 Probe spacing . . . 64
A.4 Mathematical model . . . 65

B Design tool **67**
B.1 Extended WBI assessment . . . 67
B.2 Clay erosion model . . . 68
B.2.1 Numerical erosion model. . . . 69
B.2.2 Wetland wave attenuation . . . 72

1
Introduction

1.1. Relevance of this research

Many low-lying coastal areas around the world are challenged by increasing flood risks due to a combination of climate change and human activities near coastlines (Temmerman et al., 2013; Neumann et al., 2015; Lincke and Hinkel, 2018). As coastal economic activities grow, the coastal areas are threatened by accelerating sea level rise, land subsidence and intensified storms (Temmerman et al., 2013; Lincke and Hinkel, 2018). Countries need to adapt their policies and flood safety standards, which will result in high investments in coastal reinforcements and the urge for innovative, sustainable solutions (Schoonees et al., 2019; Loon-steensma and Vellinga, 2019; Borsje, 2019). Specifically, the Netherlands recently adopted new flood safety standards for the Dutch primary flood defences, adapting to the increasing flood risks. Consequently, 1.300km of dikes are rejected by the new standards. Dike reinforcements are necessary and will cost approximately 7.3 billion euros (HWBP, 2020). This reinforcement task is assigned to the 'Hoog Water Beschermings Programma' (HWBP), which is an alliance between the Dutch water boards and Rijkswaterstaat. The water boards have already initiated several dike reinforcement projects that required asphalt revetment almost to the crest of the dike (Royal HaskoningDHV, 2020). These conventional hard solutions are expensive and do not contribute to nature and biodiversity. Therefore, nature-based solutions such as a wide green dike and coastal wetlands are considered (Loon-steensma and Vellinga, 2019; Lammers, 2019). A wide green dike is defined as a gentle sloping dike entirely covered in grass. Such dikes contribute to the biodiversity and have low maintenance costs (Loon-steensma and Vellinga, 2019; Muijs, 1999). Salt marshes and inter tidal flats are examples of coastal wetlands. These have the potential of adding value to conventional engineering methods by reducing the wave load of storm surges on dikes (Barbier et al., 2008; Gedan et al., 2011; Möller et al., 2014). The concepts of a grass cover dike and coastal wetlands already exist in the Netherlands, for example at the dike trajectory Koehool-Lauwersmeer at the Wadden Sea. Nonetheless, knowledge gaps and persistent uncertainties pose a challenge for the implementation of green dikes and coastal wetlands according to safety standards. Current guidelines and policies provide general recommendations, while technical assessment tools with respect to the performance under different boundary conditions are still lacking.

1.2. Grass cover dikes and coastal wetlands

A large part of the Dutch dikes is covered with grass. Even dikes with hard revetments have a grass cover on a significant part of the dike surface, such as the crown and inner slope. Research and experience since the mid-eighties have shown that grass covers can be of high quality in terms of erosion resistance and encouragement of development of nature (Muijs, 1999). Where conventional sea dikes have a hard revetment to deal with incoming waves, the green dike has a grass revetment that has to withstand the waves. The process of the erosion of the grass revetment and the clay layers against incoming waves is the main challenge for allowing grass revetment in the wave impact zone. For example, waves at the Wadden sea can reach heights above 2m (van Loon-Steensma et al., 2014). However, according to the Dutch safety standards, grass revetments often do not resist 1 meter high

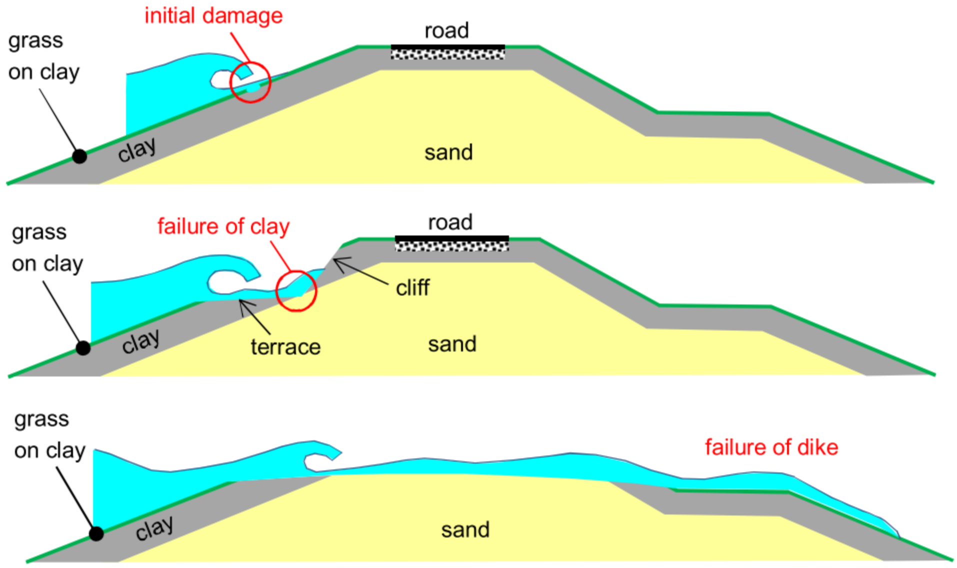

Figure 1.1: Failure of grass revetment and clay layer (adapted from Breteler (2017))

waves (Jan Klerk and Jongejan, 2016). To overcome this problem, dikes are designed with a thick clay layer that offers enough protection against the wave attack during a storm after failure of the grass revetment. Failure of the grass revetment does not necessarily lead to failure of the dike. The dike only fails if the clay layer is eroded as is presented in Figure 1.1. The failure of the grass revetment on the outer slope due to erosion (GEBU) consists of two sub-mechanisms: failure due to wave run-up and failure due to wave impact (Klerk and Jongejan, 2016). Erosion failure by wave impact is dominant over failure due to wave run-up, therefore only erosion due to wave impact is relevant for this study (Rijkswaterstaat, 2018). The new Dutch flood safety standards incorporate the assessment of a grass cover dike against the wave impact captured in the ”Wettelijk Beoordelingsintrumentatium” (WBI-2017) (De Waal, 2016). The WBI-2017 contains the methods to determine whether a flood defence system meets the safety standards.

The coastal wetlands are defined as a distinct ecosystem that are flooded by water either permanently or seasonally. The primary factor that distinguishes wetlands from other land forms or water bodies is the characteristic vegetation of aquatic plants (Gedan et al., 2011). Wetlands occur naturally on every continent. The main wetland types are swamp, salt marsh, mangrove forests and floodplains (Anderson and Smith, 2014). In this study the focus will be on salt marshes and their wave attenuating capacity. The presence of a salt marsh foreshore can lead to a reduction in failure probability of the dike behind (Gedan et al., 2011; Möller et al., 2014; Vuik et al., 2016). The hydrodynamic processes of salt marshes affecting wave attenuation are the attenuation by vegetation, wave breaking and bottom friction (Mendez and Losada, 2004; Vuik et al., 2018b). Furthermore the salt marshes stimulate biodiversity and can grow with sea level rise (Kirwan and Megonigal, 2013; D'Alpaos et al., 2011). These beneficial effects of wetlands on reducing the flood risk are not yet implemented in current safety standards. Fortunately, HWBP financed a large study on the efficiency of vegetated foreshores at the Wadden sea, which is part of a project called 'Project Overstijgende Verkenning' (POV) (Steetzel et al., 2018). This study shows promising results, but is not yet translated to assessment guidelines.

1.3. Problem definition

At the Wadden sea, grass cover dikes are being rejected by the new flood safety standards according to the WBI-2017 assessment (Wetterskip Fryslan, 2018). Herein the assessment of grass revetment on the upper part of the seaward slope has become stricter. Specifically, the Koehool-Lauwersmeer dike trajectory was previously studied and has failed in an assessment for allowing a grass cover dike in a wetland setting.

The WBI-2017 assessment on a grass cover dike differentiates between closed sods, open sods and fragmented sods, but the effect of the slope angle is not included since this has not been systematically studied (Peters, 2020). The assessment treats all slopes of a dike as a slope of 1:3. This lack of the current WBI-2017 assessment in its range of applicability for different seaward slope angles, resulted in the rejection of grass revetment at the Koehool-Lauwersmeer dike (van der Reijden, 2019; Sirks, 2019).

However, it is shown that more gentle slopes have a damping effect on the wave impact, affecting the erosion velocity of the grass revetment and clay layers (Führböter and Sparboom, 1988; Kruse, 2010; Mourik, 2015). This shows potential for the application of a wide green dike, a grass cover dike with a slope of around 1:7, which is currently rejected according to the WBI-2017. This is one of the reasons the waterboard 'Wetterskyp Fryslan' and other Dutch Water Boards want to improve the detailed assessment of a grass cover dike and specifically of the erosion processes of the grass and the underlying clay layers. A million euro Deltagoot experiment is set-up to increase the knowledge on grass and clay erosion (Breteler, 2020). Fortunately, the current assessment also shows potential to extend current knowledge numerically, which is significantly cheaper (Mourik, 2015).

Additionally, the wetlands are not part of the detailed assessment yet. Integration of coastal wetlands can add to the opportunity for allowing grass revetments on the seaward slope. It is widely shown that salt marshes in front of coastal sea dikes can reduce the nearshore wave height and also grow with sea level rise (Möller et al., 2014; Kirwan and Megonigal, 2013; Temmerman et al., 2013). However, the magnitude of wave dissipation is highly location dependent, with different coastal wetland configurations such as vegetation rigidity, stem breaking and foreshore width (Vuik et al., 2019; Willemsen et al., 2020). The studies on coastal wetlands are time consuming and expensive when considering each location separately for assessing its flood risk reduction (Steetzel et al., 2018).

To conclude, the combined effect of geometric coastal wetland settings and the seaward slope angle of a grass cover dike on the erosion processes needs to be further investigated. Detailed assessments are needed to test the feasibility of grass cover dikes taking the wetlands into account. Hereby a quick assessment tool on whether a grass cover dike in a coastal wetland setting is more feasible compared to a conventional hard solution would contribute to the development of cost-effective nature-based solutions in flood safety standards.

1.4. Research objective

The objective of this research is to assess the feasibility of a grass cover dike with a wetland in front of it. In the study the concept of feasibility includes two aspects. Firstly, the feasibility is determined by the erosion on the grass revetment and clay layers under given hydraulic design conditions. Secondly, the feasibility is determined by the construction and maintenance costs of the new grass cover dike. In order to assess the feasibility, the knowledge on the effect of the seaward slope angle on the erosion depth must be extended. For this, a numerical model is proposed (2.6). Subsequently, the study combines the effect of the seaward slope angle and the geometric wetland settings in a design tool, providing a preliminary assessment of dike design alternatives. The geometric wetland settings under consideration are the width of the foreshore and vegetation length. Finally, the applicability of the design tool is tested on a case study of the dike trajectory Koehool-Lauwersmeer. All the aforementioned is captured in the main research question stated below.

"What is the feasibility of a grass cover dike in a coastal wetland setting, considering erosion in the wave impact zone together with costs?"

The following sub-questions give answer to the main research question.

1. How does the seaward slope angle affect the wave impact load on the dike?
2. How do geometric wetland settings affect the erosion of the grass revetment and clay layers?
3. How can the described effects be combined in a design tool that assesses the feasibility of dike design alternatives?
4. What is the cost-effectiveness of a green dike design for different Koehool-Lauwersmeer dike locations compared to the current traditional designs?

The research steps are presented in Figure 1.2. The first part of the study is a literature study, which provides the necessary background knowledge for this research. The second part is a numerical analysis to extend the knowledge on the effect of slope angle on the erosion of the dike, concluding on the first sub-question. The gained knowledge of part I is used for the second part of the study. In this part a design tool is developed with the seaward slope angle, geometric wetland settings, revetment layers and costs as input parameters. The second sub-question can be answered by examining the outcome of different wetland settings. Finally, calibrating the design tool yields in the answer on sub-question 3. In a case study different alternatives are examined on the cost-effectiveness using the design tool, thereby answering the last sub-question.

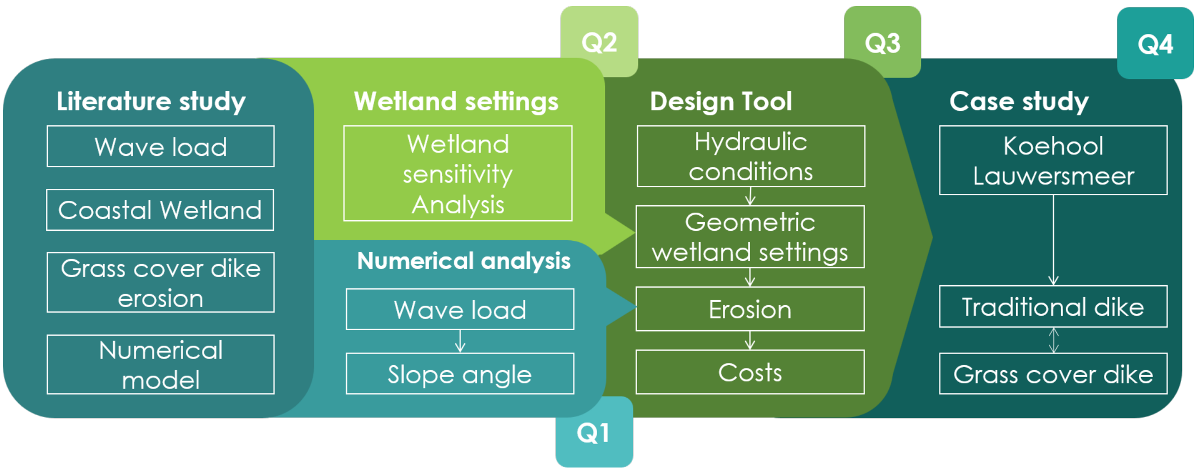

Figure 1.2: Flowchart of research steps in order to answer the main research question

1.5. Case description

This study focuses on a case study to answer the research questions. The chosen case study area is the dike trajectory of Koehool-Lauwersmeer. This trajectory is located in the north of the Netherlands at the Wadden sea coastline. The dike sections are mainly rejected on the failure mechanisms GEBU. The location of the trajectory is presented in Figure 1.3. Here a green dike is present, which is completely covered with grass revetment (green line). The remaining dike trajectory is partly covered with asphalt revetment (yellow line). The motivation for the specific dike section scenarios is based on the foreshore conditions. Where location 32.2km has a large vegetated foreshore of more than 2km, location 22.2km has a foreshore of only 700m. The third location (17.4km) has no foreshore.

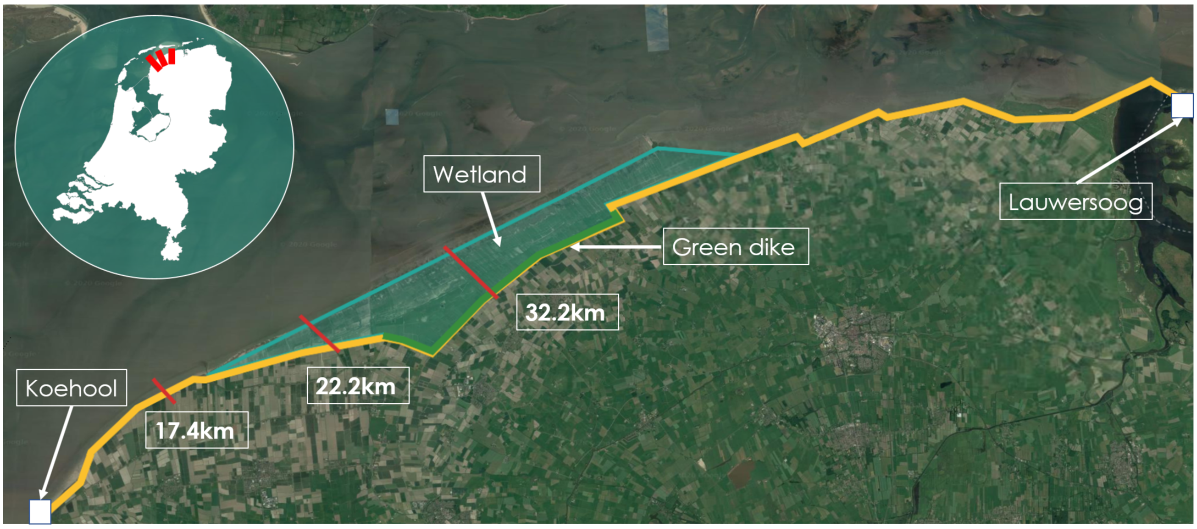

Figure 1.3: Location of dike trajectory Koehool Lauwersmeer, with three specified dike locations.

1.6. Report outline

Chapter 2	**Background**	This chapter introduces the following subjects for understanding this research: wave breaking, wave load, coastal wetlands, Grass cover dike erosion and a proposed numerical model. Each subject will be used in this study.
Chapter 3	**Methodology**	This chapter elaborates on the followed research steps in this study to answer the research question (see Figure 1.2 on the facing page). This is divided into two parts. Firstly the steps for the numerical analysis are explained. Secondly, the different components of the design tool and the necessary steps for the case study are elaborated on.
Chapter 4	**Results**	This chapter provides the results for each of the research steps explained in Chapter 3. This chapter is also divided in the numerical analysis part and the design tool part.
Chapter 5	**Discussion**	This chapter provides a general discussion on the meaning and significance of the results. Thereafter, a discussion on the applicability of the research findings is given.
Chapter 6	**Conclusion**	In the final chapter the sub-research questions are answered following on the conclusion of the main research question. The conclusion is followed by recommendations for further research and implementation of the results in a safety assessment.

2
Background

2.1. Introduction

Hydraulic engineering of dikes is a different expertise compared to coastal wetland engineering. This study combines the knowledge on these two disciplines in the coastal engineering sector. Within this chapter both disciplines are generally introduced. First, an introduction is given into wave breaking, which is related to the wave load on hydraulic structures. Secondly, the wave attenuation processes of coastal wetlands and their role in flood risk management are described. Thirdly, the assessments on grass and clay erosion is defined. Finally, a numerical model is introduced for the extension of the erosion assessments.

2.2. Wave breaking

An important parameter in describing the behaviour of waves on a slope is the breaker parameter (ξ). This parameter plays a central role in all kinds of shore protection problems. Waves can behave completely different near a structure, with different values of ξ. This relation not only provides insight into whether waves will break and how they will break, but also reflection and erosion (as non-breaking or breaking strongly determines pressures and velocities along the slope) are related to this parameter (van den Bosch, 2010). It represents the ratio of slope steepness and deep water wave steepness, and therefore combines hydraulic and structural parameters, see Equation (2.1):

$$\xi = \frac{\tan\alpha}{\sqrt{H_s/L_0}}$$

in which L_0 : (2.1)

$$L_0 = \frac{gT_p^2}{2\pi}$$

Where, ξ is the breaker parameter, α the slope angle [°], Hs is the significant wave height $[m]$, T_p is the wave period $[s]$, L_0 is the deep water wave length $[m]$ and g is the gravitational acceleration constant $[m/s^2]$. The wave height is based on the spectrum and concerns H_{m0}, however in this report it is called significant wave height, unless stated otherwise. The significant wave height H_s is the visually observed wave height and is defined as the average of the highest third parts of the waves (Peters, 2017). H_s is also used to define the deep-water wave steepness $s_o = H_s/L_0$.

The different ways of breaking of waves can be classified in three main types; surging, plunging and spilling. Table 2.1 on the following page gives an impression of the different breaker types and the range of ξ for which they occur. Obviously, the transition between the types is not sharp-cut. The main wave breaking type on dike structures is plunging waves. Dike structures have less gentle slopes, resulting in plunging breakers that range between $1 < \xi < 2.5$ (Battjes, 1974). A relatively sudden

Table 2.1: Breaker types (adopted from Peters (2017))

Breaker type	Transition value of ξ for incident waves	Dominant process	Crest Height	short wave length, gentle slope ↓ Long wave length, steep slope
Spilling	$\xi < 1$	Wave set-up	Low	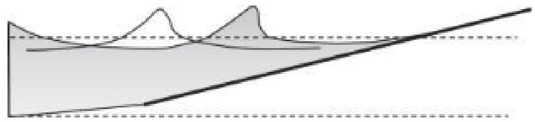
Plunging	$1 < \xi < 2.5$	Wave rundown and wave impact	↕	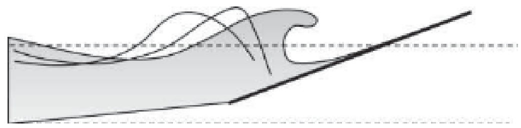
Surging	$\xi > 2.5$	Reflection rundown, run-up	High	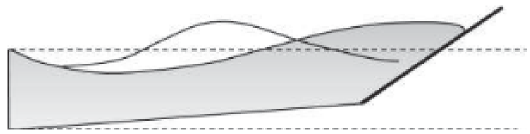

decrease of the slope reduces the speed of the wave. The top of the wave travels faster, moves over the front, and plunges or slams on the slope. In some cases the wave plunges on a water film of the previous wave pouring down. In other cases the water directly hits the revetment.

In some situations dike structures have a very gentle slope, which can result in spilling waves($\xi < 1$). These waves break like in gradually more shallow water. The high waves break distant from and the smaller waves break close to the coastline. The white-capped breakers travel over a certain distance to the coastline and gradually lose the wave energy. The least common breaker type for dike structures is surging waves, because this requires significantly higher crest heights and is therefore less cost-efficient. Table 2.1 summarizes the breaker types characteristics.

2.3. Wave loads

Wave impacts from the sea can cause significant damage to the revetment. In this process the waves reach the toe of the dike and will break and collide on the slope. Hereby a large mass of water impacts (direct impact load) on the slope, exerting a force on the cover layer. However, not all energy will be dissipated in this process, but some is lost by the water that will flow further up the slope until its velocity reaches zero (flow run-up load). Sequentially, the wave reverses direction and will flow back down the slope (flow run-down load). This process causes a shear force on the surface of the slope. The wave load is caused by the wave impact in the breaker zone and above it by flowing water in the run-up and run-down zone (Mous, 2010). Figure 2.1 on the facing page shows an example of the wave impact load of a single wave. This figure illustrates two different components of the wave load: the maximum wave impact component (P_{max}) and the quasi static component. This study focuses on P_{max}, because this is the primary damage load (van Hoven and de Waal, 2015). The type of loading by waves is strongly dependent on the breaker type. Plunging and collapsing waves have the highest impact pressure, due to their forceful process (Führböter and Sparboom, 1988). The compressibility of water and the presence of a backwash layer can reduce the magnitude of the impact pressure (Peters, 2017).

Experiments with measured peak pressures per wave impact are mainly conducted for hard revetments (Peters, 2017). In a large wave channel in Hannover, a wave impact study with different slopes was executed by Führböter and Sparboom (1988). Two prototypes with a uniform slope of 1:4 and 1:6 were tested in the facility. The dikes were covered with an asphalt layer and the maximum wave impact was measured on the slope surface.

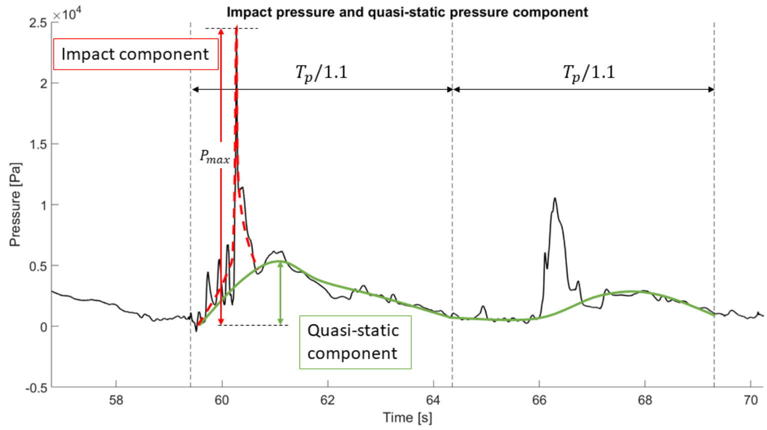

Figure 2.1: Definition of impact pressure and quasi-static component for breaking wave impact load

Based on the experiment, Equation 2.2 was established.

$$p_{max} = q\frac{1}{n}\rho_w g H \tag{2.2}$$

Here, the constant q depends on the probability of exceedance of a certain maximum pressure and the slope angle n. Several researchers have confirmed the peak pressures with a different constant q and the resulting normalized peak pressures ($p_{max}/\rho g H_s$), see Figure 2.2. In the assessment of asphalt revetments a Rayleigh distribution is used for the value of q. The highest values occur for breaker parameter values between 1 and 2, where plunging breakers appear to be strong and frequent (Peters, 2017). The pressure $p_{max,2\%}$ is an important measured maximum and represents the peak value not exceeded by more than 2% of the waves over the time series. This is captured by Equation 2.3 and also represented by the line Eq 5.42 in Figure 2.2 .

$$\frac{p_{max,2\%}}{\rho_w g H_s} = 8 - 1.6\xi_{m-10} - \frac{2}{(\xi_{m-10} - 0.2)^2} \tag{2.3}$$

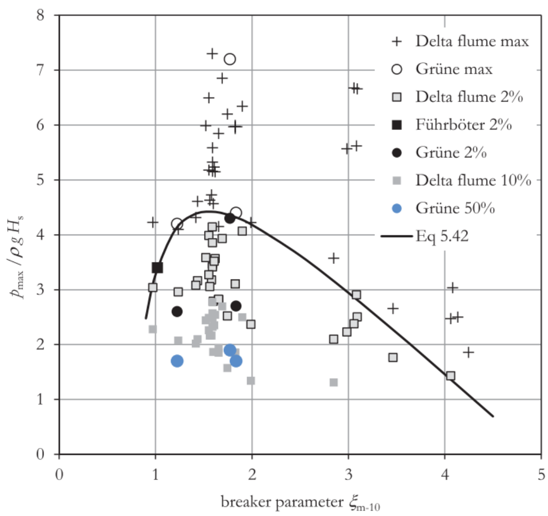

Figure 2.2: Graph of wave impact experiments on hard revetment (adopted from Peters (2017))

2.4. Wetlands in flood-risk management

The presence of a salt marsh foreshore can lead to a reduction in failure probability of the dike behind it (Vuik et al., 2019). Incorporating salt marshes in the flood protection assessment requires in-depth knowledge about the hydrodynamic processes (Losada et al., 2016). The hydrodynamic processes of salt marshes affecting wave attenuation are the attenuation by vegetation, wave breaking and bottom friction (Vuik et al., 2016). Vegetation causes wave attenuation due to the force exerted by the plants on the moving water. Following Newton's third law, the water simultaneously exerts a force equal in magnitude and opposite in direction on the plants. The flexibility of the plants determines how plant motion and wave motion interact, and determines the magnitude of the drag forces (Rupprecht et al., 2017). Nevertheless, the maximum wave height depends mainly on the water depth, which is referred to as depth induced wave breaking. Bottom friction causes lower current velocities close to the seabed as well as development of turbulence.

The stability of the vegetation is important to maintain the benefits from the wave attenuating capacity and bottom friction. Dense and tall vegetation are highly effective in dissipating wave energy, in emergent and submerged conditions (Anderson and Smith, 2014; Vuik et al., 2016). However, stem breakage may occur as wave height increases, thereby reducing the wave dissipating capacity (Rupprecht et al., 2017). This depends on the plant species and characteristics. Plants exposed to higher mean wave energy develop shorter and thicker stems which makes them less vulnerable to stem breakage (Silinski et al., 2015). Vice versa, plants exposed to low mean wave energy are most sensitive to stem breakage during severe storms.

Insight into these stability processes add to the knowledge of vertical and lateral dynamics of the salt marsh (Borsje et al., 2011; Willemsen et al., 2018). Lateral dynamics determine the cross-shore location of the marsh edge and thereby the width of a salt marsh. With these dynamics the vegetated foreshore can be considered in the original failure probability system. Vuik et al. (2019) demonstrates that the cost effectiveness of vegetated foreshores depends on how much this probability can be affected by the foreshore. Furthermore, cost effectiveness relies on the investment required to construct and maintain the foreshores in comparison to hard structures. The study by Vuik et al. (2019) qualitatively assesses the cost effectiveness of different strategies with a vegetated foreshore. It concludes that salt marsh construction is cheaper than dike heightening. Strategies considering wetland construction are foreshore heightening, foreshore combined with breakwaters and brushwood dams. In this research the strategy of foreshore construction by brushwood dams is considered, because this is already widely used at the Wadden sea, plus it has high ecological value. The foreshore construction with brushwood dams mainly depends on the accretion rate, which is $2cm/y$ for the Wadden sea (D'Alpaos et al., 2011). This morphological development is highly uncertain due to temporal and spatial variability Willemsen et al. (2018, 2020). Therefore, Salt marshes constructions with brushwood dams are limited in effect on failure probabilities, because of their dependence on sediment accretion in the inter-tidal zone.

2.5. GEBU assessment

The assessment of erosion due to wave impact consists of two parts. First the resistance of a top layer is assessed and secondly the residual strength of the clay underneath the top layer is measured. The resistance of the grass revetment is assessed by the resistance-duration and accounts for the top 20cm (van Hoven, 2015). Resistance-duration is the duration the grass revetment can withstand incoming waves and depends on the height of the waves and the quality of the grass (Ministerie van Infrastructuur en Milieu, 2016). Whenever the storm duration (t_{load}) is longer than the resistance-duration (t_{top}), the grass revetment fails and the residual strength of the clay (t_{sub}) has to be calculated (from 20cm until failure of the dike) (van Hoven, 2015). Next to the wave load characteristics there are two important aspects that affect the resistance duration of the grass revetment: the strength of the roots and the slope angle (Verheij et al., 1998). The added value of grass on top of clay, is an increased erosion resistance of the clay layer due to the tension strength of the roots of the grass (Muijs, 1999). The strength of the roots and the root density are important factors for the erosion process, while the thickness of the grass revetment and the erosion-resistance of the soil are not significantly contributing to the erosion resistance of the revetment (Verheij , Delft Hydraulics; van Loon-Steensma et al., 2014; van Hoven, 2015).

Furthermore, the residual strength of the clay layer is divided into two layers. The first layer accounts for the top 50cm minus the top 20cm of the grass revetment and assumes a stronger resistance than bare clay due to the root structure that is still present. This is captured in the method by Breteler (2017) similar to the resistance duration for the grass revetment. The second layer is the residual strength of the bare clay layer without a root structure. Recently, Mourik (2015) formulated an erosion model to account for the amount of damage caused by a storm surge translated to erosion volume (V_e) over time.

The experiments done on the resistance duration of grass and clay are limited in number. Some experiments are done on bare clay and other studies have taken a grass cover into account. From a selection of these experiments the resistance duration methods for the safety assessment of a grass revetment are generated. The erosion relation of Mourik (2015) has also used a small selection of experiments. Physical laboratory experiments, apart from being accurate, are significantly more expensive than their alternatives, such as a numerical model. Kruse (2010) introduced a method to extend the applicability of laboratory experiments with a numerical model. Mourik (2015) extended this approach and derived a relation for the erosion velocity. This research will further investigate the applicability of a numerical model for the design process of a grass cover dike.

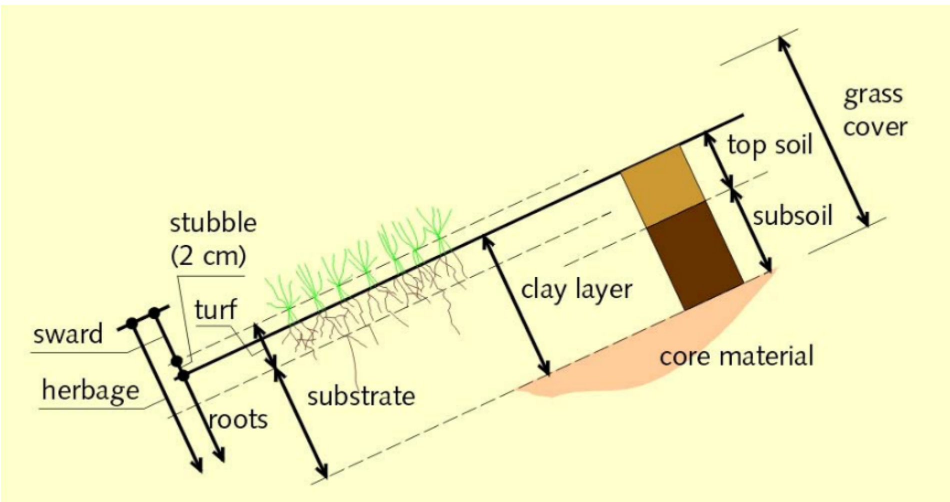

Figure 2.3: Definition sketch of grass cover Muijs (1999)

2.5.1. WBI-2017 model

The WBI-2017 describes different failure mechanisms according to the Dutch safety standards. Hereby three assessments are identified: elementary assessment, detailed assessment and the customized assessment (Ministerie van Infrastructuur en Milieu, 2016). The elementary assessment is a simple assessment based on three characteristics; wave height, whether the sod is open or closed and whether the core of the dike exists of clay. The detailed assessment consists of proposed calculations, which will be further investigated in this study. The customized assessment is used when the revetment is rejected by the detailed assessment, but with additional calculations the revetment can meet the requirements.

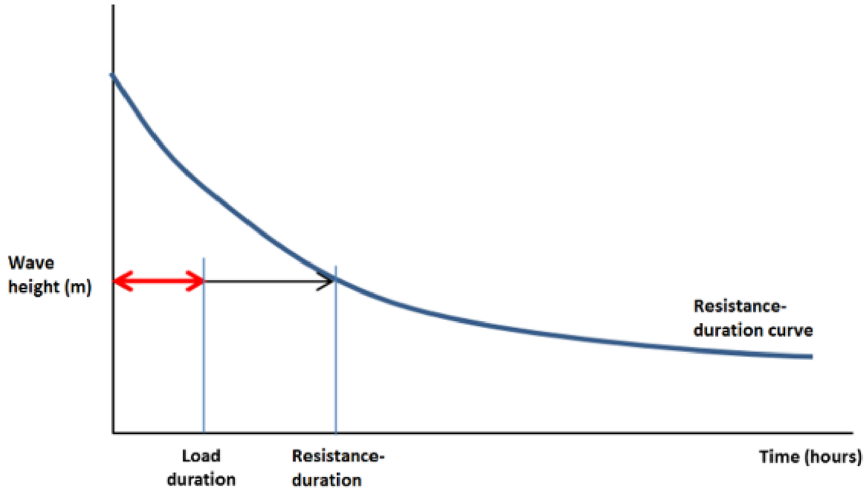

Figure 2.4: Resistance duration curve (adapted from Ministerie van Infrastructuur en Milieu (2016))

The detailed assessment is based on the resistance-duration curve shown in Figure 2.4 (Ministerie van Infrastructuur en Milieu, 2016). The resistance-duration curve describes the relation between the wave height and the maximum duration the grass revetment can resist. The grass revetment will withstand the wave attacks until the load duration exceeds the resistance-duration. The resistance-duration curve depends on empirical parameters determined from experiments (van Hoven and de Waal, 2015). The model does not present a clear distinction between load and strength, but is defined as load duration to failure. The resistance duration of the top and sub layer is determined with Equations 2.4 and 2.5.

$$t_{top} = \frac{1}{c_b} \ln\left(\frac{max((Hs - c); 0)}{c_a}\right) \tag{2.4}$$

$$t_{sub} = \frac{max((d_{tot} - 0.2); 0)}{c_d(1/3)^{1.5} max((H_s - 0.5); 0)} \tag{2.5}$$

In which, erosion of a grass cover starts at a certain threshold wave height c $[m]$ and increases with H_{m0} depending on the empirical parameters c_a $[m]$ and c_b $[h^{-1}]$. In the WBI-2017 assessment of the strength of grass revetment the effect of the slope angle is not included (Verheij et al., 1998). d_{tot} is the layer thickness of the clay layer, including the top layer with grass roots, c_d is a constant depending on the sand fraction f_{sand} elaborated on in Appendix B.2. The resistance duration is now determined by $t_{top} + t_{sub}$. During a storm, the wave heights vary. To assess the grass revetment for wave impact, the failure fraction is calculated for different wave heights. The failure fraction is calculated for a time step Δt and summed over time. Equation 2.6 shows that the top and sub layer have failed whenever $F_{frac} \geq 1$.

$$F_{frac} = \frac{\Delta t}{t_{top} + t_{sub}} \tag{2.6}$$

2.5.2. Clay erosion models

Next to the failure probability of the top and sub layer it is of interest to know the amount of erosion that occurs (Breteler, 2012, 2015; Mourik, 2015). The WBI-2017 allows for some erosion on the seaward slope, which gives the possibility to look at how much erosion occurs for a given return period. If the grass cover fails, but the erosion on the bare clay layer is relatively small, the dike still fulfils its function and will not be rejected by the WBI-2017. The approach of Breteler (2012) links the erosion velocity of bare clay with the erosion hole development presented in Figure 2.5. An erosion hole in a clay slope consists roughly of a terrace with a slope of 1:7 to 1:10 and a cliff with a slope of approximately 1:1. The erosion hole grows because the cliff retreats landward due to the wave attack.

Nowadays, for determining the erosion of bare clay the model of Mourik (2015) is used, based on the approach of Breteler (2012). The influences of wave height, wave steepness and slope angle were analysed with numerical simulations using OpenFOAM, which is a Computational Fluid Dynamic (CFD) model (see section 2.6). The main assumption in this method is that the erosion process is dominated by the significant peak pressure head (see section 2.3) accounting for the highest 33% wave impacts on the erosion profile (Kruse, 2010). Relations are derived by changing different settings as the wave steepness and the slope angle and reading out the peak pressures on the slope. The model is only validated on three Delta Flume experiments and it suggests to do more experiments (Mourik, 2015). The formula by Mourik (2015) is given in Equation (2.7).

$$\frac{\partial V_e}{\partial t} = c_e \cdot \underbrace{\left(1,32 - 0,079\frac{V_{e0}}{H_s^2}\right)}_{\text{i}} \cdot \underbrace{(16,4(\tan\alpha^2))}_{\text{ii}} \cdot \underbrace{\left(min\left(3,6;\frac{0.0061}{s_{op}^{1,5}}\right)\right)}_{\text{iii}} \cdot \underbrace{(1,7(H_s - 0,4)^2)}_{\text{iv}} \tag{2.7}$$

In this research the second term (*ii*) on the slope angle will be investigated in more detail. Elaboration on the erosion formula is given in Appendix B.2. The derivation of the relation for the slope angle is determined from Figure 2.6 on the following page. This figure shows the significant pressure head ($\phi_{s,max}$ in $[m]$). Section 3.3.2 explains the calculations on determining the maximum peak pressures. The derived relation on the slope angle is determined by simulating the peak pressures on three erosion profiles of 1:3, 1:4 and 1:5 (Equation (2.8)).

$$\phi_{s,max} = 0.56 + 4.14 \cdot \tan\alpha \tag{2.8}$$

The trend shows a linear relation between the slope angle and the significant pressure head. This relation is translated into the erosion velocity using a calibrated formula on clay erosion experiments (Equation (2.9)). With this translation the effect of slope angle is substituted in Equation (2.7).

$$\frac{\partial V_e}{\partial t} = \max\left(0; -0.5 + 0.95 \cdot \phi_{s,max}\right) \tag{2.9}$$

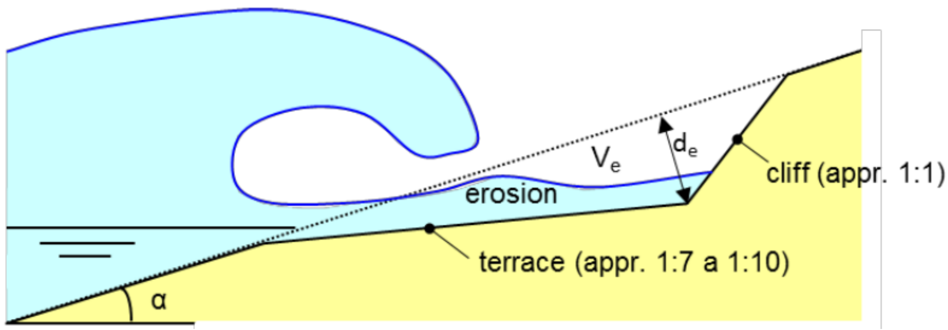

Figure 2.5: Erosion profile for the approach of Breteler (2012)

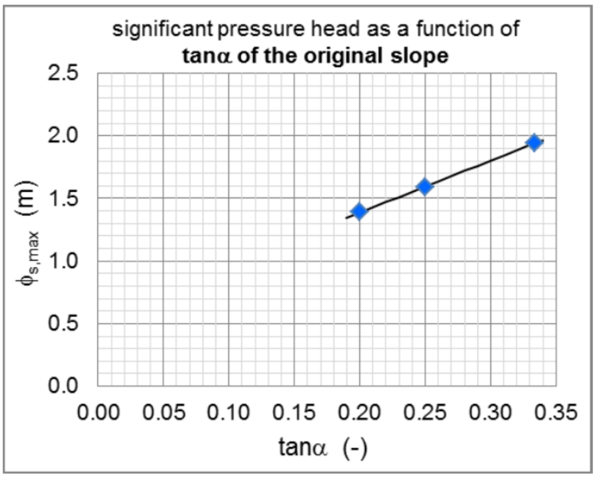

Figure 2.6: Relation between significant pressure head and the slope angle (adopted from Mourik (2015))

.

2.6. Numerical model

Several numerical model types are used to simulate wave-structure interactions that are categorized as Computational Fluid Dynamics (CFD) models. These CFD models are divided into two main categories: the nonlinear shallow water equations models (NLSW) and the Navier Stokes equations models (NS). Herein, the most complete flow description in three dimensions is represented by the Navier-Stokes differential equations. The distinction between other numerical models that it solves for very complex processes as turbulence. The equation solves for pressure, the three-dimensional flow velocity components in time and space. The downside of the model is that it causes long computation time compared to other models. Nowadays, a generally used form of the Navier-Stokes differential equations is the Reynolds-Averaged Navier-Stokes equations (RANS) combined with the volume of fluid method (VOF). A wide range of coastal engineering applications are validated and tested on RANS models (e.g. overtopping, wave loads, revetment stability, toe stability, wave-structure interaction etc.) (Jacobsen et al., 2012; Jensen et al., 2014; Higuera et al., 2014).

OpenFOAM is an example of a RANS model. The model is provided as a open source tool and accessible for everyone. The basis of the numerical framework consists of the open-source model OpenFOAM (Higuera et al., 2014). The open-source library consists of C++ libraries and codes that can solve CFD problems using finite volume discretization. Additionally, OpenFOAM is capable of handling two phase flows by linking the RANS equations to a Volume Of Fluid (VOF) method in order to capture the free surface (see Appendix A.4) . Various packages are compiled together, which is, for the sake of simplicity, called in this research as 'CoastalFOAM'. Elaboration on the formulas used in the numerical model are given in Appendix A.4. An example on post-processed data of a coastalFOAM simulation is presented in Figure 2.7.

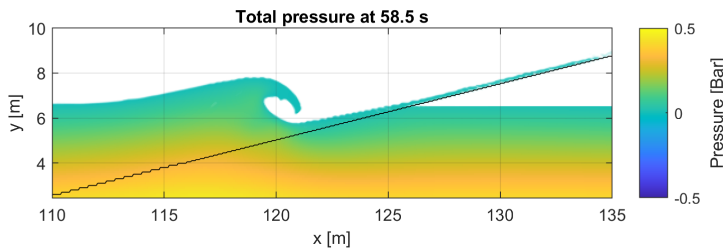

Figure 2.7: Example of a breaking wave on a dike slope showing the total pressure of a CoastalFOAM simulation

.

3

Methodology

3.1. Methodology outline

The research methodology is divided into two parts, as shown in Figure 3.1 on the next page. The first part of the methodology is focused on the numerical analysis of different geometries and the induced pressures on the slope of the dike. This part begins with a numerical model set-up, motivating hydraulic conditions, geometries and mesh properties. As follow-up a mesh sensitivity analysis is necessary to optimize the computation duration and examine the skill of the model. The skill of the model is defined by how accurately it can capture the maximum pressures. A post-processing method on the pressure data is given, which results in the local maximum pressure per wave on the slope. The next step is formulating and running the simulations by concluding on the numerical set-up and the mesh refinements. A linear trend is obtained from the geometric settings and the maximum simulated pressure. The last part of the numerical analysis is the validation on empirical data and models. First, using experiments and relations on hard revetment by Führböter and Sparboom (1988). Additionally, the relation of Mourik (2015) on the erosion velocity of clay is compared with the obtained relation from the simulations. Lastly, The WBI model is extended by concluding on the linear trend for different slope angles.

The second part of the methodology describes the design tool set-up. The tool builds on the extended WBI-model using a variable water level and hydraulic conditions during a storm from the Hydra-NL software. Wetland strategies are computed and validated, which result in a reduction factor on the hydraulic input conditions. At last construction and maintenance costs are computed for the different geometric settings. The final part of the methodology describes how the design tool can be used in a case study of the Koehool Lauwersmeer dikes. The three dike locations are examined whether a grass cover dike is feasible.

3.2. Numerical analysis

Having outlined the numerical framework in Chapter 2, a method for a numerical wave flume is presented in this section. Multiple aspects are discussed: geometry settings, hydraulic conditions and mesh properties.

3.2.1. Geometry settings

Different geometries and hydraulic conditions are considered to come to an optimal choice for the numerical wave flume set-up. The goal of the numerical analysis is to examine two different geometrical relations. One is to numerically verify the relation Peters (2020) has concluded on. Herein the relation of Führböter and Sparboom (1988) most accurately fitted the experimental data on grass cover erosion. The second relation consideres the study by Mourik (2015) on the erosion velocity of clay for different slopes. In conclusion, the two relations are derived from two geometry profiles, which are defined as a flat profile and an erosion profile. A detailed description on the geometries is described in Appendix A. The important choices on the geometry profiles are given below.

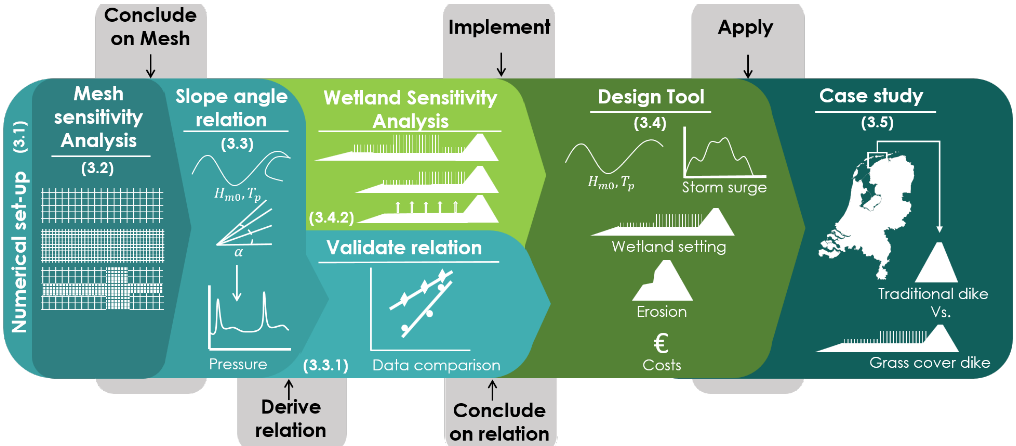

Figure 3.1: Methodology

- **Flat profile:** the relation of Führböter and Sparboom (1988) is derived from experiments on a flat profile with a slope of 1:4 and 1:6 (see section 2.3). To extend and verify this relation flat slope profiles of 1:4, 1:6 and 1:8 are considered.
- **Erosion profile:** the erosion profiles examined by Mourik (2015) are three flat slopes of 1:3, 1:4 and 1:5 (see section 2.5.2). The erosion profiles are based on the method of Breteler (2012). In this research the erosion profiles for slopes of 1:6 and 1:8 are adopted as well. The erosion profiles have an erosion volume of $V_e = 5m^3/m$, which corresponds to an erosion depth of $d_e = 1.0m$.

3.2.2. Hydraulic conditions

The hydraulic conditions of the flat profile deviates from the hydraulic conditions of the erosion profile. Extending the relations for the different geometries, as described in previous paragraph, requires to imitate the hydraulic settings of these studies. The numerical analysis by Mourik (2015) uses hydraulic conditions corresponding to river dikes. Therefore, the forcing is relatively low. This results in a relatively small wave steepness compared to the wave steepness at the Wadden Sea.

The hydraulic conditions of the flat slopes are based on sea swell waves at the Wadden sea. These waves are higher than 2 meters for the trajectory norm (Wetterskip Fryslan, 2018). The wave impact pressure associated with wave heights above $H_s = 1.6m$ will increase the peak pressure linearly with the wave height H (Peters, 2017). Therefore, a wave height above $2m$ is not considered, because this can linearly be interpolated. Next to that the currently running Delta Flume experiments focus on a wave height of $2m$. The wave period also based on the Wadden Sea conditions, which has a high wave steepness and therefore a low wave period of $T_p = 5.7s$.

The depth of the numerical flume is chosen such that the degree of non-linearity of the incoming waves (Ursell number) is equal for all simulations. This research focuses on the influence of wave height and should not be obscured by the influence of the water depth. The Ursell parameter is a measure to define the shape of a wave which is an important aspect of the depth influence. The Ursell parameter is described by the following formula:

$$U = \frac{H_s L_p^2}{h^3} \tag{3.1}$$

with, U as the Ursell parameter $(-)$, L_p as the wave length at shallow water, belonging to the peak of the spectrum (s) and h is the water depth (m). The parameter is chosen between 10 and 13 for all simulations, which means that incoming waves near the toe of the dike still are nearly sinusoidal. It is expected that there will be no unwanted influence of the water depth because of this choice (Mourik, 2015).

Table 3.1: Hydraulic conditions and geometric settings

simulation	experiment	$Hs[m]$	$Tp[s]$	$sop[-]$	$tan[-]$	Depth $[m]$	Duration $[s]$	$Ve[m^3/m]$	$de[m]$
CoastalFOAM Flat profile									
1	F10_slope4	2.0	5.7	0.039	0.250	6.50	570	-	-
2	F11_slope6	2.0	5.7	0.039	0.167	6.50	570	-	-
3	F12_slope8	2.0	5.7	0.039	0.125	6.50	570	-	-
CoastalFOAM Erosion profile									
4	E10_slope3	1.20	5.0	0.031	0.333	4.50	530	5.00	1.00
5	E11_slope4	1.20	5.0	0.031	0.250	4.50	530	5.00	1.00
6	E12_slope5	1.20	5.0	0.031	0.200	4.50	530	5.00	1.00
7	E13_slope6	1.20	5.0	0.031	0.167	4.50	530	5.00	1.00
8	E14_slope8	1.20	5.0	0.031	0.125	4.50	530	5.00	1.00

A summary of the geometric settings and the hydraulic conditions is given in Table 3.1. Each simulation is performed with a Jonswap-spectrum at the inlet of the numerical flume. The hydraulic conditions for the flat profile are set to $H_s = 2m$, $T_p = 5.7$ and a water depth of $d = 6.5m$. The hydraulic conditions of the erosion profiles are based on the study of Mourik (2015), with $H_s = 1.2m$, $T_p = 5.0s$ and a water depth of $d = 4.5m$.

3.2.3. Mesh properties

For this study a two-dimensional simulation in a vertical plane (2DV) is performed. Although wave breaking is a three dimensional process, a 2DV model is able to simulate the governing wave breaking characteristics with a reasonable accuracy as shown by several other 2DV numerical studies in literature (Jacobsen et al., 2012; Devolder and Troch, 2018; Larsen and Fuhrman, 2018). The dimensions of the mesh shown in Figure 3.2 on the next page depend on the intermediate wave length ($0.05 < h/L < 0.05$), because the wave generation zone needs to be one wavelength. The free zone is also one wave length, where the incident waves and reflective waves from the structure interact with each other. The toe of the structure starts directly after the free zone. The wave impact zone is where the waves break on the structure. For the numerical stability of the model a wave relaxation zone at the end of the mesh is placed. The cells that are located within the structure are excluded from the simulation in order to safe computation time.

As a reference the studies of Kruse (2010) and Mourik (2015) are used, in which respectively the cell sizes of $0.1 \times 0.1m$ and $0.05 \times 0.05m$ are presented. The grid size is generally expressed by its number of cells per wave height and length. A relatively fine mesh with square cells($\Delta x = \Delta y$) is used , which according to Jacobsen et al. (2012) gives the most accurate results considering wave propagation towards the structure. Mesh refinement can have significant influence on the output, but also on the computation time. Further elaboration on this is given in the next section on mesh sensitivity analysis.

The model stability is indicated by the Courant number, which during the simulation needs to be lower than a pre-defined value (e.g. 0.35). To reach numerical stability, the time step is set to be variable, so that the Courant number is kept below 0.35. Also the Courant number is kept low to avoid smearing of the interface.

$$C_0 = \frac{u \cdot \Delta t}{\Delta x} \tag{3.2}$$

Where, u is the velocity, Δt the time step and Δx a fixedvalue based on pre and post processing meshing tools. Since the wave celerity cannot be altered, nor can the resolution of the grid during the simulation (fixed mesh is used), only time can be adapted ensuring a low Courant number. the Courant number is always below 1, but varies for each study and the purpose of the study (Devolder et al.; Devolder and Troch, 2018; Jacobsen et al., 2018). Because this study focuses on maximum pressure peaks, which typically have a duration of 0.35 seconds, the Courant number is chosen to be relatively low 0.35 [-].

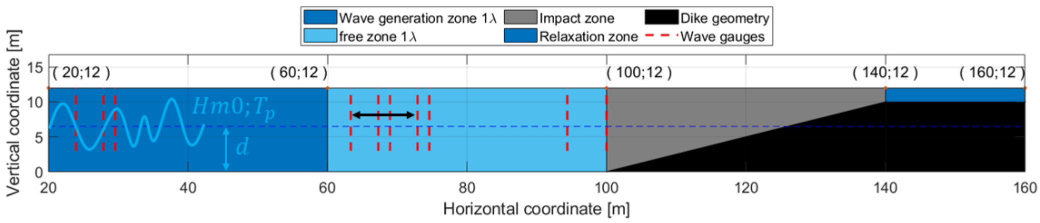

Figure 3.2: An example of the mesh dimensions and wave gauge spacing

3.3. Mesh sensitivity analysis

In the mesh sensitivity analysis different grid sizes and grid refinementss are examined on their computation time and model accuracy. Table 3.2 shows the different grids that are examined. A coarse and fine uniform ($\Delta x_1 = \Delta y_1$) structured grid are considered following the studies of Kruse (2010) and Mourik (2015). Next to that the mesh is optimized by applying local refinements in the zones where the most wave interaction is. The zones of interest are around the sea water level zone ($\Delta x_2 = \Delta y_2$) over the whole grid and the breaking zone ($\Delta x_3 = \Delta y_3$) on the structure. Next to the base meshes, two local refinement tools are used in openfoam.

The multigrading tool manipulates the spacing of the grids in the x and y direction with a pre-defined number of cells. The x and y are divided into three blocks. For the x direction this results in a domain from: the inlet to the toe of the dike, the toe of the dike to the wave breaking zone and the end of the breaking zone to the outlet. The y domain is divided in the interest zone around the sea water level of $1.5H_s$ and the domain below and above. Figure 3.3 on the next page clarifies where the zones of interest are located with the darkest grey spaces having a grid size of $0.05 \times 0.05m$. This reduces the number of cells compared to the fine mesh, but results in non-uniform rectangular cells. The non-uniform grid sizes are for example located in front of the dike around the sea water level where the spacing is $0.1 \times 0.05m$. This non-uniformity is examined in the sensitivity analysis.

Another tool is the snappy hex mesh tool, in which local refinements can be applied and the grids are snapped to the structure surfaces. This makes that all the cells are uniformly sized. The dark line on the slope of Figure 3.3d on the facing page indicates the snapped region on the slope with a grid size of $0.05 \times 0.05m$. the underlying base mesh is still $0.1 \times 0.1m$, reducing the total number of cells.

The mesh sensitivity analysis is conducted for a flat profile case of slope 1:4, with the corresponding hydraulic conditions described in previous section. In total four different sensitivity simulations with four different grids are conducted with a duration of 20 wave periods plus a warm-up time of 3 wave periods. Hereby we follow the approach of Devolder et al., which also used 20 waves for the validation of the numerical model. The model accuracy is validated on the reflection coefficient and the generated maximum pressures.

Table 3.2: Gridsizes mesh sensitivity analysis

Grid	**Base Mesh** $\Delta x_1 = \Delta y_1 [m]$	**SWL refinement** $\Delta x_2 = \Delta y_2 [m]$	**Profile refinement** $\Delta x_3 = \Delta y_3 [m]$	N_y/H_s	N_x/L	N_{total}
Coarse	0.1	0.1	0.1	20	400	128000
Fine	0.05	0.05	0.05	40	800	296000
Multi grading	0.1	(0.1:0.05)≠0.05	(0.1:0.05)≠(0.1:0.05)	40	(800:400)	240000
Snappy Hex Mesh	0.1	0.05	0.05	40	800	186648

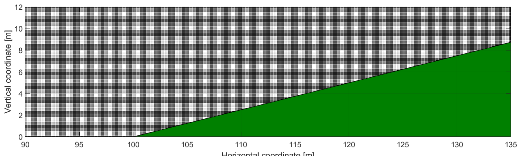

(a) Coarse grid

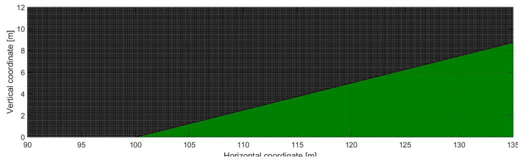

(b) Fine gird

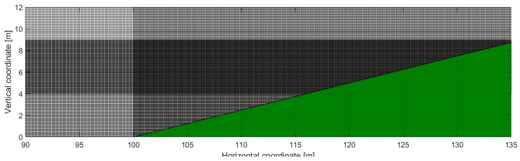

(c) Multi grading grid

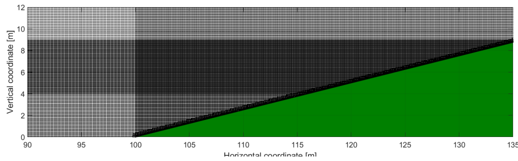

(d) Snappy hex mesh

Figure 3.3: Grid spacing of the different meshes. (a) Coarse grid $dx = dy = 0.1$, (b) Fine gird $dx = dy = 0.05$, (c) Multi grading grid $dx_1 = dy_1 = 0.1; dx_2 = dy_2 = 0.05$, (d) Snappy hex mesh $dx_1 = dy_1 = 0.1; dx_2 = dy_2 = 0.05; dx_3 = dy_3 = 0.025$.

3.3.1. Reflection

The reflection coefficient is widely used to show the strength(or weakness) of a numerical model (Oumeraci et al., 2010; Mourik, 2015; Moretto, 2020). The reflection-coefficient is defined as the wave height of the reflected wave with respect to the incoming wave height shown in Equation (3.3).

$$K_r = \frac{Hm0_r}{Hm0_i} \tag{3.3}$$

Where $Hm0_r$ is the reflected wave height and $Hm0_i$ the incoming spectral wave height. The incoming and reflective wave height are derived from a least square method by Mansard and Funke (1980). This method requires at least three wave gauges in reasonable proximity from each other. In addition, more wave gauges result in higher accuracy, therefore 2 wave gauge arrays of respectively 3 and 4 wave gauges are used in the analysis (Zelt et al., 1993). The wave gauges are specified with the red dotted lines in Figure 3.2 on the facing page.

The derivation of a theoretical solution for reflection of breaking waves is hardly possible. An useful approach is given by Allsop (1999). This approach implies that the reflection coefficient is proportional to ξ^2 (see (Battjes, 1974)). For values of ξ below the breaking limit, the following formula was found experimentally for a smooth impermeable slope:

$$K_r \approx= \frac{0.96 \cdot \xi^2}{4.8 + \xi^2} \tag{3.4}$$

Equation (3.4) will be used to compare the results of the sensitivity simulations. Next to that, the study of Mourik (2015) also conducted reflection coefficients, which give a validation case with the numerical simulations of this research.

3.3.2. Pressure head

The pressure time-series on the geometry profiles are read out from pre-defined probes on the slope. These probes provide the calculated data in the cell they are located in. Appendix A.3 provides a detailed description on the probe spacing. Figure 2.1 on page 9 shows a typical output from one of the probe locations. As described in section 2.3 the wave impact is divided into an impact component and a quasi-static component. For the analysis we are interested in the impact component P_{max} for every wave. The peak pressure per wave is extracted by dividing the time-series over the average wave period $T_m = Tp/1.1$. For the sensitivity analysis this gives 20 values from 20 waves. The pressure head is used instead of the pressure, to focus on the dynamic aspect of the pressure. The pressure head ϕ concerns the total pressure P minus the static hydraulic pressure as shown in Equation (3.5) on the next page.

$$\phi = \frac{P}{\rho g} - z \tag{3.5}$$

with, ϕ being the pressure head in$[m]$, P is the total pressure in $[Pa]$, g is the gravitational acceleration in $[m/s^2]$, rho the density of water in $[kg/m^3]$ and z is the vertical coordinate of the location relative to the water level $[m]$. Before cutting the time series into small parts the data is filtered. Artefacts of unrealistic high pressures during a period of $t = 0.01s$ in one grid cell are removed from the signal. Thereafter a slight moving average over the location is used $(0.25 \cdot P_{x_i-1} + 0.50 \cdot P_{x_i} + 0.25 \cdot P_{x_i+1})$ to remove the largest noise from the calculated probe signals. The pressure head distribution over the profile will be examined on its $\phi_{2\%}$, $\phi_{10\%}$ and significant pressure head ϕ_s. The percentages indicated with the pressure head correspond to the percentage of the highest maximum pressures occurring. These are values that are also used in corresponding experiments, also called design parameters (Peters, 2017; Kruse, 2010; Mourik, 2015).

3.4. Relation between geometry and pressure

After concluding on the mesh sensitivity analysis the simulations are conducted conform Table 3.1 on page 17. Each profile is analysed on its peak pressure head, herein a distinction is made between the flat profiles and the erosion profiles. Führböter and Sparboom (1988) adopted the relation from the maximum peak pressures (see section 2.3), therefore it is analysed on $\phi_{2\%}$ and $\phi_{10\%}$ compared to the slope angle. The relation is derived by conducting a linear regression line through the simulated peak pressures in relation to the slope angle.

For the erosion profile the significant pressure head is used conform the assumption of Kruse (2010). It is expected for the erosion process that the significant value of the peak pressures is more relevant than an extreme value, or an average value (Kruse, 2010; Mourik, 2015). The significant value is the average of the highest 33 % of the peak pressures. The regression line for the erosion profiles is conducted similarly as the flat profiles.

3.4.1. Validation on empirical relations

The next step is validating the geometry relations with the derived relations of Führböter and Sparboom (1988) and Mourik (2015). The hypothesis is that the slope of the regression lines will have a statistical linear correlation with the empirical relations. The simulated data will show an error compared to experimental data. However, it is assumed this error will be the same for each geometry setting, which makes that it still can describe the linear trend. The linear relation is summarised in Table 3.3.

Each regression line is examined on the coefficient of determination R^2 which evaluates the quality of a linear fit of a model on data. It expresses what fraction of variability of the dependent variable (P_{max}) is explained by the independent variable ($tan(\alpha)$) (ref, 2008). Another common statistical method is used to determine the significance of the linear fit, which is the $pvalue$. A small $pValue$ means that there is stronger evidence in favor of the hypothesis of a linear fit (Dahiru, 2011).

Next to that the experiments on wave impact pressure on hard revetment are compared with the simulated flat profile data. The data of Figure 2.2 on page 9 is used to assess the skill of the numerical model in simulating the design parameters explained in previous section.

Table 3.3: Overview of geometry relation on wave impact pressure

Studies	Description	Relation
Führböter and Sparboom (1988)	Slope angle on hard revetment from wave impact pressure	$\tan\alpha$
Mourik (2015)	Slope angle on erosion profile from numerical wave impact pressures	$\tan\alpha$

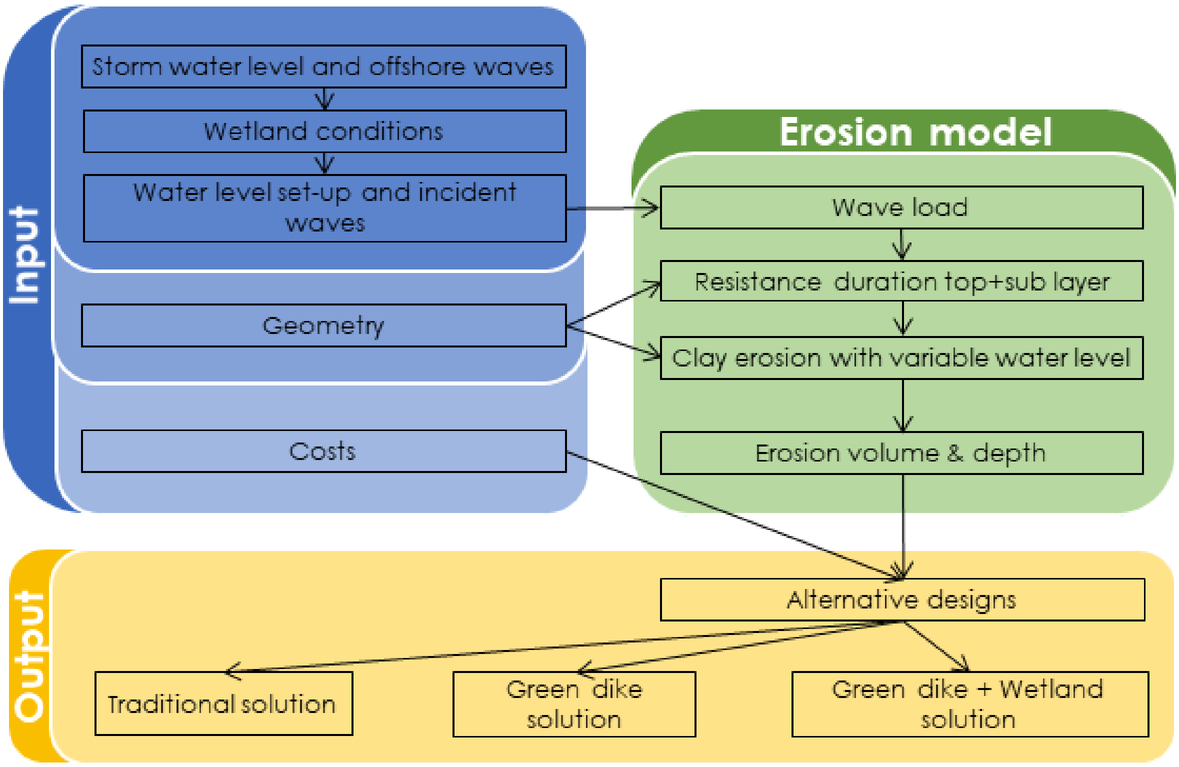

Figure 3.4: Design tool framework

3.5. Design tool

The second part of this research methodology describes the design tool set-up. Figure 3.4 shows the proposed framework of the design tool. The input consists of three components, which have their own settings and parameters influencing the erosion model. The first input considers the water level set-up and wave height during the design conditions. Wave attenuation by vegetation is calculated from the wetland settings together with the already given hydraulic conditions. This results in lower hydraulic conditions which are input for the erosion model. The slope of the dike is divided into sections in which for each section the failure fraction is calculated. The geometry input is used for the calculation of the resistance duration of the top and sub layer, but also for the bare clay layer. When the wave load exceeds the resistance duration of the top and sub layer at a section, the erosion of bare clay is being calculated. The output gives the erosion volume per section, which is translated into the erosion depth. Finally, different settings of the geometry slope and wetland conditions can be adjusted for calculating new design alternatives. The costs of constructing and maintaining new design alternatives are given as output of the model. A distinction is made between the traditional dike design and a grass cover dike solution with or without variable wetland strategies.

3.5.1. Hydraulic input conditions

Figure 3.5 on the following page shows how the hydraulic conditions of a storm is being simulated. The steps for each location are explained as follows. The maximum water level is abstracted form the Hydra-NL data, which is used to determine the water level set-up during the storm. The water level during a storm is the combination of the tide and the storm surge which is extracted from the software Waterstandsverloop. The tide of the Wadden sea has an amplitude of 1.35m and a period of 12.5 hours. The peak of the combined effect of the tide and the storm surge is limited to the already determined maximum water level. The output locations of Hydra-NL are placed approximately 50m in front of the dike. Extensive research at the Wadden Sea has led to the incorporation of the effect of depth induced wave breaking of the foreshore into the H_s-value and T_p-value 50m in front of the dike (Lammers, 2019; Steetzel et al., 2018). Therefore, Hydra-NL data 50m in front of the dike is used to generate the wave height H_s and period T_p per water level (steps of 0.5m). The wave height between

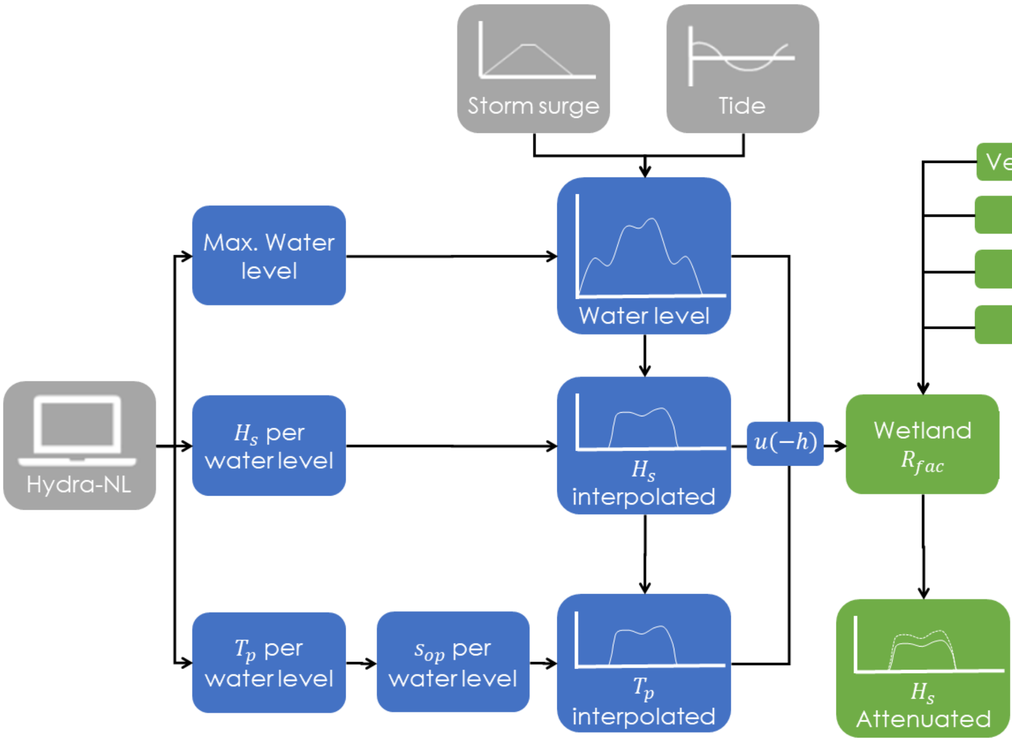

Figure 3.5: Hydraulic input conditions for the erosion model

the 0.5m intervals is interpolated with the water level set-up. For the wave period this is different, because the change in wave period is squared in comparison with the wave height. Therefore, the wave steepness is firstly calculated and interpolated with the interpolated wave height H_s. This given, the wave period is calculated with Equation 3.6.

$$T_p = \sqrt{\frac{2\pi H_s}{9.81 s_{op}}} \tag{3.6}$$

The water level set-up, interpolated H_s and T_p are the raw hydraulic input conditions for the tool. With these three parameters using linear wave theory the orbital velocity is calculated at the bottom (given the inundation depth, see Equation).

$$u(z) = \frac{\omega H_s}{2} \frac{cosh(k(z+h))}{sinh(kh)} \tag{3.7}$$

with, ω the angular frequency $[rad/s]$, k the angular wave number $[rad/m]$, h the inundation depth $[m]$ and $u(z)$ is the orbital velocity at inundation depth z in $[m/s]$. The orbital velocity is necessary to simulate stem breaking of vegetation, which is explained in section 3.5.2.

3.5.2. Wetland input strategies

The geometric wetland settings and resulting wave attenuation is explained in this section. Section 2.4 explains wetland wave attenuation has three processes which are depth induced wave breaking, bottom friction and attenuation by vegetation (Vuik et al., 2016). Because depth induced wave breaking is already incorporated in the Hydra-NL data for already present foreshores, it is advised for a detailed assessment of revetment to incorporate only additional wave attenuation by vegetation (Steetzel et al., 2018). Accordingly, this phenomena is integrated into the model using Figure 3.6 on the next page. This figure shows a 1D SWAN analysis for several wetland settings in the Wadden Sea, such as the

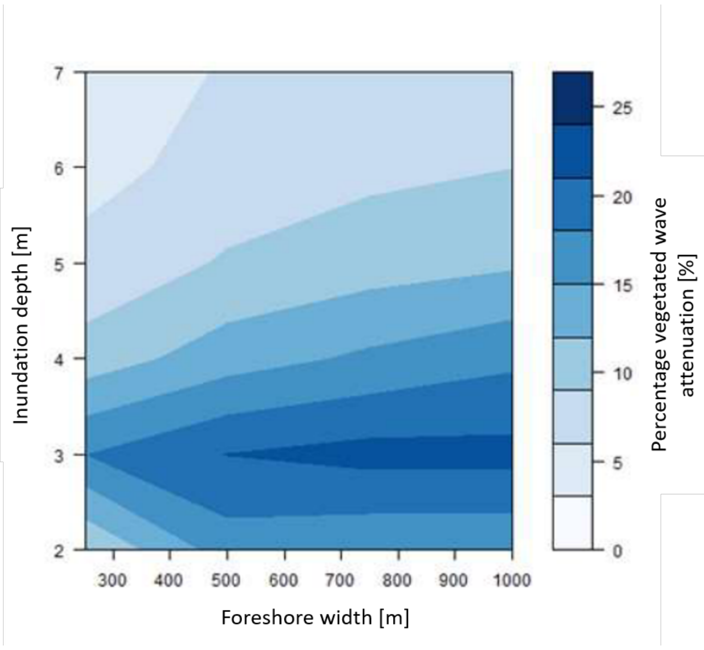

Figure 3.6: Percentage wave attenuation due to vegetation in relation to the inundation depth and foreshore width. This figure adopted from Steetzel et al. (2018) shows the result of a SWAN analysis done on Wadden Sea wetlands with long vegetation and a roughness height of $k_N = 0.09m$

Table 3.4: Summary of the vegetation characteristics

Vegetation category	Vegetation name	Source for attenuation by vegetation	u_c $[m/s]$	Factor compared to high marsh vegetation	Stem breaking factor
Short marsh vergetation	Puccinellia maritima Suaeda maritima	Möller et al. (2014) Rupprecht et al. (2017)	> 1.1	0.4	-
Middle marsh vegetation	Artemisia maritima Festuca rubra Agrostis stolonifera	Steetzel et al. (2018)	$0.9 - 1.4$	0.6	0.4
High marsh vegetation	Spartina anglica (pioneer veg.) Elymus athericus repens Aster tripolium	Vuik et al. (2018a) Steetzel et al. (2018)	$0.9 - 1.4$	1	0.4

foreshore width (B_{fs}), inundation depth (z_{fs}) and long vegetation. It purely shows the percentage of wave height attenuation by vegetation. From the figure, dissipation curves are generated for inundation depth of 2m to 6m with an interval of 1m for each foreshore width (see Appendix B.2.2 for more details). The percentages of attenuation for a specific foreshore width is interpolated over the inundation depths. In each time step of the storm surge the corresponding attenuation percentage with inundation depth and foreshore width is translated to a reduction factor on the raw wave height H_s. This gives a reduction factor compared with the raw input, which is calculated with Equation (3.8).

$$R_{fac}(t) = \frac{H_{s,raw}(t)}{H_{s,attenuated}(t)} \tag{3.8}$$

With, R_{fac} being the reduction factor, which changes over the time depending on the foreshore width and inundation height.

Vegetation length categories

An extra parameter is added to the tool describing different vegetation lengths. As already mentioned the reference Figure 3.6 simulates attenuation by long vegetation, however there are a lot of different vegetation heights and characteristics on the foreshore. Therefore Three categories of vegetation height are specified in Table 3.4. The vegetation species and their characteristics are derived from

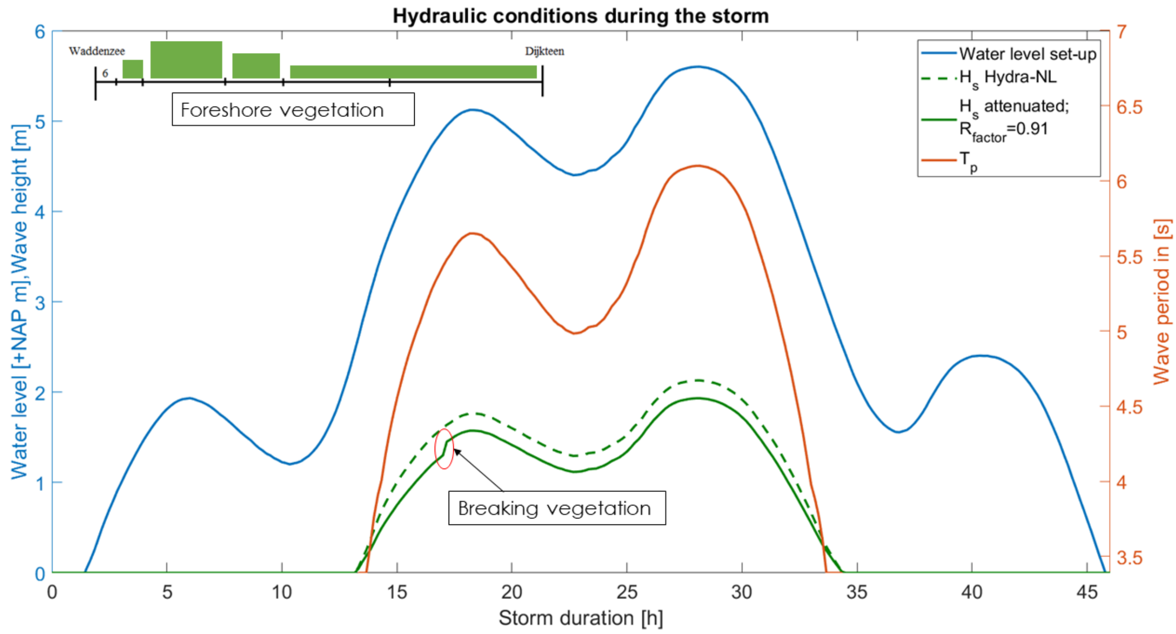

Figure 3.7: Hydraulic conditions during the storm surge which is input for the erosion model.

the sources that are specified. The short marsh vegetation is linked with short mowed grass (0.2m) (Möller et al., 2014; Rupprecht et al., 2017). The middle marsh vegetation is categorized between 0.2m and 0.5m (Steetzel et al., 2018). The long vegetation has a vegetation height of 0.5m and 0.8m (Vuik et al., 2018a; Rupprecht et al., 2017; Steetzel et al., 2018). Wave flume experiments showed that short mowed grass have a factor 0.4 lower wave attenuating capacity than long vegetation (Möller et al., 2014; Rupprecht et al., 2017). Therefore the Figure 3.6 on the preceding page is initially reduced with a factor 0.4. The middle marsh vegetation is based on another SWAN simulations which shows the Madsen roughness height of different vegetation at the foreshore dike location 32.2km (van der Reijden, 2019). Appendix B.2.2 explains the derivation of a 0.6 factor on the long vegetation attenuation.

Stem breaking

The fourth column in Table 3.4 on the previous page gives an indication of the critical orbital velocities for vegetation to break. This is an important factor in designing with vegetated foreshores, because the vegetation lose wave attenuating capacity ones they break. Section 2.4 describes there are different forms of breaking of vegetation (Rupprecht et al., 2017; Vuik et al., 2016). Additionally, several studies suggest not all vegetation will break in a storm leaving some attenuation capacity left. However, with a storm of ones in 200.000 years it is assumed all vegetation will break after the critical orbital velocity is exceeded. A study showed that almost no vegetation was left for a storm of ones in 4000 years with a critical orbital velocity of $u_c = 1.04 - 1.24[m/s]$ (Steetzel et al., 2018). An example of the eventual output of the hydraulic conditions is shown in Figure 3.7. Herein the moment of breaking of vegetation is shown where the orbital velocity exceeds the critical value. Furthermore the vegetation length settings are given in the left top corner.

Calibration attenuation by vegetation

The calibration case for the vegetation reduction factor is computed for dike location 32.2 km, which is used in the SWAN analysis by van der Reijden (2019). The specific results and vegetation characteristics of this study are given in Appendix B.2.2. The wetland settings consisted of a foreshore width of $1857m$ divided in short middle and high marsh vegetation and came down to a vegetation reduction factor of $R_{factor} = 0.91$. The exact same settings are duplicated for the design tool and shown in the top left corner of Figure 3.7. The height of the green blocks indicate the vegetation height concerning the three categories. The factors in Table 3.4 on the preceding page are adjusted to derive similar results.

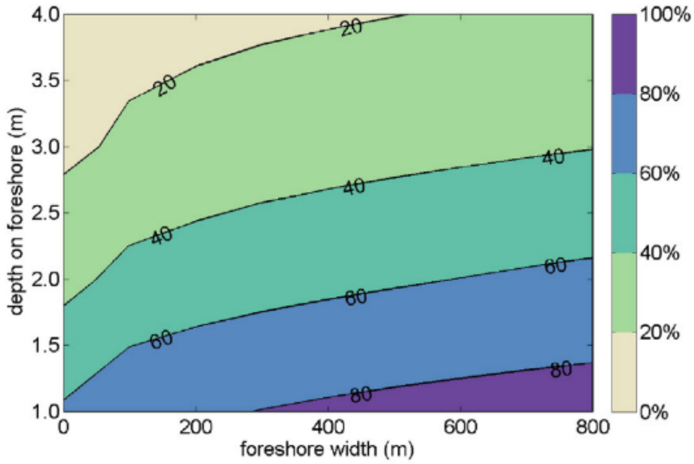

Figure 3.8: Percentage wave attenuation due to vegetation and depth induced wave breaking in relation to the inundation depth and foreshore width. This figure adopted from Vuik et al. (2016) shows the result of a SWAN analysis done on Zeeland wetlands.

Sensitivity analysis

A sensitivity analysis is performed on the critical orbital velocities and inundation depths. Because literature gives a wide range of critical orbital velocities the range is verified from $u_c = 1.04 : 1.34 m/s$ following Table 3.4 on page 23. Furthermore, the foreshore height can have uncertainties depending on the accretion rate compared to sea level rise, therefore foreshore heights of $z_{fs} = 0.5 : 1.5m$. The results are evaluated on the erosion depth, which will be explained in section Section 3.5.5 on the following page.

Foreshore construction

The last option in the design tool for wetland strategies is constructing a wetland, where no foreshore already exists. In this case depth induced wave breaking needs to be accounted for, because the Hydra-NL data has not incorporated these locations. The method for deriving the depth induced wave attenuation is similar to the vegetated attenuation in the first paragraphs of this section. Figure 3.8 is a similar SWAN analysis, but computed in Zeeland (Vuik et al., 2016). Different foreshore widths with varying water depth give a wave attenuating percentage. The figure shows higher attenuating percentages compared to the vegetation attenuation. This is because the wave height to depth ratio is limited and accounted for in this process. The percentages of foreshore construction are calibrated for the dike location 22.2km with a foreshore width of 700m. A difference is calculated between the raw data output with depth induced wave breaking integrated in Hydra-NL and the foreshore output of Hydra-NL with deep water conditions. The design tool reduction factor for foreshore construction is evaluated on this difference, whether it provides the same reduction as Hydra-NL.

3.5.3. Geometry input

The geometry input for the design tool imports the coordinates of the current dike, which is being evaluated. An asphalt revetment can be specified with the asphalt height, if there is one. Furthermore, the clay layer thickness and the new slope angle of the dike need to be specified. An extra feature in the design tool is reducing the crest height due to the gentle slope. This reduces the construction and maintenance cost of the dike. A gentle slope reduces the hydraulic loading on the structure (HBN) conform WBI-2017. From Hydra-NL the new HBN is calculated. This new HBN height is the height at which the gentle slope insects with the current dike. The remaining part of the current dike stays untouched.

3.5.4. Costs input

The last input component are the costs for construction and maintenance of alternative designs. The costs are summarized in Table 3.5 on the following page provided with a description. Al the costs are related to the construction of 1m dike. These costs are based on insight knowledge of Royal

Table 3.5: Unit costs of dike reinforcement

	Costs [€]	unit	description
Construction Costs			
Soil excevation	9.10	m^3	
WBA removal	9.50	m^2	0.20m top layer
Construction sand layer	12.55	m^3	50% reusable sand
Construction clay layer	14.05	m^3	50% reusable clay
Construction grass revetment	2.40	m^2	30cm top layer
Construction of WBA	46.00	m^2	0.20m top layer
Construction of Brushwood dams	85.00[1]	m	foreshore width $B_{fs} = 300m$
LCC			
Dike+sand maintenance	41.64	$100y/m$	2 per 100 year with 18m grassrevetment
Grass revetment mainenance	79.21	$100y/m$	mowing 2 per year with 18m grass revetment
WBA maintenance	91.07	$100y/m$	restoration of cracks, damage, replacement with 20 m^2/m
Brushwood dams maintenance	23.60[1]	$100y/m$	foreshore width $B_{fs} = 300m$

Table 3.6: Parameter settings for the erosion model

Variable	Symbol	Unit	Parameter
Parameter grass strength	c_a	[m]	1.83
Parameter grass strength	c_b	[1/h]	-0.05
Parameter grass strength	c_c	[m]	0.5
Fraction of sand in clay	f_{sand}	[-]	0.35
Thickness clay layer with roots	d_{tot}	[m]	0.5
Erosion coefficient	c_e	[-]	0.55

HaskoningDHV. Except from the brushwood dams which are derived by Vuik et al. (2019). The soil excavation costs are determined by using polygon intersection tools in MATLAB, subtracting regions that need to be excavated from the current dike. The Life Cycle Costs (LCC) are for a design period of 100 years which is the period for the Koehool Lauwersmeer dike. In the description the costs are described for a certain length of revetment, therefore these values are recalculated to the specific revetment length of the dike.

3.5.5. Erosion model

The erosion model is divided in two components, where firstly the erosion resistance of the top and sub layer is determined. The second part takes the residual strength of the bare clay layer into account, which results in the eventual erosion depth. Each component is explained separately. Before erosion is being calculated the slope of the dike is divided in sections of $\Delta z = 0.25m$ from the toe to the crest of the dike. In each section the wave load duration is determined (t_{load}) for each time step.

Top and sub layer

The resistance duration of the top and sub layer is adjusted for the slope angle confirm the study of Peters (2020). The equations uses the reference WBI slope of 1/3 divided by the real slope angle. The impact zone considered for calculating the resistance duration is shown in Equations 3.9 and 3.10.

$$t_{s,top} = \frac{tan(1/3)}{tan(\alpha)} \cdot t_{top} \tag{3.9}$$

$$t_{s,sub} = \frac{tan(1/3)}{tan(\alpha)} \cdot t_{sub} \tag{3.10}$$

[1]Construction and maintenance costs for brushwood dams are derived from Vuik et al. (2019), where costs are based on two zones with sedimentation fields of 300m wide (perpendicular to the dike) and 200m long (parallel to the dike). For constructing this system, a 5 km brushwood dam is needed per 1 km dike.

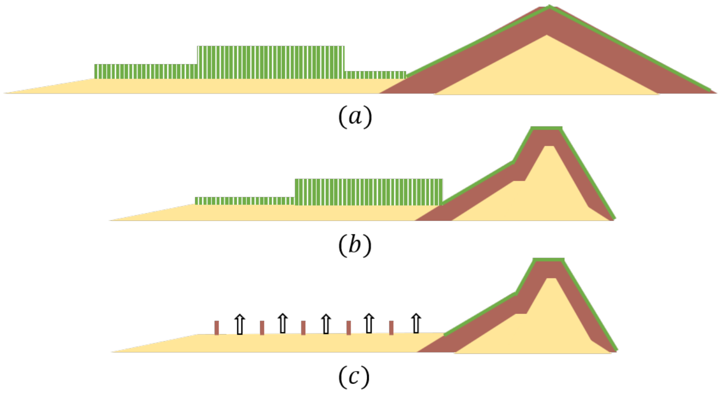

Figure 3.9: Dike location scenarios

The parameter settings are summerised in Table 3.6 on the preceding page, where the grass strength parameters calibrated by the study of Peters (2020) is used. The model calculates for each time step the resistance duration for the wave height occurring on that moment. With this the failure fraction for each time step is calculated (see Equation (2.6) on page 12). Whenever the failure fraction of a section is greater than 1 the bare clay layer erosion model starts calculating the erosion at that specific section.

Bare clay layer

The clay layer erosion is calculated with the erosion model of Mourik (2015). This is under the assumption the numerical analysis shows a good agreement for the linear relation with the slope angle. The model is extended towards an erosion process with a variable water level conform Breteler (2015). The model starts with an initial erosion corresponding to an erosion depth of $d_e = 0.5m$ (depth of top and sub layer), which has an erosion volume of $V_e = 1.7m^3/m$ (Mourik, 2015). In every time step the impact zone is determined, which is different from the impact zone for the top layers. Thereafter the already present erosion in the wave impact zone is determined. This is necessary to calculate the additional erosion, with the erosion formula of Mourik (2015) (see Appendix B.2). By calculating the average erosion depth per section the failure of clay layer can be checked. This method shows more realistic results compared to a method with a constant water level Breteler (2015). A detailed description on the calculation of the erosion of bare clay with a variable water level is given in Appendix B.2.

3.6. Case study

Lastly, the case study of Koehool Lauwersmeer is evaluated on different design alternatives. The three dike locations specified in section 1.5 are analysed on the possibility of constructing a grass cover dike. Three different scenarios are examined shown in Figure 3.9. The first scenario is assessed with the design tool on the current grass cover dike at location 32.2km. The dike is evaluated on the erosion depth with the current wetland settings compared to the WBI assessment (see Figure 3.9 (a)). The second and third scenario consider different alternatives compared to the current traditional dike, which is elaborated on in the next paragraphs.

Return period

This section gives a technical outline of the three dike locations specified in Figure 1.3 on page 5. A cross section of the specific dike location is given in Figure 3.10 on the following page. The design year of the dike locations is a period of 100 years including climate change scenario W+ (Schaap, 2015). Climate scenario W+ is the most extreme scenario corresponds to a sea level rise of 60cm for a design period of 100 years (Schaap, 2015). The hydraulic conditions depend on the return period of the dike locations. The trajectory norm is a 1/3000 year storm. For a grass cover dike the failure probability of GEBU is calculated with Equation (3.11).

$$P_{norm,dsn} = \frac{P\omega}{N} \tag{3.11}$$

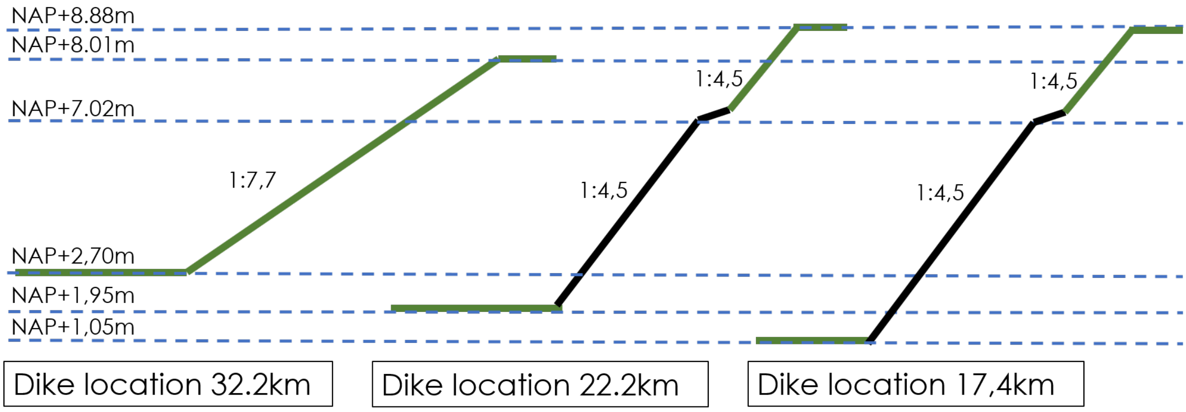

Figure 3.10: Current cross-section waterside slope of the dike locations

With, N (3) being the length-factor and P the probability of failure of the trajectory norm (1/3000y). ω is the failure margin factor which is 0.05 for GEBU (Ministerie van Infrastructuur en Milieu, 2016). This results in a return period of 1/18000 years, however following the norm the probability of this is 90% for grass and clay which results in a return period of 1/200000 years.

Traditional dike vs grass cover dike solution

Dike location 22.2km is a traditional dike with a wetland of 700m in front of it. At this point in time the asphalt revetment needs to be replaced, which makes it a perfect case to consider different design alternatives. Because the dike already has a foreshore, the possibility of constructing a grass cover dike is even more plausible. The geometric settings are varied in such a way to find the most optimal design alternatives. A grass cover dike with a slope of 1/8 is examined combined with different clay layer thickness (see Figure 3.9 on the preceding page (b)).

Traditional dike vs grass cover dike + wetland solution

The dike location 17.4km is considered because it does not have any foreshore yet. Therefore, the depth induced wave breaking model is used to simulate the construction of a foreshore assuming brushwood dams as presented in Figure 3.9 on the previous page (b). Brushwood dams are a 'Building with Nature' solution which have a positive influence on the ecosystem (Vuik et al., 2019). With an accretion rate of 2cm/year at the Wadden Sea the foreshore can grow almost with 2m for a design period of 100 years (Vuik et al., 2019). Therefore, this case examines a variable foreshore height next to the geometric and foreshore settings. An important factor is the foreshore height z_{fs}, because the accretion on the foreshore is highly uncertain by depending on the sediment supply (Vuik et al., 2018a).

4

Results

4.1. Mesh sensitivity analysis

The different grid refinement methods are analysed on the computation time as described in the previous chapter. The hydraulic conditions are summarised in Table 4.1 with the corresponding computation time. Herein the coarse grid shows a computation time one third shorter than the fine grid. Similarly the snappy hex mesh shows a faster computation time compared to the fine grid. This in contrast to the multi grading grid, which is significantly longer than the fore mentioned grids, but is still five hours shorter than the fine grid. These differences in computation time will make a significant difference when simulating with higher number of waves.

Another criteria on the grid refinement performance is the reflection coefficient. Table 4.1 shows a small variance in the hydraulic conditions, however the reflection coefficient shows some discrepancies. As a reference Equation 3.4 is plotted with the reflection data in Figure 4.1b on the following page. In general the simulation data is in good agreement with Equation 3.4, which has a coefficient of variation of $\sigma' = 10\%$ (Allsop, 1999). The fine grid shows the best fit followed by the multi grading grid.

An indication on the performance of the different grids on the pressure is shown in Figure 4.1b on the next page. Herein the significant pressure is formulated in a dimensionless parameter by division of the wave height. The boxplots presents the distribution of the highest 33% of the waves on the probe location where the highest pressures occurs. Next to that the important design parameters $P_{2\%}$, $P_{10\%}$ and P_s are given. Apparently the coarse grids is less capable of simulating higher peak pressures compared to the other grids. The other three grids seem to have comparable distributions, however the multi-grading grid simulates slightly higher peak pressures.

Concluding the snappy hex mesh grid shows the best agreement with the pressure data compared to the fine grid. Next to that the reflection coefficient is within the boundaries of Equation 3.4 based on physical experiments. Finally it has a significant shorter computation time, therefore the snappy hex mesh grid is used for the following numerical simulations.

Table 4.1: Sensitivity analysis results

Grid	$Hs_{toe}[m]$	$T_{p,toe}[s]$	$s_{op,toe}[-]$	K_r	N waves $[-]$	Computation time $[h]$
Fine	2.040	5.676	0.041	0.229	22	32.47
Coarse	2.037	5.676	0.041	0.204	22	21.59
Multi grading	2.022	5.679	0.040	0.223	22	27.02
Snappy hex mesh	2.040	5.676	0.041	0.255	22	23.58

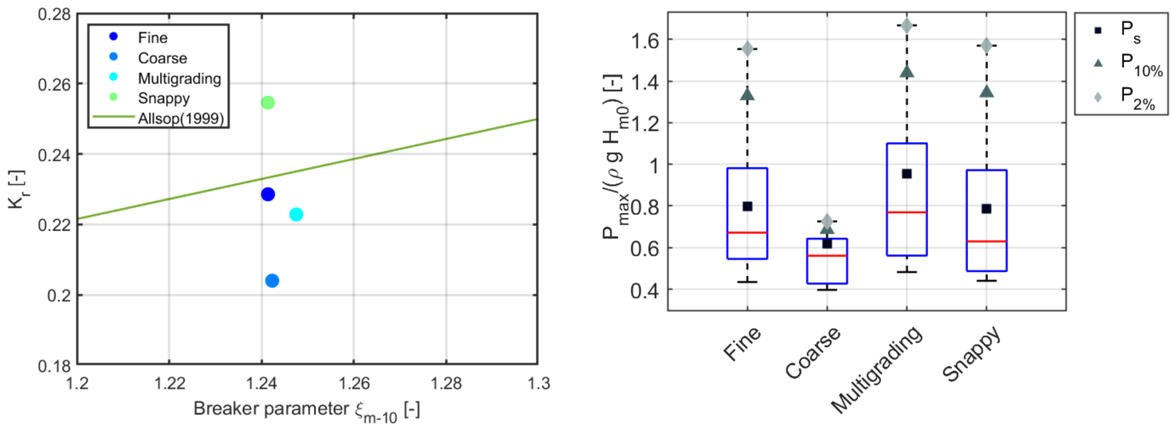

(a) Reflection coefficient

(b) significant pressure head distribution

Figure 4.1: Results sensitivity analysis: (a) Reflection coefficients of the different grids compared to Equation (3.4) on page 19, (b) This figure shows the distribution of the highest 33% of the waves for different grid resolutions

4.2. Relation between geometry and pressure

This section describes the simulations for the different geometry profiles. Every profile is evaluated on the pressure distribution over the slope and the resulting relations. First the results of the flat profiles are discussed. Secondly the results of the erosion profiles are presented. A summary of the simulated hydraulic conditions are presented in Table 4.2. The reflection coefficient consists of a wave spectrum analysis, therefore the wave spectra are only presented in the Appendix A.2.

4.2.1. Flat profile simulations

Figure 4.2 on the facing page presents the maximum peak pressure distribution over the vertical profile ($y[m]$). The figure is subdivided into the three design parameters $P_{2\%}$, $P_{10\%}$ and P_s for the three different flat profiles. The $P_{2\%}$ distribution clearly shows a high peak for the 1/4 profile half a meter under the water level ($y = 6.5m$). This is in contrast to the 1/6 and 1/8 slope, which show almost a evenly distributed $P_{2\%}$ over the slopes. However the 1/6 slope still performs higher $P_{2\%}$ pressures compared to the 1/8 slope. The high peak in the $P_{2\%}$ subplot is shifted upward and flattened out when increasing the number of waves ($P_{10\%}$ and P_s subplots). However the peak in the 1/4 slope remains below the water level, where the 1/6 and 1/8 show a peak shift towards the water level.

Table 4.2: summary of the hydraulic conditions and pressure results

simulation	experiment	$H_{s,toe}[m]$	$Tp_{toe}[s]$	$sop[-]$	$tan[-]$	$K_r[m]$	$\phi_{2\%}$ [m]	$\phi_{10\%}$ [m]	ϕ_s [m]
CoastalFOAM Flat profile									
1	F10_slope4	1.98	5.9	0.037	0.250	0.223	6.94	3.68	2.28
2	F11_slope6	2.01	5.9	0.037	0.167	0.207	4.23	2.66	1.70
3	F12_slope8	2.01	5.9	0.037	0.125	1.960	2.82	2.14	1.50
CoastalFOAM Erosion profile									
7	E10_slope3	1.23	5.2	0.029	0.333	0.475	5.98	3.91	2.24
8	E11_slope4	1.23	5.2	0.029	0.250	0.314	4.04	2.75	1.75
9	E12_slope5	1.22	5.2	0.029	0.200	0.268	3.51	2.18	1.37
10	E13_slope6	1.23	5.1	0.030	0.167	0.251	2.22	1.23	0.97
11	E14_slope8	1.20	5.2	0.029	0.125	0.206	1.75	0.77	0.59

Validation numerical model

From the peak pressure distribution in Figure 4.2 on the next page the maximum values are derived and presented in Figure 4.3 on the facing page. As a validation case for the numerical model the pressure

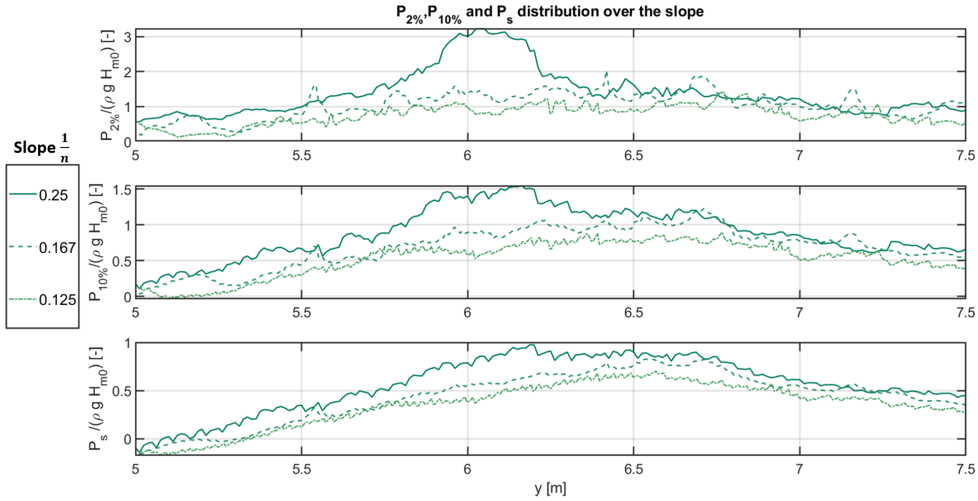

Figure 4.2: Maximum pressure distribution $P_{2\%}$(top), $P_{10\%}$(middle) and P_s(bottom) over the slope elevation

data is compared with experiment data adopted from Peters (2017). The figure shows the $P_{2\%}$ and $P_{10\%}$ data for different breaker parameters as discussed in section 2.3. Equation (2.3) on page 9 is denoted as Eq5.42 in the figure, because of convenience with the already presented figure on this matter (Figure 2.2 on page 9). The domain of the $P_{2\%}$ and $P_{10\%}$ pressures are visualized to indicate whether the simulated data lies within this domain. The simulation with the highest breaker parameter corresponds to the 1/4 slope and breaker parameters in further descending order correspond to the 1/6 and 1/8 slope. The $P_{2\%}$ simulated pressures of the 1/4 slope lies within the $P_{2\%}$ domain, which indicates that it is agreement with other experimental data. However for the same slope the $P_{10\%}$ pressure is being underestimated by the simulation data, because it lies outside the $P_{10\%}$ domain.

The $P_{2\%}$ data point of Führböter and Sparboom (1988) is highlighted, because this is the only data point for a 1/6 slope. The experiment data is located on the boundary of the line Eq5.42 (Equation 2.3) describing the maximum wave impact peak pressure. This experiment has a higher breaker parameter in comparison to the $P_{2\%}$ CoastalFOAM data for the same slope, because a longer wave length is used. Therefore, the breaker type is still in the spectrum of plunging waves explaining also higher peak pressures.

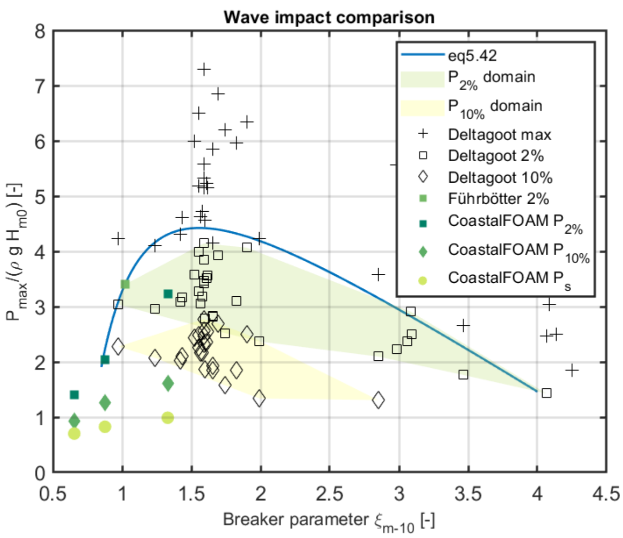

Figure 4.3: Wave impact experiment data adopted from Peters (2017) together with the the simulation data

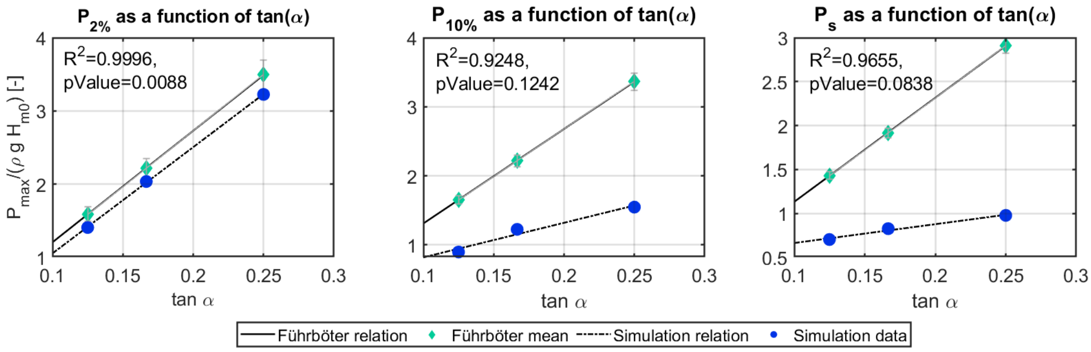

Figure 4.4: Linear relation between the geometry and design parameters, where the most left describes the relation for $P_{2\%}$, the middle $P_{10\%}$ and the right graph depicts the P_s data.

Nonetheless it is interesting to see the 1/6 $P_{2\%}$ CoastalFOAM data is also positioned on the boundary of line Eq5.42 (Equation 2.3) for a lower breaker parameter. This suggest an agreement with the experimental data for the $P_{2\%}$ pressures of the 1/6 slope. The breaker parameter of the 1/8 slope is of the scope of the experimental data done on hard revetments. The wave impact peak pressures are lower compared to the surging waves ($\xi > 2.5$), which is logical because energy is already lost by breaking of the waves, where surging waves do not break and conserve more energy resulting in a higher pressure.

Relation

A linear relation between the geometry and design parameters $P_{2\%}$, $P_{10\%}$ and P_s is drawn in Figure 4.4. The relation is compared with the relation of Führböter and Sparboom (1988) Equation (2.2) on page 9 as described in section 3.4. The error-bars around the F√ºhrb√∂ter data indicate the standard deviation of 10000 iterations calculating the maximum pressures. Furthermore the R^2 coefficient of determination is given, showing the goodness of fit of the linear relation. Also the $pValue$ is given which indicates if the data is significant if $pValue < 0.05$ (Dahiru, 2011).

The left plot with the $P_{2\%}$ as a function of $\tan(\alpha)$ shows a good linear fit according to the R^2 and $pValue$ statistics. Furthermore, it approximates the relation of Führböter and Sparboom (1988), however the data still lies out of the error-bars. The middle plot with the $P_{10\%}$ relation shows a less good linear fit with a lower R^2 value and $pValue > 0.05$. Also, the data deviates a lot compared to the Führböter and Sparboom (1988) relation. The last right plot shows even larger deviation with the Führböter and Sparboom (1988) relation, nonetheless it gives a good linear fit according to the statistical parameters. For each design parameter a linear trend is formulated in Equations 4.1, 4.2 and 4.3.

$$\frac{P_{2\%,max}}{\rho_w g Hm0} = 14.28 \tan(\alpha) - 0.36 \tag{4.1}$$

$$\frac{P_{10\%,max}}{\rho_w g Hm0} = 5.18 \tan(\alpha) + 0.33 \tag{4.2}$$

$$\frac{P_{s,max}}{\rho_w g Hm0} = 2.24 \tan(\alpha) + 0.44 \tag{4.3}$$

The above-mentioned preliminary results give a good impression of the influence of the slope angle. Where the $P_{2\%}$ results show the most reliable results compared with experimental data.

4.2.2. Erosion profile simulations

Figure 4.5 presents the maximum peak pressure distribution in the x direction for $P_{2\%}$(top), $P_{10\%}$(middle) and P_s(bottom). All the simulations show a clear peak in the pressure data that occurs directly after the start of the cliff of the erosion profile. A decreasing trend in the peak can be observed with the slope angle. An phenomena that is only observed with the $P_{2\%}$(top) plot, is that it shows some small bumps in the pressure data in front of the cliff. These bumps indicate some waves breaking on the erosion terrace before reaching the erosion cliff.

Relation

The maximum values of the peak pressure distribution of P_s are derived and presented in Figure 4.6 on the following page. As a reference the data of Mourik (2015) for the significant pressure head on the erosion profiles are given. Note the pressure head is presented none dimensionless in contrary to Figure 4.5, because the data of Mourik (2015) is only given in this way. The peak pressures for a 1/3 and 1/4 slope are relatively overestimated with the simulation data compared to the data of Mourik (2015). Where the 1/5 slope surprisingly matches the data of Mourik. On the contrary the simulation data of the less steep slopes are underestimated.

It is not necessarily important that the data matches precisely with the data of Mourik (2015), but it should describe a linear trend corresponding to the trend by Mourik (2015). The simulation data shows a linear trend for the significant pressure head as a function of $tan(\alpha)$ conform the statistic parameters R^2 and $pValue$. The influence of the slope angle of the original profile on the pressure head is given in Equation 4.4.

$$\phi_{s,max} = 7.91\tan(\alpha) - 0.32 \tag{4.4}$$

The other pressure data on $P_{2\%}$ and $P_{10\%}$ are left out of the analysis, because the scope of this study is to extend the data of Mourik (2015), which only uses the P_s data.

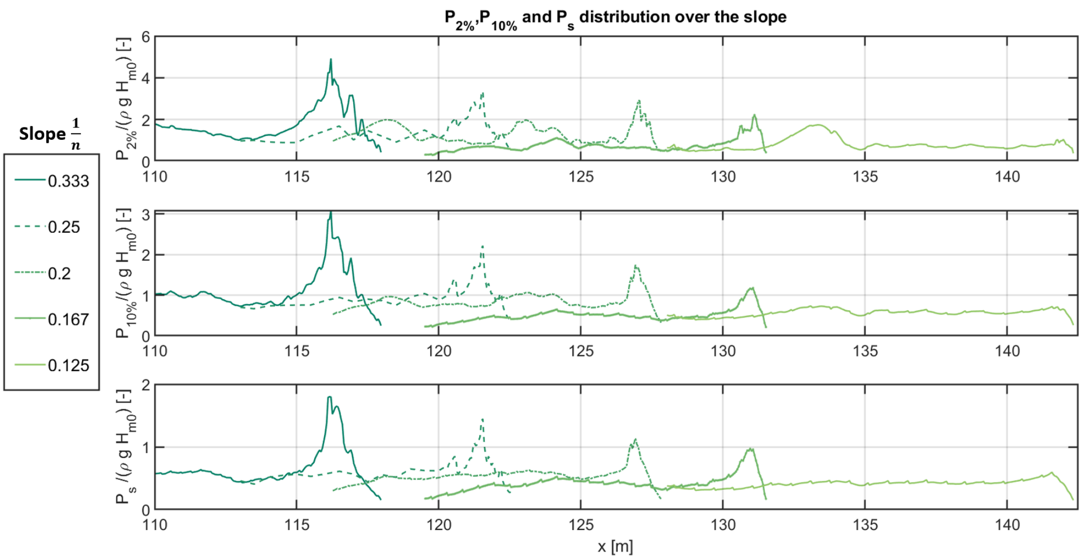

Figure 4.5: Maximum pressure distribution $P_{2\%}$(top), $P_{10\%}$(middle) and P_s(bottom) over the erosion profile in the x direction.

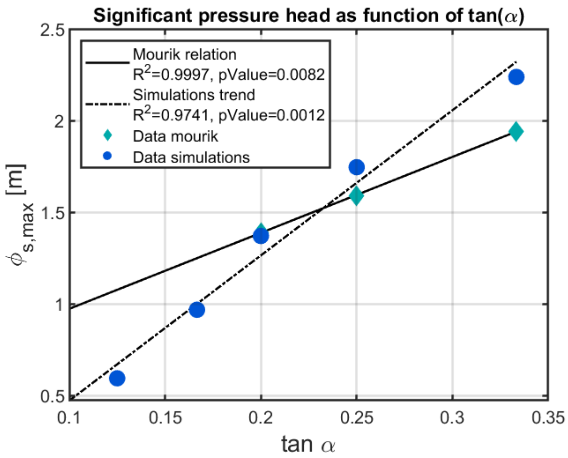

Figure 4.6: Linear relation between the original slope angle and design parameters, where the most left describes the relation for $P_{2\%}$, the middle $P_{10\%}$ and the right graph depicts the P_s data.

Table 4.3: Summary of the design conditions

Location [km]	Return period [/y]	Design water level [NAP+m]	H_s [m]	T_p [s]	R_{factor}	$H_{s,veg}$
32.2	1/200000	5.71	2.16	5.41	0.9	1.94
22.2	1/200000	5.64	2.14	5.35	0.94	2.01
17.4	1/200000	5.61	2.51	5.53	1	2.51

4.3. Design tool

In this section the results of the different components of the design tool are presented. The three dike locations of Koehool-Lauwersmeer are considered as input for the tool. Dike location 32.2km is used as a validation case for the performance of the wetland attenuation. Furthermore, the costs and the performance of the erosion model are given. At last different design alternatives are presented for the dike locations 22.2km and 17.4km.

4.3.1. Hydraulic input conditions

Three dike cases considered as input are presented in Figure 4.7 on the next page. Next to that a summary of the design conditions are given in Table 4.3. The first figure (4.7a) shows the conditions of location 32.2km, with a peak water level at $\zeta = NAP + 5.71m$. It can be seen that H_s and T_p both peak for the water level of $\zeta = NAP + 5.0m$ and stay constant, while the water level increases. On first sight this might seem wrong, however Hydra-NL considers probability of the different phenomena for maximum water level set-up and maximum wave height not to be in sync. This means that the wave height reaches a maximum even when the water level increases. Because T_p and H_s are correlated T_p also has a peak for a water level of $\zeta = NAP + 5.0m$. Furthermore, can be observed stems break at a water level of $\zeta = NAP + 4.5m$, which has a inundation depth of $h = 3.0m$. This is indicated by the jump in the attenuated wave height at 15h of storm. A reduction factor by the vegetated wave attenuation is $R_fac = 0.9$, which will be further discussed in the next section.

The second dike location 22.2km is shown in Figure 4.7b. Similar to the first case the H_s and T_p show a maximum after a water level of $\zeta = NAP + 4.6m$. Because this location has a lower foreshore of $z_{fs} = NAP + 1.0m$ waves already occur at lower water levels. Since the foreshore width is significantly smaller than the first case, the wave attenuation factor is also lower $R_{fac} = 0.94$. This also explains why the jump in the stem breaking is less noticeable. The third location has no foreshore, which makes that the reduction factor $R_{fac} = 1$. Next to that the maximum Hydra-NL wave height is significantly higher than the other cases $H_s = 5.51m$. This is also the reason of the wave height and period peaking with the water level.

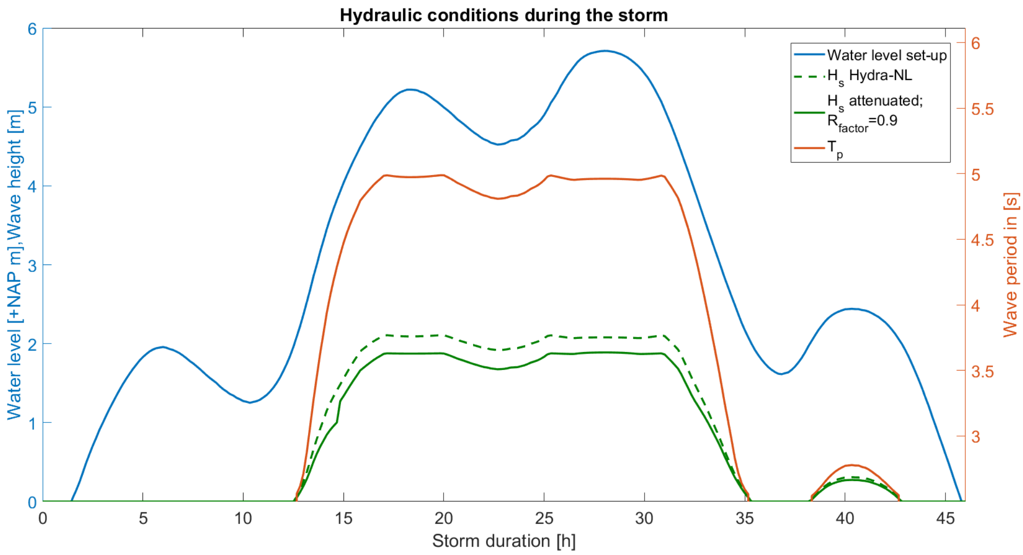

(a) Dike location 32.2km

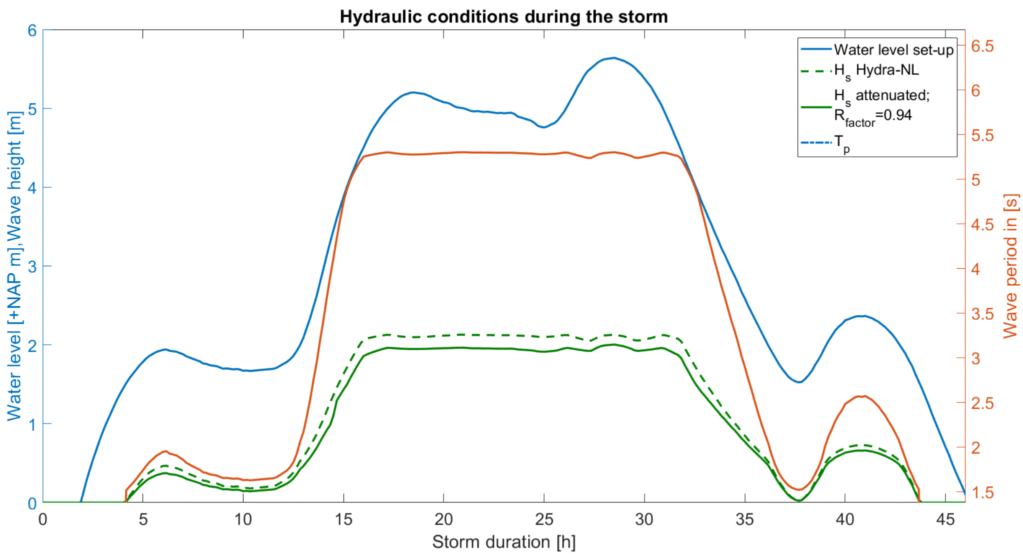

(b) Dike location 22.2km

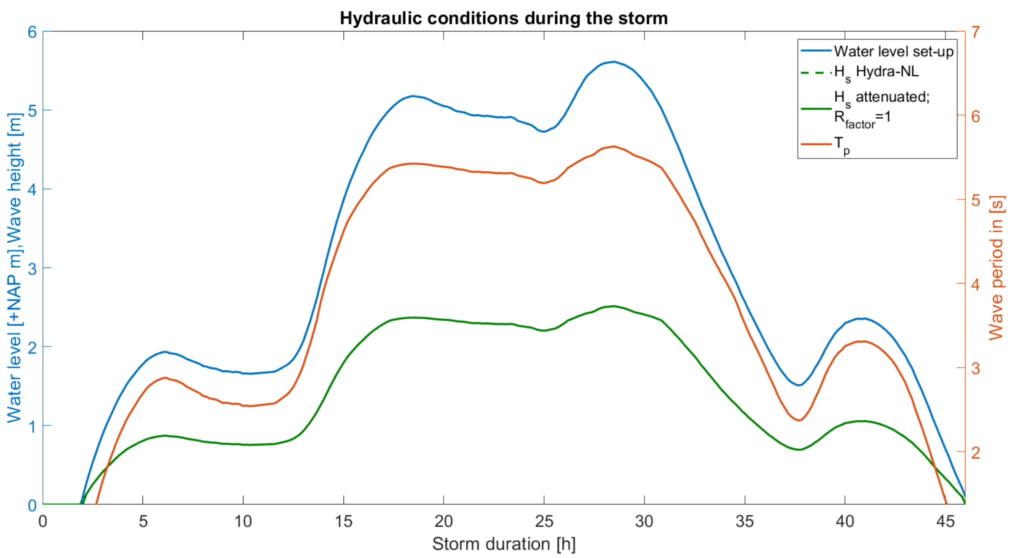

(c) Dike location 17.4km

Figure 4.7: Interpolated Hydra-NL hydraulic conditions for the different dike locations: (a) loc. 32.2km has a foreshore of 1850m foreshore, (b) loc. 22.2km has a foreshore of 700m and (c) loc. 17.4km has no foreshore.

4.3.2. Wetland model performance

Chapter 3.5.2 provides a detailed description for determining the wetland attenuation of vegetation for different inundation depths. The result is given in Figure 4.8, where the left plot describes the attenuation for a high vegetation roughness derived from Steetzel et al. (2018). This roughness corresponds to long vegetation with a roughness height of $k_N = 0.09m$ following the Madsen approach for bottom roughness(Madsen and Sorensen, 1992). The results show a decrease in wave height from $5 - 15\%$ with a water level of $NAP + 5m$, $10 - 17.5\%$ with $NAP + 4m$ and $15 - 22.5\%$ with $NAP + 3m$ compared to a low bottom roughness ($k_N = 0.001m$). The middle marsh and short marsh vegetation are based on the left plot and are a factor 0.6 and 0.4 respectively smaller (see Table 3.4 on page 23). The vegetated wave attenuation is calibrated with the study of van der Reijden (2019) as described in section 3.5.2. By changing the factor of short vegetation and broken vegetation to 0.3 give the best results for the same foreshore settings as is shown in Table 4.3 and Figure 4.7a.

Next to the vegetated wave attenuation the depth induced wave breaking is determined (Figure 4.9). As described in section 3.5.2 the depth induced wave breaking is based on the simulation setting of Vuik et al. (2016). After calibration with the foreshore hydraulic conditions of location 22.2km the percentages were reduced by a factor 2 (see Appendix B.2.2). The Figure shows that low inundation has significantly more influence on the wave attenuation compared to higher inundations. This is in line with the concept of depth induced wave breaking, where the H_s/h ratio is limited by the inundation depth.

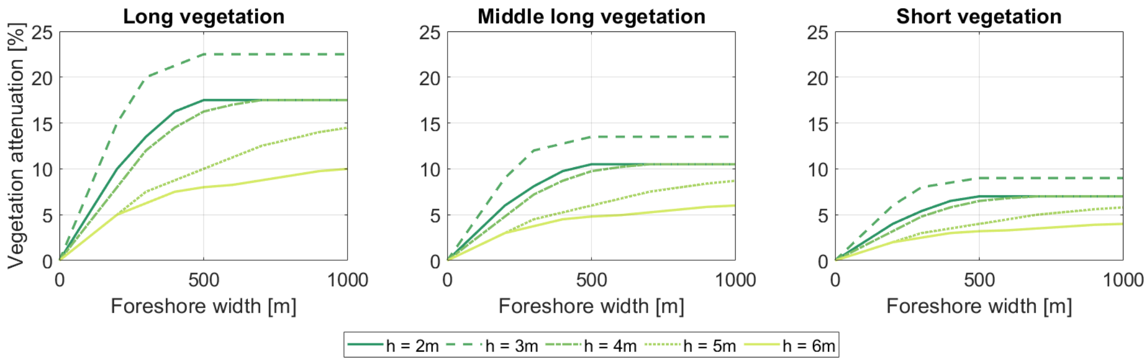

Figure 4.8: Percentage wave attenuation per foreshore width and inundation depth (adopted from Steetzel et al. (2018).

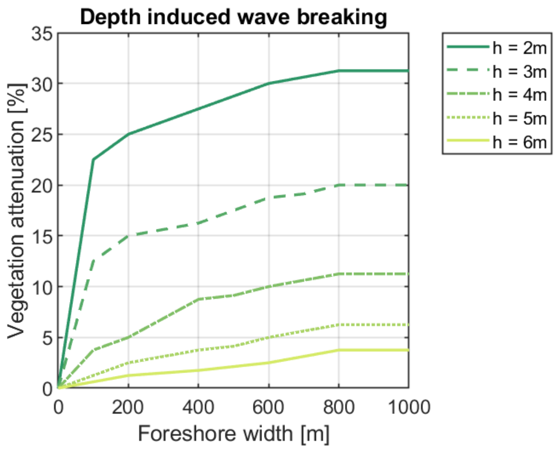

Figure 4.9: Depth induced wave breaking adjusted from Vuik et al. (2016)

Wetland sensitivity

A sensitivity analysis on the stem breaking by the critical orbital velocity is presented in Figure 4.10, herein the critical orbital velocity is varied between $u_c = 1.04 - 1.34m/s$. Furthermore the foreshore elevation is varied, where the left plot presents a foreshore elevation of $z_{fs} = NAP + 0.5m$, the middle $z_{fs} = NAP + 1.0m$ and the right plot $z_{fs} = NAP + 1.5m$. Each scenario is simulated with a 900m of wetland with a varying vegetation height described in the legend. The left plot shows a significant decrease of erosion depth for increasing orbital velocities, remarkably even no erosion occurs for a wetland with only long vegetation (explained in section 5.1.2). Furthermore, it is noticed that for lower inundation depths (middle and right plot) the overall erosion depth decreases. An interesting trend is the shift of the critical orbital velocity having influence on the erosion depth with decreasing inundation depths. Where higher inundation depths can have lower critical orbital velocities, leading to less erosion (left plot) compared to higher inundation depths (right plot).

The long vegetation has the most influence on the wave attenuation, when the stems don't break (each third bar). However, the order of high and low vegetation also makes a difference in the wave attenuation, because some low vegetation can already attenuate waves in order for longer vegetation not to break as is shown in the last bars. As an example, the scenario of short vegetation (600m) followed by long vegetation (300m) leads to no erosion compared to a scenario with only short vegetation (left plot, $u_c = 1.34m/s$).

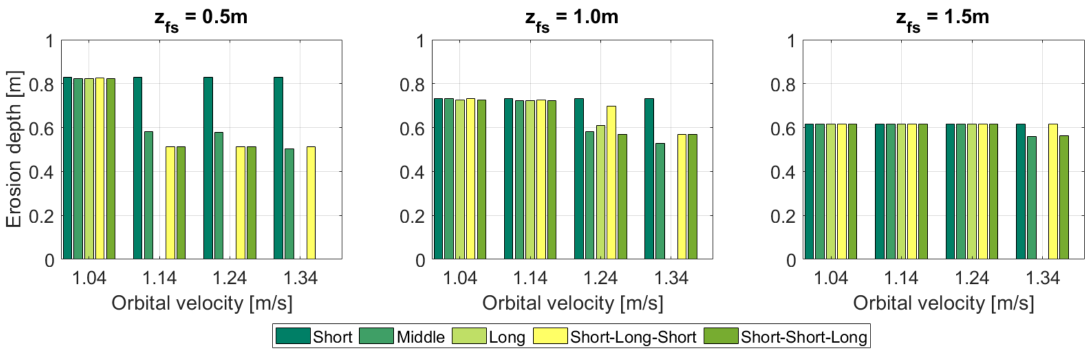

Figure 4.10: Sensitivity of vegetation attenuation with u_c and $z_{f}s$ and a foreshore width of 900m.

4.3.3. Erosion model

This section shows the difference between the GEBU assessment by the current WBI and the extended version the WBI model. Figure 4.11 on the next page shows the results of three simulations with the hydraulic conditions of location 32.2km (Figure 4.7a). Herein the current green dike profile is simulated with the current assessment, extended assessment and the extended assessment with the current vegetated wetland. The clay layer thickness is $d_c = 1.5m$ with a grass revetment on top. The current WBI assessment (slope 1/3) shows it fails after 30.8 hours with an erosion depth of $d_e = 1.55m$ (blue line). This is just after the peak of the storm (see Figure 4.7a on page 35).

The extended WBI assessment shows the dike will not fail when we account for a slope angle of approximately 1/8. The extended assessment shows an erosion depth of $d_e = 1.31m$, which gives a residual clay thickness of almost 20cm (red line). If we also account for the wave attenuation by vegetation the erosion depth reduces to $d_e = 0.71m$ (green line). With a foreshore width of $B_{fs} = 1770m$ using the vegetation settings described in section 3.5.2.

4.4. Alternative designs

The final results of the design tool are given in this section. First different design alternatives are given for dike location at 22.2km, with an asphalt revetment up to NAP+7.09m and a foreshore of $B_{fs} = 700m$. Secondly a similar dike is assessed on different alternatives for location 17.4km. However, in this case no initial foreshore is present.

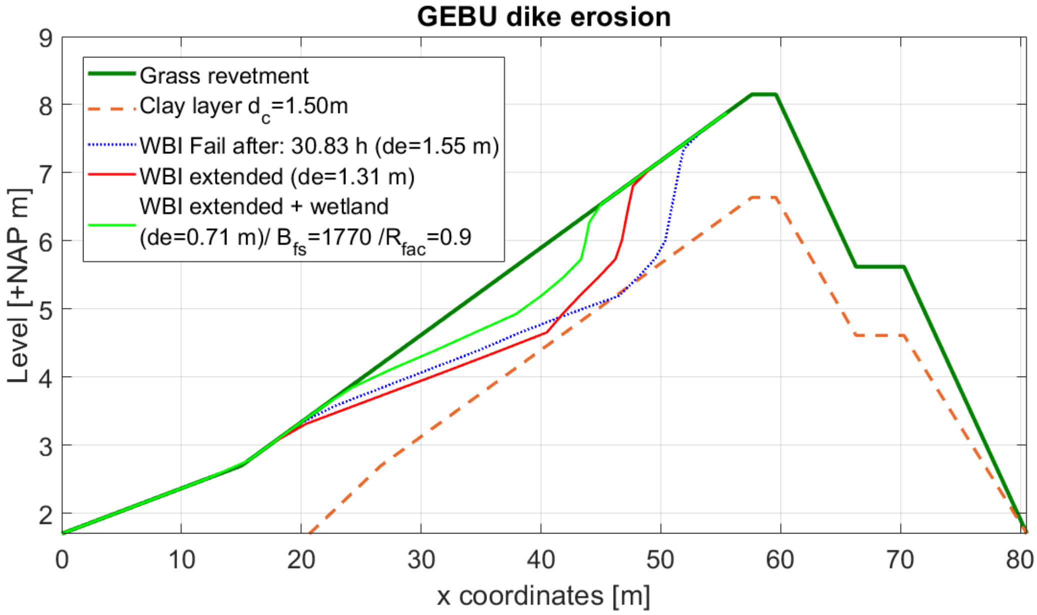

Figure 4.11: Extention of the WBI model, dike location 32.2km

4.4.1. Traditional dike vs green dike (Loc. 22.2km)

Four grass cover dike alternatives are considered in comparison with the current traditional asphalt dike. All the alternatives have a slope of 1/8 and the same geometric wetland setting. The first alternative has no crest reduction in order to compare the effect of crest reduction on the total costs. The other alternatives only vary in clay layer thickness. An overview of the design settings is presented in Table 4.4. An example is given for the fourth alternative shown in Figure 4.12 on the facing page. The traditional dike is presented with the asphalt revetment in black, the top part of the slope is grass revetment (light green) and the dark dotted line as the clay layer. No GEBU dike erosion occurs for the traditional dike, because the asphalt layer is located far above the design water level. The new alternative (dark green line) has an 1/8 slope, which results in an erosion depth of $d_e = 0.92m$. This alternative appears to be a possible solution replacing the traditional dike. The following step for the design tool is to calculate the construction and maintenance costs. The final output is presented in Figure 4.13 on page 40.

The output presents the different costs for construction and maintenance of the dike (see section 3.5.4 for calculations). The current dike appears to be most expensive over a period of 100 years per meter dike. This is because the current asphalt revetment has reached its end of life and needs to be replaced before the maintenance cost for the coming hundred years can be calculated. Overall, the alternatives show promising results considering their costs and erosion depths. Alternative 1 with no crest reduction and a clay layer of $d_c = 1.5m$ has the highest costs, because more soil has to be excavated plus the construction cost of clay are higher. Alternative 2 and 3 are more conservative compared to alternative 4, which has a marginal residual clay thickness left $0.08m$.

Table 4.4: Different design alternatives for dike location 22.2km

Alternative	slope angle $[-]$	Foreshore width $[-]$	R_{fac} $[-]$	HBN_{reduc} $[m]$	Clay thickness $[m]$	Erosion depth $[m]$	Construction Cost [€/m]	Maintenance Cost [€/m]
'Current dike'	0.245	0	1	-	1.5	0	1474	820
'Alternative 1'	0.125	700	0.94	0	1.5	0.917	1526	375
'Alternative 2'	0.125	700	0.94	2.27	1.5	0.917	1483	348
'Alternative 3'	0.125	700	0.94	2.27	1.25	0.917	1280	348
'Alternative 4'	0.125	700	0.94	2.27	1.0	0.917	1171	348

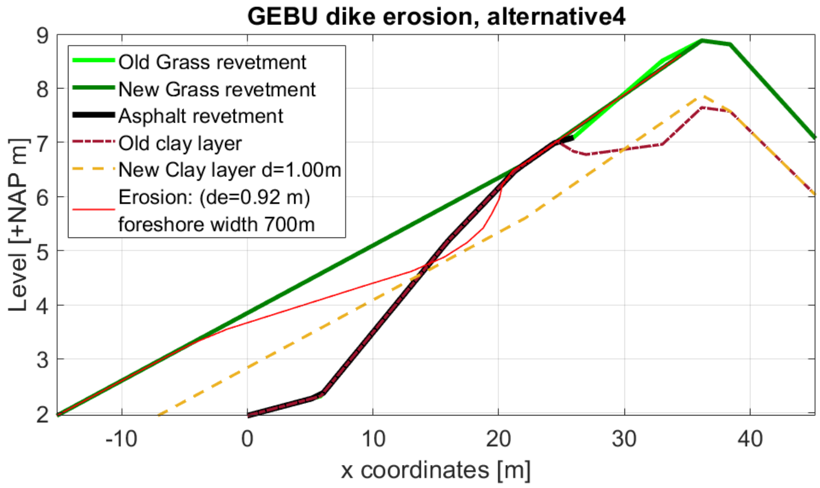

Figure 4.12: Example of the calculation output on the erosion depth for alternative 4 with crest height reduction.

4.4.2. Traditional dike vs green dike + wetland construction (Loc. 17.4km)

Alternatives on foreshore construction with brushwood dams is presented for the dike location 17.4km (Figure 4.14 on page 41). The settings of the five alternatives with a slope of 1/8 and a crest reduction of 1.68m are given in Table 4.5. Note the wave height reduction factor is a sum of the vegetation attenuation factor and the depth induced wave breaking factor. The first alternative is a case without foreshore and a $d_c = 2.5m$ meter thick clay layer as a reference to the other alternatives, however this a unrealistic thick clay layer. This case shows there is some residual clay strength left, but is only 0.1m thick. The foreshore height is varied between $z_{fs} = 1.0m - 1.5m$ to consider the uncertainty in accretion of the foreshore. Alternative 2 and 3 have a foreshore height of $z_{fs} = 1.0m$ and a width of 350m and 550m respectively. Alternative 4 and 5 have the same foreshore settings but a foreshore height of $z_{fs} = 1.5m$. A clear result is the reduction in erosion depth by the higher foreshores. This allows for a thinner clay layer, resulting in a cheaper alternative. Furthermore, A foreshore width of 350m shows there is just enough residual strength left by the clay layer (0.13m). Alternative 3 and 5 have a wider foreshore which results in lower erosion depths. This allows for a thinner clay layer and therefore lower costs. It can be seen that the costs on a thicker clay layer are higher than construction and maintenance of the foreshore.

Table 4.5: Different design alternatives for dike location 17.4km

Alternative	slope angle $[-]$	Foreshore width $[m]$	R_{fac} $[-]$	z_{fs} $[NAP+m]$	Clay thickness $[-]$	Erosion depth $[m]$	Construction Cost [€/m]	Maintenance Cost [€/m]
'Current dike'	0.245	0	1	0.5	1.5	0	1474	820
'Alternative 1'	0.125	0	1	0.5	2.5	2.42	2292	350
'Alternative 2'	0.125	350	0.93	1.0	2.0	1.87	2194	433
'Alternative 3'	0.125	550	0.9	1.0	1.5	1.23	1961	480
'Alternative 4'	0.125	350	0.88	1.5	1.5	1.14	1791	433
'Alternative 5'	0.125	550	0.84	1.5	1.0	0.86	1653	480

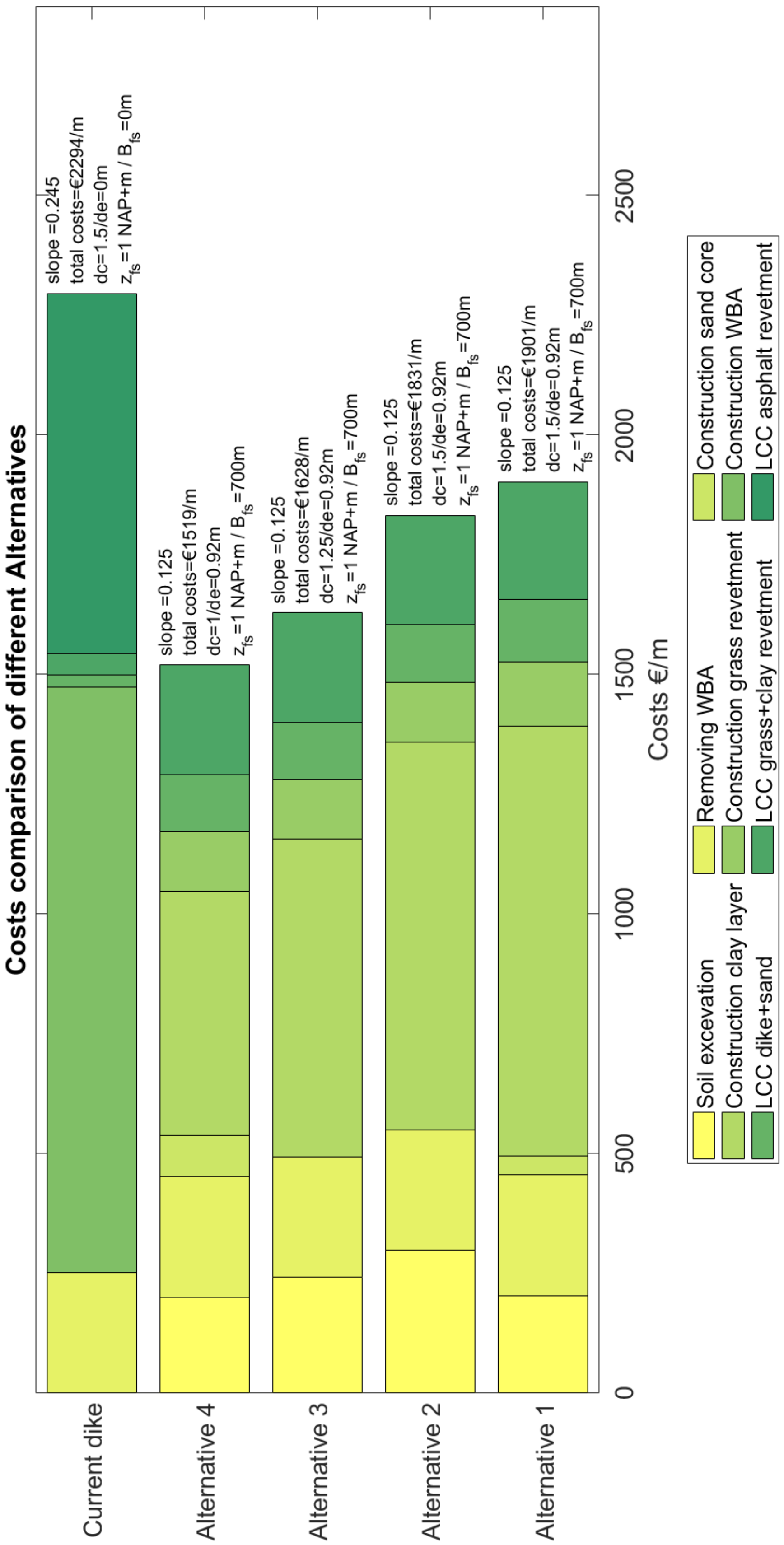

Figure 4.13: Final output of the design tool, giving a cost comparison of the different alternatives at location 22.2km.

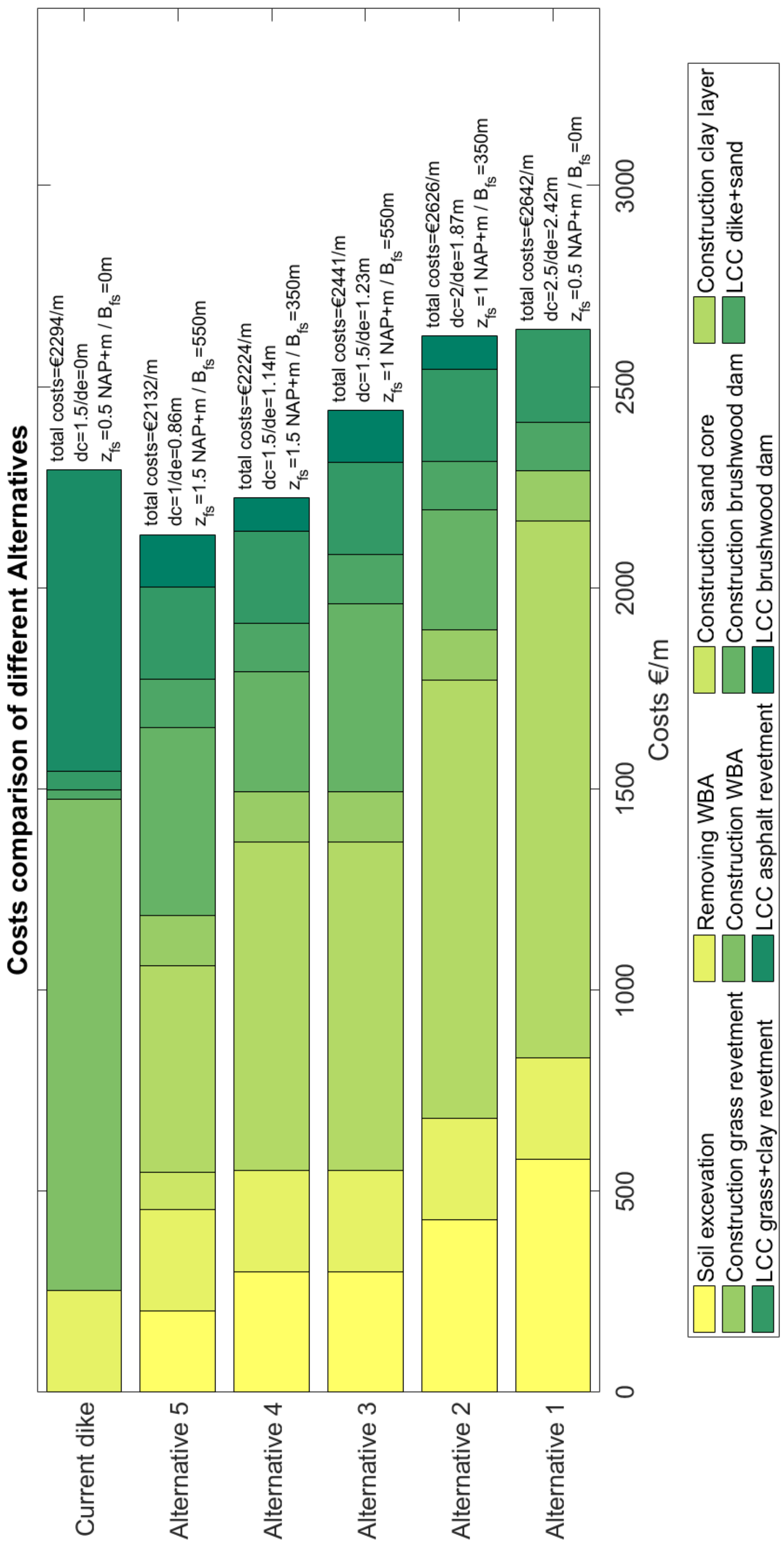

Figure 4.14: Final output of the design tool, giving a cost comparison of the different alternatives at location 17.4km

5

Discussion

This chapter discusses the feasibility of grass cover revetments in a wetland setting, in terms of the erosion depth and construction and maintenance costs. The results show that a gentle dike slope with a coastal wetland in front of it reduces the erosion on the grass and clay layers, thus making a grass cover dike a feasible option. First, the meaning and significance of the results are discussed in this chapter. Thereafter, the applicability of the research findings is discussed.

5.1. Insights and limitations of this study

The results of this study are divided into two parts. In the first part, numerical analysis shows the linear relation between the seaward slope angle and impact pressures on the dike. In the second part, using the design tool, the results show the effect of different wetland settings on the erosion depth. Additionally, results on the Koehool-Lauwesmeer dike trajectory present the feasibility of a grass cover dike. All the aforementioned results are separately discussed in this section.

5.1.1. Seaward slope angle relation

The numerical simulations show a clear decrease in impact pressure for decreasing slope angles. However, the data is not directly validated with flume experiments, therefore only generates indicative results. This means that the model can show trends in the slope angle - pressure relations similar to previous studies, but the derived relations cannot be directly applied in new relations for erosion models (Kruse, 2010; Mourik, 2015). The resulting trends are discussed for the flat profile and erosion profile.

Flat profile

The simulation on a flat slope shows a clear difference in wave impact for different geometric settings (see Figure 4.2 on page 31. The peak pressure results of the gentle slopes 1/6 and 1/8 are significantly reduced over the slope compared to a 1/4 slope. This effect is in line with literature (see section 2.2):, the gentle slopes have a lower breaker parameter, indicating waves behave more like spilling waves with a lower wave impact energy than plunging waves (Führböter and Sparboom, 1988; Peters, 2017). Additionally, the remaining thin water layer generated by, from previous waves, becomes larger for less steep slopes, thus causing a damping effect (Verheij , Delft Hydraulics). The highest reduction in peak pressures is captured by the $P_{2\%}$ results over the different slope angles. This implies that the damping effect is largest on the highest peak pressures simulating the wave impacts onconsidering the gentle slopes. Sequentially, the damping effect of lower peak pressures the($P_{10\%}$ and P_s) results over the slopes become smaller. The reason for this reduced effect is that there is an overall shift from the impact component to the quasi-static component over the total amount of waves (see section 2.3). The effect of the shift in pressure type becomes larger considering a higher percentage of the total wave impact pressures. Additionally, this explains the wider distribution of wave impacts over the slope, compared to the peak in $P_{2\%}$ in Figure 4.2 on page 31. The quasi-static pressures are caused by the waves surging on the slope, therefore the peaks in the pressure results shift more upward for $P_{10\%}$ and P_s.

The CoastalFOAM simulations are compared with data from physical experiments on hard revetment (see Figure 4.3 on page 31). However, care must be taken because no real time series are used to calibrate the model. The comparison shows that the $P_{2\%}$ results have some agreement with real life experiments in the Delta Flume. Nevertheless, only the $P_{2\%}$ of a 1/4 slope shows some similarities. The $P_{10\%}$ data point is slightly underestimated compared to the Delta Flume experiments in Figure 4.3 on page 31. A reason for this can be due to the relatively small amountnumber of waves tested. The Delta flume data is derived from several hours of testing, resulting in approximately more than 2000 waves, where the simulation data consists of 100 waves. Therefore, the highest 10 percent of the Delta Flume experiments will be higher compared to the simulations, because it consists of more waves filtering out the effect of spilling waves. Next to the 1/4 slope, the gentle slope angle results are less comparable with the experiments. However, tThe 1/6 slopes is on the edge of the domain of the empirical relations Equation (2.3) on page 9. This indicates that the model shows some correlation to the empirical data for a slope of 1/6, but the significance can not be validated. The 1/8 slope is hard to compare with the experimental data, because no experiments have been conducted on this slope.

All in all, the simulation on a flat profile does not have a direct relation to the erosion of the grass revetment. Only a few studies have shown a relation between wave impact pressure and grass erosion, which are barely validated (Stanczak et al., 2007; Mous, 2010). Nevertheless, the main reason to simulate the effects of a flat slope is to determine the accuracy of the CoastalFOAM model. Next to the validation on hard revetments, it is linked to the wave impact relation of Führböter and Sparboom (1988). This relation has proven to show most accurately the effect of slope angles on grass cover experiments (Peters, 2020). Similar to the validation case (see Figure 4.3 on page 31), the trend of the $P_{2\%}$ data shows a correlation with the Führböter and Sparboom (1988) relation in Figure 4.4 on page 32. This demonstrates that CoastalFOAM gives realistic results on its highest peak pressure data ($P_{2\%}$). Furthermore, the $P_{10\%}$ and P_s show the same discrepancy as with the Delta Flume experiments. This can be a result of two things, one is the aforementioned argument on a small number of waves. The second reason can be due to the fact that the Führböter and Sparboom (1988) relation is derived from maximum pressures as the $P_{2\%}$ results. All things considered, the flat profile simulations give an indication on the accuracy of the model and adds to the validity off the erosion profile simulations, which is discussed in the next section.

Erosion profile

The erosion profiles demonstrate, comparable to the flat profiles, a clear decrease in peak pressure for a decreasing slope angle (see Figure 4.5 on page 33). The form of the peak pressure graphs show the same peaks at the starting location of the cliff as in the study of Mourik (2015). As described in the results the $P_{2\%}$ plots shows small bumps on the erosion terrace. These bumps are caused by early breaking of the waves on the terrace. This phenomena is only observed for the $P_{2\%}$ results and not for the higher percentage peak pressures, because the effect of a single high wave impact is more dominant in the $P_{2\%}$ results.

During this study it has been found that the influence of the cliff height is influences the peak pressure outcomes. Whenever the still water level is above the starting cliff height point, the peak pressures increased. Therefore, care must be taken in the implementation of the erosion profile following the approach of Breteler (2012). The erosion profiles are copied from the study by Mourik (2015), which should give correct results in comparing the two studies (slopes of 1/3, 1/4 and 1/5). However, the gentle slopes are based on the erosion profile of a 1/5 slope and extended on the method of Breteler (2012). This simplification could affect the results considering the sensitivity of the cliff location.

Kruse (2010) determined that the erosion velocity of the clay correlates with the significant peak pressures, because the erosion process is most likely influenced by an ongoing process of wave impacts rather than by one single high wave impact. However, following the discussion of the flat profiles it can be argued whether the significant peak pressures are accurately described by the CoastalFOAM model. Herein, the $P_{2\%}$ show a correlation with empirical data, where the higher percentage peak pressures show an underestimation. Nonetheless, the significant peak pressures describe a similar trend in pressure reduction as the 2% peak pressures. Also, the same numerical settings are used as in the study by Mourik (2015) and showed the same linear trend. Therefore, it is assumed that the significant peak pressures can be used in the derivation of the linear relation.

The CoastalFOAM data on the erosion profile show a linear trend according to the statistical parameters ($R^2 > 0.95$ and $pValue < 0.05$). This is in line with the study by Mourik (2015) which only considered slope angles of 1/3, 1/4 and 1/5. Adding the gentle slopes to the analysis adds to the assumption on the linear relation between seaward slope angle and wave impact pressure. Consequently, the current erosion model can be extended for gentle slopes down to a slope of 1/8.

5.1.2. Geometric wetland settings

The studies by Steetzel et al. (2018) and Vuik et al. (2016) on wave attenuation of coastal wetlands are implemented in the design tool. Both studies account for a different hydrodynamic process of wetland wave attenuation. Steetzel et al. (2018) simulated the effect of wave attenuation by vegetation in a 1D SWAN model, whereas Vuik et al. (2016) simulated the combined effect of depth induced wave breaking and wave attenuation by vegetation in a comparable model. The vegetated wave attenuation model is adjusted for different vegetation lengths and categorized for different plant species. This approach shows some shortcomings due to difference in the wave attenuating capacity of plants within a category (Rupprecht et al., 2017). For example, the stiffness of the stem or leaning angle could make the difference in wave attenuating capacity. Implementing depth induced wave breaking large adjustment needed to be made to the model by Vuik et al. (2016). The model has been reduced with a factor 2, because the resulting wave attenuation was unrealistically high compared to Hydra-NL data. Therefore, care should be taken into interpreting the results on foreshore construction in this study. Nevertheless, similar results are shown compared to the situation with initial foreshore conditions with only vegetated attenuation. An important assumption for the wave attenuation by vegetation is that the hydraulic conditions 50m in front of the dike are used to calculate the orbital velocities. This causes the orbital velocities to be underestimated at the edge of the foreshore and therefore overestimates the wave reduction factor.

In this study, the critical orbital velocity is assumed to be similar for all the vegetation categories (see Table 3.4 on page 23). However, there are remarkable differences in plant species sensitive to wave-induced stresses (Vuik et al., 2018a). For most wetlands there are several plant species present that will have different critical orbital velocities. Therefore, the design tool should be extended by integrating plant specific critical orbital velocities. The variation in individual stem properties can easily be implemented in the tool, because the tool allows for spatially varying vegetation lengths. Coupling the lengths to spatially varying critical velocities would be sufficient. Vuik et al. (2018a) provides a formula determining the critical orbital velocity of a plant species, which could be used as a first estimate on the stability of other plant species (Vuik et al., 2018a). Additionally, plant specific critical orbital velocities should also be correlated to seasonal variations of the plant stability. The long vegetation characteristics are based on roughness heights for full grown vegetation. Nonetheless, seasonal variations also have influence on the vegetation length and stem diameter, which could result in overestimation of the reduction factor (Steetzel et al., 2018; Vuik et al., 2016).

The sensitivity analysis shows the importance of hydrodynamic processes on the wave load on the dike. High inundation depths cause lower orbital velocities, which result in less stem breaking (see Figure 4.10 on page 37). Additionally, the effect of long vegetation on the wave attenuation increases with higher inundation depths. This could even result in no erosion of the dike behind.

The wave impact load reduction on the dike due to vegetation decreases when stem breakage occurs. Considering the extreme situation for the GEBU assessment (1/20000y) all vegetation breaks. However, there is still some wave height reduction by the broken vegetation, given the wave flume experiments of Möller et al. (2014). The residual wave height reduction of the broken vegetation still has a considerable effect on the erosion depth reduction (see Figure 4.11 on page 38). For the case location 32.2km the reduction in erosion depth by vegetation results in 0.6m.

5.1.3. Design Tool

The design tool aims to assess the feasibility of a grass cover dike in a coastal wetland setting in terms of the failure of the grass revetment and clay layers together with costs on construction and maintenance. This tool is based on analytical or semi-empirical approximations, which provides a quick analysis compared to detailed numerical model approaches. There are 3 hydrodynamic process-based steps for the assessment of the failure of the revetment. Firstly, the offshore hydrodynamic conditions are determined. The key result of this step is an assessment of the extreme offshore hydrodynamic conditions in the study area. Secondly, effects of the coastal wetland vegetation on the hydraulic conditions are derived. The nearshore wave and surge interact with the coastal wetland vegetation, which results in wave attenuation and wave height reduction. Thirdly, the resulting wave load is translated to the erosion of the dike. The storm surge water level and wave heights initially cause erosion to the grass revetment. Whenever the grass revetment fails the resulting erosion depth is calculated. The hydrodynamic processes are based on several assumptions. Herein, the hydrodynamic wetland processes are already discussed in section 5.1.2.

In this study the potential wave run-up was not included. When the water level increases, it is possible that the grass is damaged due to wave run-up before the waves directly attack that particular location on the dike. However, this effect will probably not lead to different results since wave impact is dominant over wave run-up (van Hoven, 2015). Another assumption is that the erosion model is only reliable for closed sods, because it is derived from experiments with closed sods. For open or fragmented sods different top and sub layer relations must be determined. Furthermore, the relation is only reliable for slope angles between 1:3 and 1:8 since this was the range of slopes used in the simulations. Considering the erosion of the bare clay layer, there is a threshold in the erosion depth between no erosion and an erosion depth of $0.5m$. This is because of the following reason: if the grass revetment does not fail according to the extended WBI-2017 assessment there will not be erosion, but when it does fail the model starts with an initial erosion depth of $0.5m$ accounting for the failure of top and sub layer.

The cost efficiency of crest height reduction is presented in Table 5.1. Dike location 22.2km has a crest height reduction of 2.27m, which is lower compared to location 17.4km. This difference is due to the lower hydraulic loading at location 22.2km. The costs are respectively 70 and 57 [€/m], which could save a lot of costs considering 100 kilometres of dike.

Table 5.1: Cost reduction by lowering gentle slope crest height

Location $[km]$	HBN Traditional dike $[+NAPm]$	HBN Green dike $[+NAPm]$	Cost reduction [€/m]
22.2	7.94	6.61	70
17.4	8.82	7.14	57

5.1.4. Case study

A case study is conducted for the remaining two dike locations at the Koehool-Lauwersmeer trajectory. The locations are assessed using the design tool. Results show for both locations positive results on the applicability of a grass cover dike with a failure probability of 1/200000y. Changing the different parameters in the design tool gives insight in how the system works and what is needed to come to a grass cover dike solution. First, dike location 22.2km with an initial foreshore width of 700m is assessed on a new grass cover dike with a seaward slope of 1/8. The results show an erosion depth of 0.92m, which would allow for a 1.5m thick clay layer. However, this would be too conservative while a 1 m thick clay layer would be too optimistic considering a safety margin of 0.2m. Therefore, a 1.25 thick clay layer would be optimal for a grass cover dike design. Next to that the solution shows to be substantially cheaper compared to the current traditional dike. Figure 4.13 on page 40 shows that the clay layer thickness has a substantial effect on the construction and maintenance costs, therefore design optimization can lead to considerable cost reductions.

For the dike location 17.4km alternatives with construction of brushwood dams are considered. Construction of brushwood dams has shown to be possible solutions for construction of green dikes. The alternatives considered accounted for different accretion rates depending on the sediment supply. Literature states a range between 1 and 2.5cm rise per year resulting in 1 to 2.5m foreshore heightening (Vuik et al., 2019). The alternatives show two different options for dike managers. Herein a relative conservative design can be chosen for assuming foreshore heightening of $z_{fs} = 1.0m$ by accretion. Another option is a more optimistic approach assuming a foreshore height of $z_{fs} = 1.5m$. Both options have their own solution as shown in Figure 4.14 on page 41 where logically the conservative approach is more expensive.

5.2. Applicability of this research

The numerical model has shown to be a useful supplement to current assessment tools by extending the experimental data numerically. The model is able to capture a linear trend without calibrating the model to experimental time-series. Therefore, the model also could be applied for analysis on different geometries and coastal settings.

Varying geometric parameters in the design tool shows the weaknesses and strengths of the grass cover dike in a wetland setting solution. Most coastal protection tools and models are specifically designed for one process in the whole system of coastal protection, mainly because the processes are complex. Nonetheless, these tools and models provide semi-empirical solutions, which are applied in the design tool of this study (Vuik et al., 2016; Steetzel et al., 2018; Mourik, 2015). Some research is done on the combined effect of coastal wetland attenuation and the dike failure in behind (Vuik et al., 2018a, 2019). However, a quick feasibility assessment tool on the combined effect is not developed yet. This study is a first step in combining the semi-empirical data into a design tool for a grass cover dike solution in a coastal wetland setting. This tool gives an advantage over numerical models and detailed assessments, considering the preliminary phase of dike reinforcement projects.

Following the results on the current grass cover dike at dike location 32.2km, it is not necessary to replace the current grass cover dike with a traditional dike when accounting for the slope angle and wetland settings. The extended WBI assessment shows that there is residual strength left, considering a geometry profile of 1/8 (see Figure 4.11 on page 38). It could be argued that the 0.2m remaining clay thickness won't be a safe margin, therefore taking also the wetland into account adds up to a residual strength of 0.6m (van Hoven and de Waal, 2015). Because erosion with a variable water level is applied the outcomes give more visually realistic outcomes. This is more attractive for dike managers to get insight in what really happens in the erosion process.

6

Conclusion and Recommendations

6.1. Conclusion

This research aims to asses the feasibility of a grass cover dike with a wetland in front of it. The four sub-questions and main question are answered in this chapter.

1. How does the seaward slope angle affect the wave impact load on the dike?

The three steps in the numerical analysis evaluate that the effect of the seaward dike slope on the maximum peak pressures occurring on the dike provided for the following conclusions. First, by applying the Mesh sensitivity analysis that evaluates computation time, reflection coefficients and peak pressures, it can be concluded that the snappy hex mesh grid with local refinements performs best on the peak pressure performance and computation time compared to the other grids. Secondly, the flat profile and erosion profile simulations show a significant linear relation between the seaward slope angle and the wave impact pressure. Whereby, the highest damping effect, due to the gentle slopes slopes (1/6 and 1/8), is observed for the highest peak pressures ($P_{2\%}$). Lastly, comparing the relations derived from the numerical data with physical experiments on hard revetment, it is concluded that the numerical data shows some agreement with the empirical data for the $P_{2\%}$ results of a 1/4 slope. Nonetheless, comparison with other slopes gave inconclusive results. The main conclusion on the relation of the seaward slope angle is the extension of the WBI model for different dike slopes up to 1/8. Therefore, it is advised to use the relation of Führböter and Sparboom (1988) to estimate the resistance duration for cases with a gentle slope. Furthermore, the relation of Mourik (2015) has a wider range of applicability for gentle slopes, according to this research.

2. How do geometric wetland settings affect the erosion of the grass revetment and clay layers?

Geometric wetland settings are determined by two vital hydrodynamic processes: wave attenuation by vegetation and wave attenuation by depth induced wave breaking. Important wetlands conditions are the inundation depth and critical orbital velocity for stem breaking. Design tool results introduce a reduction factor of 0.9 only considering vegetation and a reduction factor of 0.84 for the combined effect of vegetation and depth induced wave breaking. It can be concluded that the consequently reduced wave heights allows for the application of a grass cover dike in the wave impact zone. In addition, we show that cost can be reduced due to tolerating thinner clay layers when adopting the wetland. This is confirmed by the coastal wetland construction case assessment in which 350m construction of brushwood dams is sufficient for a grass cover dike.

3. How can the described effects be combined in a design tool that assesses the feasibility of dike design alternatives?

A design tool has been developed to help assess the feasibility of dike design alternatives. The multi-feature tool combines wetland strategies with geometric setting of the dike slope, the residual strength of the clay layer and costs for construction and maintenance. Herein the wetland strategies can be adjusted on the foreshore width B_{fs}, foreshore height z_{fs}, vegetation length categorized by Table 3.4

on page 23 and the corresponding orbital velocity u_c. The geometric settings can be extended with a numerical analysis, which increases the reliability of gentle slopes up to 1/8. The tool allows for combining the resistance duration curves of the top and sub layer together with the erosion model of Mourik (2015). the erosion model accounts for the residual strength of the bare clay layer, whereby the erosion depth can be calculated. Lastly, different alternatives can be evaluated for construction and maintenance costs compared to the original dike. The tool should be used and interpreted rather as indicative, showing the effect of different alternatives.

4. What is the cost-effectiveness of a green dike design for different Koehool-Lauwersmeer dike locations compared to the current traditional designs?

A case study for three locations at the dike trajectory of Koehool Lauwersmeer shows positive results for the design alternatives of a green dike. For each location several possible green dike alternatives are found. Which are most of the time cheaper than considering the current traditional dike with an asphalt revetment. Next to that a case has been considered without a foreshore showing potential for constructing a foreshore with brushwood dams. Because maintenance of brushwood dams is relatively intensive, this solution makes it an expensive alternative although it has a higher ecological value compared to the conventional solutions. Given these alternatives, we conclude that a gentle dike slope of 1/8 allows for a cost-effective grass cover dike in the wave impact zone for Wadden sea conditions at Koehool Lauwersmeer.

Provided the answers on the four sub questions, we conclude with respect to the main research question:

What is the feasibility of a grass cover dike in a coastal wetland setting, considering erosion in the wave impact zone together with costs?

This study shows that a grass cover dike in a coastal wetland setting is feasible. A gentle seaward sloping dike of 1/8 significantly damps the effect of the wave impact on erosion of the grass and clay layers. Additionally, integrating wave attenuation of a coastal wetland into the assessment allows for a grass cover dike in the wave impact zone. Furthermore, presenting the feasibility in a design tool provides dike managers quick insights into the applicability of a grass cover dike in a wetland setting. Lastly, a first step towards the practical implementation of coastal wetland research is taken. A case study at the dike trajectory of Koehool-Lauwesmeer shows feasible grass cover dike designs compared to the traditional design. This reduces the costs and adds to the biodiversity.

6.2. Recommendations

Several recommendation are formulated in this study. witch are classified as recommendations for further research and recommendations for the safety assessment nowadays.

6.2.1. Further research

this section on further research is separated in the numerical wave impact analysis, coastal wetlands and the design tool.

Numerical wave impact analysis

In the numerical analysis several aspects came across, which are worthy for further investigation. The mesh sensitivity considers different refinement strategies, which are examined on the pressures and reflection coefficients. Nonetheless, only two refinement resolutions are examined, which are the coarse and fine resolutions based on previous studies (Kruse, 2010; Mourik, 2015). It would be interesting to see the effect of finer grid resolution on the peak pressure outcomes. Additionally, the mesh sensitivity analysis is simulated for only 22 waves, which is statistical insignificant (>100) Mourik (2015). Nonetheless the results showed clear differences between the different refinement strategies, therefore it is advised to conduct mesh sensitivity analysis for at least 20 waves, which safes computational time in the phase of the numerical set-up of the model.

This study shows that the higher peak pressure percentages ($P_{10\%}$ and P_s), are underestimated due to a relatively small amount of simulated waves (100 waves). It is recommended to simulate more waves to provide better estimation of the design pressure parameters. However, this is a difficult task, because there is a fine balance between the accuracy of the model and computational time. Solutions on reducing the computation time can be found in mesh refinement methods as used in this model. Nonetheless, grid refinement also needs further investigation on the effect on breaking and estimating the pressures accurately of the model.

An important assumption in the numerical extension of the seaward slope angle relation are the geometry profiles. During this study the effect of the geometry profiles on the pressure outcome had a considerable influence on the peak pressure results. Specifically the gentle slope erosion profiles of 1/6 and 1/8 are derived from a 1/5 erosion profile following the method of Breteler (2012). Therefore, it is recommended to investigate the erosion profiles of gentle slopes in a physical experiment.

The CoastalFOAM simulations show some correlation with experimental data on Hard revetments. Therefore it would be interesting to do more research on the validity of the model compared to experimental data. Calibrating the model on a experimental time series would add to the validity. Furthermore, there is no direct relation between the impact pressure and the erosion process of the grass revetment and clay layers in behind. Current models consider the processes as a black box, where impact pressures are linked to the erosion velocity. Only a few studies have shown a relation between wave impact pressure and the erosion of the grass revetment and clay layer, which is barely validated (Stanczak et al., 2007; Mous, 2010). Additional studies are needed to improve the understand of the load on the revetment due to wave impact. The force that damages the grass revetment is the uplifting force and extra studies could contribute in understanding the translation of the wave impact to the uplift pressure.

Coastal wetlands

A first step in the practical implementation of wetland research is provided in this research. This model has shown how a stem breakage model and geometric wetland settings can be applied in a design tool. The findings on the application of coastal wetlands in the design tool address the importance of the inundation depth. Figure 4.10 on page 37 and Figure 4.14 on page 41 both show the sensitivity of the foreshore height on the erosion depth. A difference in half a meter foreshore height has a huge impact. Therefore, it is important to reduce the uncertainty on the morphological development of coastal wetlands. The importance of morphological development is also stressed in other studies (Vuik et al., 2019; Willemsen et al., 2020). Consequently, analysis on the long-term temporal variability of the salt marsh foreshore is the next step for the application of salt marsh foreshores for coastal protection.

Design tool

Due to a small amount of experiments on wave impact, the uncertainty of the erosion model is high. Next to that the knowledge on the effect of different conditions on the erosion process is limited. Extra fullscale wave impact experiments on grass revetments can contribute to a decrease in the uncertainty. It is recommended to execute the experiments on gentle slopes, because most experiments are executed on a steep slope of around 1:3 and 1:4. Additionally, it is recommended to focus on the wave height for design conditions of around 2 meter.

6.2.2. Safety assessment

This study has shown the added value of using CoastalFOAM to improve or extend current assessment guidelines. Additionally, the model can give more in depth knowledge on the complex processes such as wave breaking and resulting wave loading. Next to investigating the wave impact load on coastal structures, the wave run-up and overtopping processes can be studied in detail.

The main finding of this study is the extension of the WBI model for different dike slopes up to a 1/8 slope. Therefore, it is advised to use the relation of Führböter and Sparboom (1988) to estimate the resistance duration for cases with a gentle slope. Furthermore the relation of Mourik (2015) has a wider range of applicability for gentle slopes, according to this research. It is recommended to use the extended relations in the customised assessment of the WBI. More research as is mentioned above, has to be executed to increase the reliability of the effect. The effect of the slope angle was found to be large, thus it should be implemented in the detailed assessment as soon as possible.

Next to the slope angle the wetland attenuation by vegetation should be considered in the coastal protection. This study shows that a combined effect of a gentle slope and a vegetated wetland reduce the erosion depth considerably allowing grass revetments instead of asphalt. the semi-empirical implementation of geometric wetland settings in the design tool needs further development for incorporation into the safety standards.

Furthermore it is recommended for dike managers to consider this tool when redesigning a new dike. This tool gives first of all insight in the whole system from foreshore to the erosion of the dike. Furthermore different strategies can be evaluated on the cost efficiency, providing insights in choosing for conservative designs or more optimistic designs. These conservative or optimistic designs are mainly depending on the morphological development of the foreshore location. Thus, from the quick assessment it can be determined whether a detailed morphological study is required to optimize the design.

Bibliography

Coefficient of Determination. In *The Concise Encyclopedia of Statistics*, pages 88–91. Springer New York, New York, NY, 2008. ISBN 978-0-387-32833-1. doi: 10.1007/978-0-387-32833-1{_}62. URL https://doi.org/10.1007/978-0-387-32833-1_62.

N.W.H. Allsop. Probabilistic Design Tools for Vertical Breakwaters - Volume IIa hydrodynamic aspects. 0041, 1999.

M E Anderson and J M Smith. Wave attenuation by fl exible , idealized salt marsh vegetation. *Coastal Engineering*, 83:82–92, 2014. ISSN 0378-3839. doi: 10.1016/j.coastaleng.2013.10.004. URL http://dx.doi.org/10.1016/j.coastaleng.2013.10.004.

Edward B. Barbier, Evamaria W. Koch, Brian R. Silliman, Sally D. Hacker, Eric Wolanski, Jurgenne Primavera, Elise F. Granek, Stephen Polasky, Shankar Aswani, Lori A. Cramer, David M. Stoms, Chris J. Kennedy, David Bael, Carrie V. Kappel, Gerardo M.E. Perillo, and Denise J. Reed. Coastal ecosystem-based management with nonlinear ecological functions and values. *Science*, 319(5861): 321–323, 2008. ISSN 00368075. doi: 10.1126/science.1150349.

J A Battjes. *Computation of set-up, longshore currents, run-up and overtopping due to wind-generated waves*. PhD thesis, TU Delft, 1974. URL http://resolver.tudelft.nl/uuid:e126e043-a858-4e58-b4c7-8a7bc5be1a44.

Edin Berberović, Nils P. Van Hinsberg, Suad Jakirlić, Ilia V. Roisman, and Cameron Tropea. Drop impact onto a liquid layer of finite thickness: Dynamics of the cavity evolution. *Physical Review E - Statistical, Nonlinear, and Soft Matter Physics*, 79(3), 2009. ISSN 15393755. doi: 10.1103/PhysRevE.79.036306.

Bas W. Borsje. Living Dikes - Realizing resilient and climate proof coastal protection. Technical Report 5, 2019.

Bas W Borsje, Bregje K Van Wesenbeeck, Frank Dekker, Peter Paalvast, Tjeerd J Bouma, Marieke M Van Katwijk, and Mindert B De Vries. How ecological engineering can serve in coastal protection. *Ecological Engineering*, 37(2):113–122, 2011. ISSN 0925-8574. doi: 10.1016/j.ecoleng.2010.11.027. URL http://dx.doi.org/10.1016/j.ecoleng.2010.11.027.

Mark KLein Breteler. Erosie van een dijk na bezwijken van de steenzetting door golven. Technical report, deltares, 2012.

Mark KLein Breteler. Residual strength of grass on clay in the wave impact zone. Technical report, delatres, 2015.

Mark KLein Breteler. Residual strength of grass on clay in the wave impact zone. 2017.

Mark Klein Breteler. Erosie van kleibekleding met gras op buitentalud van zee- en meerdijken. 2020.

T Dahiru. P-Value, a true test of statistical significance? a cautionary note. *Annals of Ibadan Postgraduate Medicine*, 6(1):21–26, 2011. ISSN 1597-1627. doi: 10.4314/aipm.v6i1.64038.

A. D'Alpaos, S. M. Mudd, and L. Carniello. Dynamic response of marshes to perturbations in suspended sediment concentrations and rates of relative sea level rise. *Journal of Geophysical Research: Earth Surface*, 116(4):1–13, 2011. ISSN 21699011. doi: 10.1029/2011JF002093.

J.P. De Waal. Basisrapport WBI 2017. Technical report, Deltares, 2016.

Brecht Devolder and Peter Troch. Performance of a buoyancy-modified k- ω and k- ω SST turbulence model for simulating wave breaking under regular waves using OpenFOAM ®. (June 2019), 2018. doi: 10.1016/j.coastaleng.2018.04.011.

Brecht Devolder, Pieter Rauwoens, and Peter Troch. Application of a buoyancy-modified k- ω SST turbulence model to simulate wave run-up around a monopile subjected to regular waves using OpenFOAM ®. 125(July 2017):81–94.

A Führböter and U Sparboom. Shock pressure interactions on prototype sea dykes caused by breaking waves. *Modeling Soil-Water-Structure Interactions*, 1988.

Keryn B. Gedan, Matthew L. Kirwan, Eric Wolanski, Edward B. Barbier, and Brian R. Silliman. The present and future role of coastal wetland vegetation in protecting shorelines: Answering recent challenges to the paradigm. *Climatic Change*, 106(1):7–29, 2011. ISSN 01650009. doi: 10.1007/s10584-010-0003-7.

Pablo Higuera, Javier L. Lara, and Inigo J. Losada. Three-dimensional interaction of waves and porous coastal structures using OpenFOAM®. Part II: Application. *Coastal Engineering*, 83:259–270, 2014. ISSN 03783839. doi: 10.1016/j.coastaleng.2013.09.002. URL http://dx.doi.org/10.1016/j.coastaleng.2013.09.002.

HWBP. HoogWaterBeschermingsProgramma, 2020. URL https://www.hoogwaterbeschermingsprogramma.nl/.

Niels G Jacobsen, David R Fuhrman, and Jørgen Fredsøe. A wave generation toolbox for the open-source CFD library : OpenFoam r. pages 1073–1088, 2012. doi: 10.1002/fld.

Niels G Jacobsen, Marcel R A Van Gent, Alex Capel, and Mart Borsboom. Numerical prediction of integrated wave loads on crest walls on top of rubble mound structures. *Coastal Engineering*, 142(October):110–124, 2018. ISSN 0378-3839. doi: 10.1016/j.coastaleng.2018.10.004. URL https://doi.org/10.1016/j.coastaleng.2018.10.004.

Wouter Jan Klerk and Ruben Jongejan. Semi-probabilistic assessment of wave impact and runup on grass revetments. Technical report, Deltares, 2016.

Bjarne Jensen, Niels Gjøl Jacobsen, and Erik Damgaard Christensen. Investigations on the porous media equations and resistance coefficients for coastal structures. *Coastal Engineering*, 84:56–72, 2014. ISSN 03783839. doi: 10.1016/j.coastaleng.2013.11.004. URL http://dx.doi.org/10.1016/j.coastaleng.2013.11.004.

Dorothea Kaste and Mark KLein Breteler. Rekenmodel voor kleierosie bij variërende waterstand. Technical report, Deltares, 2015.

Matthew L Kirwan and J Patrick Megonigal. Tidal wetland stability in the face of human impacts and sea-level rise. pages 3–10, 2013. doi: 10.1038/nature12856.

Wouter Jan Klerk and Ruben Jongejan. Semi-probabilistic assessment of wave impact and runup on grass revetments. Technical report, Deltares, 2016.

M Kruse. Studie voor richtlijnen klei op dijktaluds in het rivierengebied. 2010.

Jan Lammers. Risicoanalyse HR. 2019.

Bjarke Eltard Larsen and David R Fuhrman. On the over-production of turbulence beneath surface waves in Reynolds-averaged Navier – Stokes models. pages 419–460, 2018. doi: 10.1017/jfm.2018.577.

Daniel Lincke and Jochen Hinkel. Economically robust protection against 21st century sea-level rise. *Global Environmental Change*, 51(April):67–73, 2018. ISSN 09593780. doi: 10.1016/j.gloenvcha.2018.05.003. URL https://doi.org/10.1016/j.gloenvcha.2018.05.003.

Jantsje M Van Loon-steensma and Pier Vellinga. How " wide green dikes " were reintroduced in The Netherlands : a case study of the uptake of an innovative measure in long-term strategic delta planning. *Journal of Environmental Planning and Management*, 62(9):1525–1544, 2019. ISSN 0964-0568. doi: 10.1080/09640568.2018.1557039. URL https://doi.org/10.1080/09640568.2018.1557039.

Iñigo J Losada, Maria Maza, and Javier L Lara. A new formulation for vegetation-induced damping under combined waves and currents. *Coastal Engineering*, 107:1–13, 2016. ISSN 0378-3839. doi: 10.1016/j.coastaleng.2015.09.011. URL http://dx.doi.org/10.1016/j.coastaleng.2015.09.011.

Per A Madsen and Ole R Sorensen. A new form of the Boussinesq equations with improved linear dispersion characteristics . Part 2 . A slowly-varying bathymetry. 18:183–204, 1992.

E.P.D. Mansard and E.R. Funke. The measurement of incident and reflected spectra using a least square method. pages 154–172, 1980.

Fernando J Mendez and Inigo J Losada. An empirical model to estimate the propagation of random breaking and nonbreaking waves over vegetation fields. 51:103–118, 2004. doi: 10.1016/j.coastaleng.2003.11.003.

Ministerie van Infrastructuur en Milieu. Regeling veiligheid primaire waterkeringen 2017(Bijlage I I I, sterkte en veiligheid). Technical report, Rijkswaterstaat, water Verkeer en Leefomgeving, 2016.

Iris Möller, Matthias Kudella, Franziska Rupprecht, Tom Spencer, Maike Paul, Bregje K. Van Wesenbeeck, Guido Wolters, Kai Jensen, Tjeerd J. Bouma, Martin Miranda-Lange, and Stefan Schimmels. Wave attenuation over coastal salt marshes under storm surge conditions. *Nature Geoscience*, 7 (10):727–731, 2014. ISSN 17520908. doi: 10.1038/NGEO2251.

M L A Moretto. An efficient numerical approach to model wave overtopping of rubble mound breakwaters. 2020.

G.C. Mourik. Prediction of the erosion velocity of a slope of clay due to wave attack. Technical report, Delta, 2015.

B C Mous. *Wave impact on grass covered outer slopes*. PhD thesis, Delft University of Technology, 2010.

J.A. Muijs. Grass cover as a dike revetment. Technical Report February, Technical Advisory Committee for Flood Defence (TAW), 1999.

Barbara Neumann, Athanasios T. Vafeidis, Juliane Zimmermann, and Robert J. Nicholls. Future coastal population growth and exposure to sea-level rise and coastal flooding - A global assessment. *PLoS ONE*, 10(3), 2015. ISSN 19326203. doi: 10.1371/journal.pone.0118571.

Hocine Oumeraci, Tijl STAAL, Saskia PFÖRTNER, and Gisa LUDWIGS. Hydraulic performance, wave loading and response of ELASTOCOAST revetments and their foundations. 988(988):709–740, 2010. doi: 10.5150/jngcgc.2010.082-o.

D.J. Peters. *Design of Pattern-placed Revetments*. 2017. ISBN 9789055841745. doi: https://doi.org/10.4233/uuid:0b67a0dd-a951-46f3-bbaa-86270e546c4e.

Martijn Peters. A study of the effect of the slope angle of a green dike on the failure of the grass revetment due to wave impact. 2020.

Water Verkeer en Leefomgeving Rijskswaterstaat. Schematiseringshandleiding grasbekleding (WBI 2017). Technical Report april, Ministerie van Infrastructuur en Milieu, 2018.

Royal HaskoningDHV. Dijkversterking Lauwersmeer- Vierhuizergat. Technical report, 2020.

F. Rupprecht, I. Möller, M. Paul, M. Kudella, T. Spencer, B. K. van Wesenbeeck, G. Wolters, K. Jensen, T. J. Bouma, M. Miranda-Lange, and S. Schimmels. Vegetation-wave interactions in salt marshes under storm surge conditions. *Ecological Engineering*, 100:301–315, 2017. ISSN 09258574. doi: 10.1016/j.ecoleng.2016.12.030. URL http://dx.doi.org/10.1016/j.ecoleng.2016.12.030.

Ben Schaap. KNMI'14-klimaatscenario's voor Nederland; Leidraad voor professionals in klimaatadaptatie. 2015.

T. Schoonees, A. Gijón Mancheño, B. Scheres, T. J. Bouma, R. Silva, T. Schlurmann, and H. Schüttrumpf. Hard Structures for Coastal Protection, Towards Greener Designs. *Estuaries and Coasts*, 42(7):1709–1729, 2019. ISSN 15592731. doi: 10.1007/s12237-019-00551-z.

Alexandra Silinski, Maike Heuner, Jonas Schoelynck, and Sara Puijalon. Effects of Wind Waves versus Ship Waves on Tidal Marsh Plants : A Flume Study on Different Life Stages of Scirpus maritimus. pages 1–16, 2015. doi: 10.1371/journal.pone.0118687.

E. Sirks. Vervolg toets op maat groene dijk - Verkenning Waddenzeedijk Koehool-Lauwersmeer. Technical report, Witteveen + Bos, 2019.

Grzegorz Stanczak, Hocine Oumeraci, and Andreas Kortenhaus. Laboratory tests on the erosion of clay revetment of sea dike with and without a grass cover induced by breaking wave impact. *FLOODsite*, page 48, 2007.

Henk Steetzel, Jacco Groeneweg, and Vincent Vuik. Effectiviteit Voorlanden HR - Onderzoeksrapportage Fase C. page 187, 2018.

Stijn Temmerman, Patrick Meire, Tjeerd J. Bouma, Peter M.J. Herman, Tom Ysebaert, and Huib J. De Vriend. Ecosystem-based coastal defence in the face of global change. *Nature*, 504(7478): 79–83, 2013. ISSN 00280836. doi: 10.1038/nature12859.

I. C. van den Bosch. Numerical modeling of wave run-up on a dike. *Lecture Notes in Computational Science and Engineering*, 71:373–401, 2010. ISSN 14397358. doi: 10.1007/978-3-642-03344-5{_}13.

I.M.H. van der Reijden. *Effectiviteit van vegetatie op voorlanden*. PhD thesis, technical university Delft, 2019.

Andre van Hoven. WTI 2017 Onderzoek en ontwikkeling landelijk toetsinstrumentarium. Technical report, Deltares, 2015.

Andre van Hoven and Hans de Waal. Failure Mechanism Module Grass Wave Runup Zone Requirements and Functional Design. Technical report, Deltares, 2015.

J.M. van Loon-Steensma, H.A. Schelfhout, M.E.A. Broekmeyer, M.P.C.P. Paulissen, W.T. Oostenbrink, C. Smit, and E. Jolink. Nadere verkenning Groene Dollard Dijk. Technical report, Wageningen, Alterra Wageningen UR (University & Research centre), 2014.

H.J. Verheij, G.A.M. Kruse, J.H. Niemeijer, J.T.C.M. Sprangers, J.T. de Smidt, and P.J.M. Wondergem. Technisch rapport Ersosiebestendigheid van grasland als dijkbekleding. Technical report, TAW, 1998.

H.J. Verheij (Delft Hydraulics), G.A.M. Kruse (Geodelft), J.H. Niemeijer(Heidemij Advies), J.T.C.M. Sprangers (Agricultural University Wageningen), J.T. de Smidt (University of Utrecht), Wondergem (Road, and P.J.M. Hydraulic Engineering Institute, Delft). Technical report Erosion resistance of grassland as dike covering. Technical report, Technical Advisory Committee for Flood Defence in The Netherlands (TAW), 1997.

V. Vuik, S. N. Jonkman, B. W. Borsje, and T. Suzuki. Nature-based flood protection: The efficiency of vegetated foreshores for reducing wave loads on coastal dikes. *Coastal Engineering*, 116:42–56, 2016. ISSN 03783839. doi: 10.1016/j.coastaleng.2016.06.001. URL http://dx.doi.org/10.1016/j.coastaleng.2016.06.001.

Vincent Vuik, Hannah Y. Suh Heo, Zhenchang Zhu, Bas W. Borsje, and Sebastiaan N. Jonkman. Stem breakage of salt marsh vegetation under wave forcing: A field and model study. *Estuarine, Coastal and Shelf Science*, 200:41–58, 2018a. ISSN 02727714. doi: 10.1016/j.ecss.2017.09.028. URL https://doi.org/10.1016/j.ecss.2017.09.028.

Vincent Vuik, Saskia van Vuren, Bas W. Borsje, Bregje K. van Wesenbeeck, and Sebastiaan N. Jonkman. Assessing safety of nature-based flood defenses: Dealing with extremes and uncertainties. *Coastal Engineering*, 139(December 2017):47–64, 2018b. ISSN 03783839. doi: 10.1016/j.coastaleng.2018.05.002. URL https://doi.org/10.1016/j.coastaleng.2018.05.002.

Vincent Vuik, Bas W. Borsje, Pim W.J.M. Willemsen, and Sebastiaan N. Jonkman. Salt marshes for flood risk reduction: Quantifying long-term effectiveness and life-cycle costs. *Ocean and Coastal Management*, 171(January):96–110, 2019. ISSN 09645691. doi: 10.1016/j.ocecoaman.2019.01.010. URL https://doi.org/10.1016/j.ocecoaman.2019.01.010.

Wetterskip Fryslan. Beoordeling Waddenzeedijk Koehool-lauwersmeer. Technical report, 2018.

P. W.J.M. Willemsen, B. W. Borsje, S. J.M.H. Hulscher, D. Van der Wal, Z. Zhu, B. Oteman, B. Evans, I. Möller, and T. J. Bouma. Quantifying Bed Level Change at the Transition of Tidal Flat and Salt Marsh: Can We Understand the Lateral Location of the Marsh Edge? *Journal of Geophysical Research: Earth Surface*, 123(10):2509–2524, 2018. ISSN 21699011. doi: 10.1029/2018JF004742.

Pim W J M Willemsen, Bas W Borsje, Vincent Vuik, Tjeerd J Bouma, J M Suzanne, and H Hulscher. Field-based decadal wave attenuating capacity of combined tidal flats and salt marshes. *Coastal Engineering*, 156(January):103628, 2020. ISSN 0378-3839. doi: 10.1016/j.coastaleng.2019.103628. URL https://doi.org/10.1016/j.coastaleng.2019.103628.

J. A. Zelt, James E. Skjelbreia, and Wave Technologies. Estimating incident and reflected wave fields using an arbitrary number of wave gages. *Proceedings of the Coastal Engineering Conference*, 1:777–788, 1993. ISSN 08938717.

A

Numerical analysis

A.1. Geometry profiles

The geometry profiles for the numerical analysis are presented in Figure A.2 on the following page and Figure A.3 on page 61. The geometries of the erosion profiles are determined following Breteler (2012). Using the erosion profile schematisation in Figure A.1.

$$E_p = \frac{h_{terrace}}{\sin \alpha_t} \cdot \sin(\alpha - \alpha_t) \tag{A.1}$$

This formula is used to calculate the erosion depth of each profile, that has to correspond to a depth of 1m. The derivation of the gentle slope profiles of 1/6 and 1/8 are conform Equation (A.2) in Figure A.1.

$$\cot \alpha_t = \frac{1}{2}(\cot \alpha + 1 + \sqrt{\frac{2V_e}{d_t^2}(\cot \alpha - 1) + \frac{1}{4}(\cot \alpha - 1)^2} \tag{A.2}$$

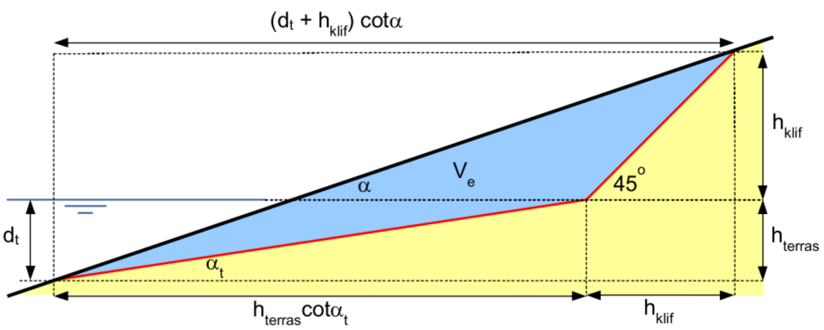

Figure A.1: Erosion profile for gentle slopes.

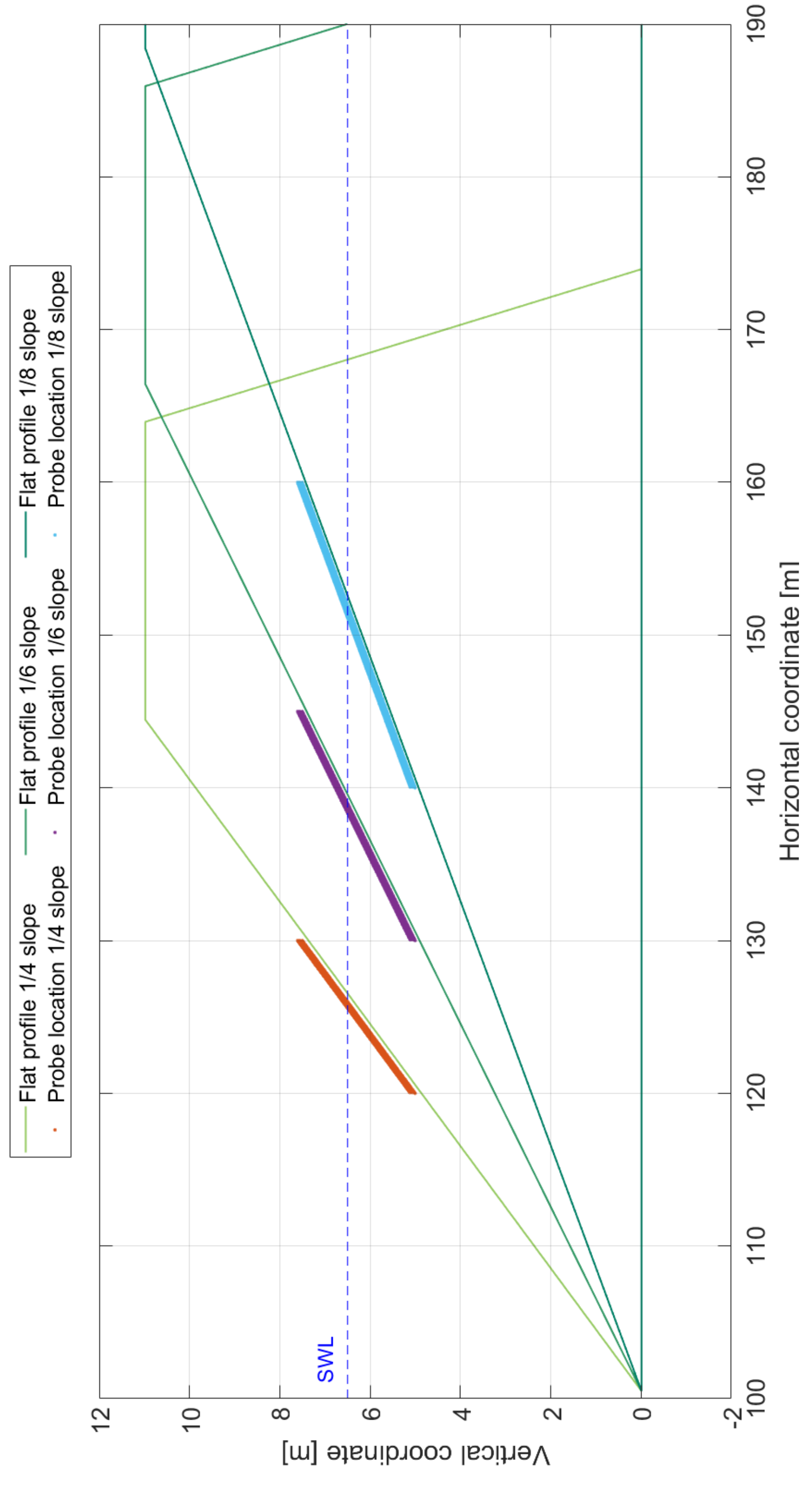

Figure A.2: Geometries of flat profile and the erosion profile

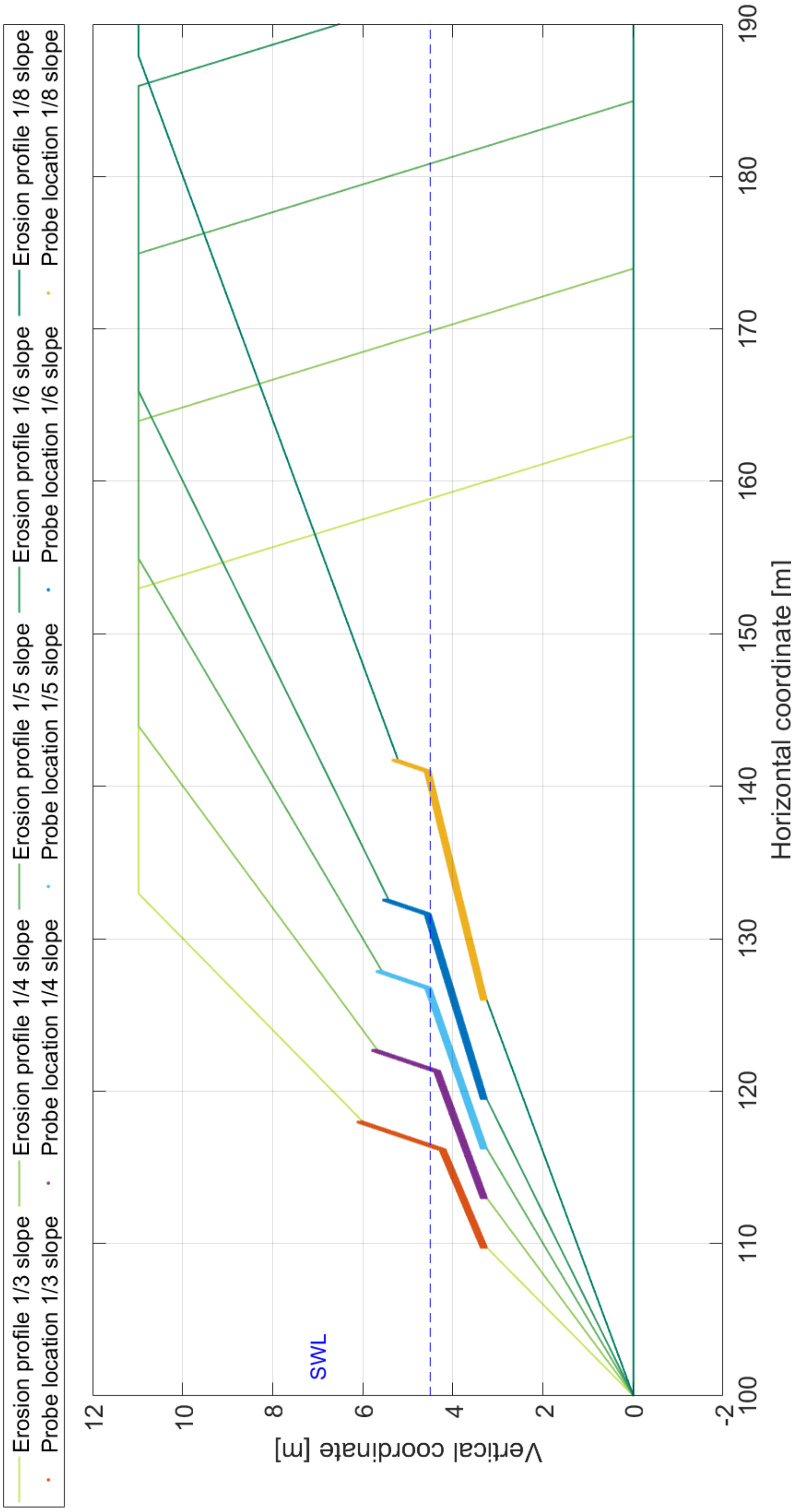

Figure A.3: Geometries of flat profile and the erosion profile

A.2. Wave spectra

This section shows the resulting wave spectra from the wave gauges in Figure A.4 on the next page. For the separation of wave gauges the following mathematical statements are used from Mansard and Funke (1980).

$$\begin{gathered} X12 = L/10 \\ L/6 < X13 < L/3 \text{ and } X13 \neq L/5 \text{ and } L13 \neq 3L/10 \end{gathered} \tag{A.3}$$

$X12$ is the distance between the first and the second wave gauges [m] and L as the wave length [m]. $X13$ is the distance from the first and third wave gauge [m]. From the wave gauge surface elevation data the wave spectra and reflection waves are determined using a Matlab tool.

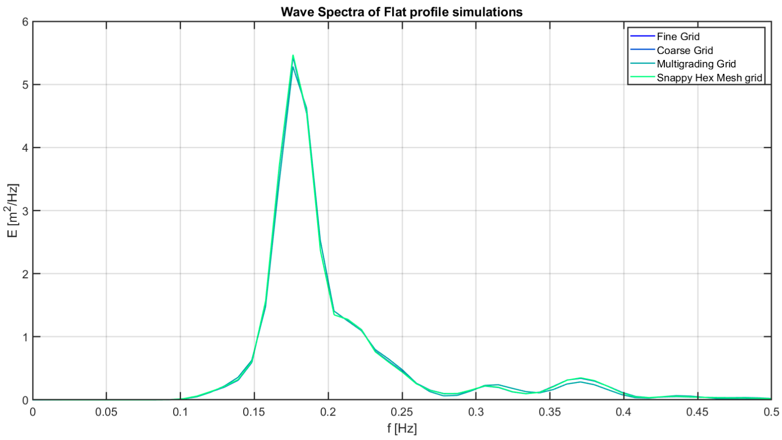

(a) Sensitivity wave spectrum

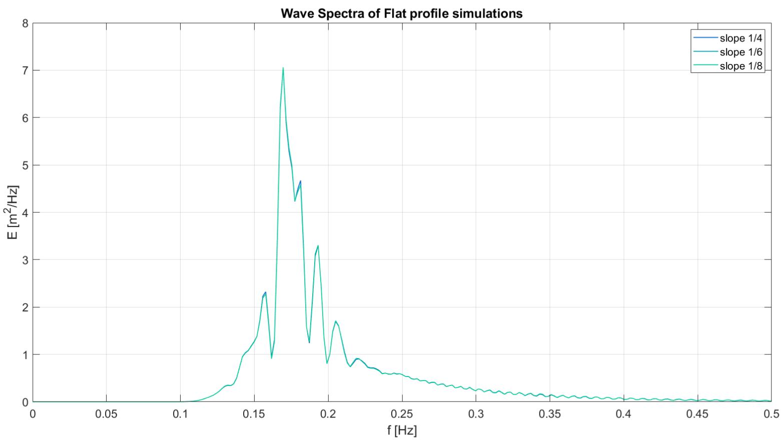

(b) Flat profile wave spectrum

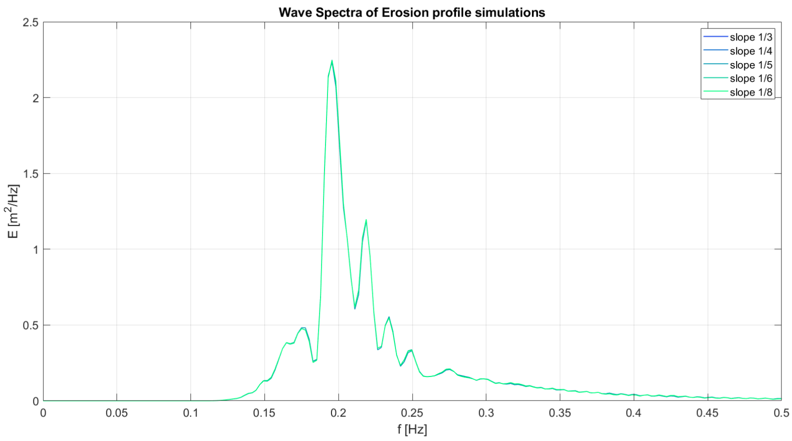

(c) Erosion profile wave spectrum

Figure A.4: Wave spectra of the numerical analysis

A.3. Probe spacing

The location of the probes on the erosion profiles is shown in Figure A.2 on page 60 and Figure A.3 on page 61. Because it is not possible to calculate the pressure directly on the profile, it is derived from the results of the two grid cells above the profiles, see Figure A.5. The pressure on the slope results from linear extrapolation. At least half of the lower grid cell has to be above the profile. In this way errors in one of the probes can be filtered out, when interpolating over the the other two probes. Figure A.5 shows the difference in the snappy hex mesh grids and the unsnapped grids.

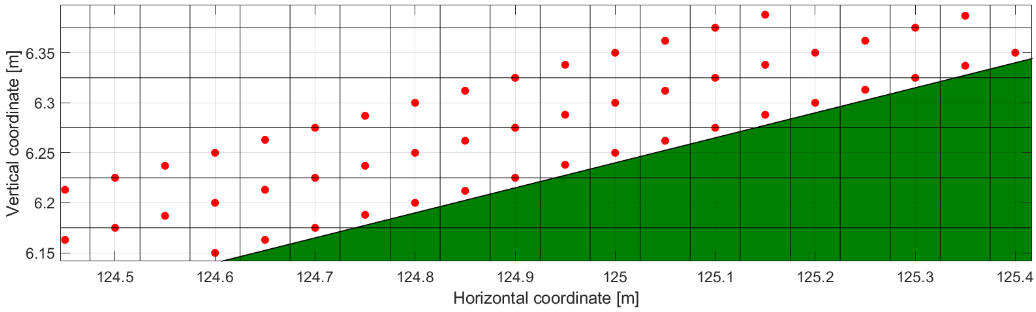

(a) Snappyhexmesh probe spacing

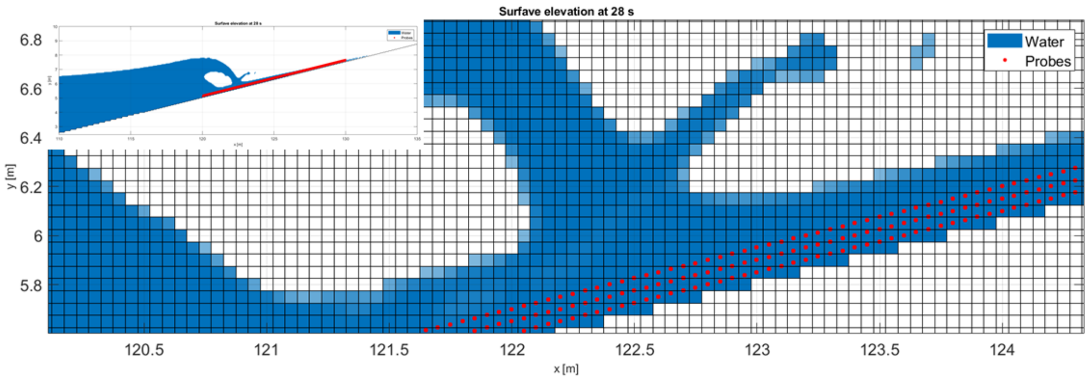

(b) Unsnapped probe spacing

Figure A.5: Probe spacing for (a) Snapped grid, (b) unsnapped grid

A.4. Mathematical model

The numerical framework is explained in section 2.6, A detailed description of the mathematical equations used in the numerical analysis are described below.

Hydrodynamic model

As already described in 2.6 the Reynolds Averaged Navier-Stokes (RANS) equations describe the hydrodynamic model. The RANS model uses the continuity mass and continuity equations. The velocity is defined as the filter velocity in the Navier-Stokes equations (see Equations A.4 and A.5; mass and momentum conservation respectively) (Jensen et al., 2014).

$$\nabla\vec{U} = 0 \tag{A.4}$$

$$(1 + C_m) \cdot \frac{\partial\rho\vec{U}}{\partial t n_p} + \frac{1}{n_p}\nabla\frac{\rho}{n_p} \cdot (\rho\vec{U}\vec{U})^T - \nabla \cdot (\mu_{eff}\nabla\vec{U}) = -\nabla p^* - \vec{g} \cdot \vec{x} \cdot \nabla\rho + \frac{1}{n_p}\nabla\vec{U} \cdot \nabla\mu_{eff} - \vec{F_p} \tag{A.5}$$

Where C_m is the added mass coefficient, t is the time, ρ is the density of the fluid, u is the filter velocity expressed in Cartesian coordinates, $p*$ is the excess pressure, x is the Cartesian coordinate vector ($[x, y, z]$), μ_u is the dynamic viscosity of the velocity field and F_p is the resistance induced on the flow by the presence of permeable coastal structure. The excess pressure is defined as $p* = p - \rho g \cdot \vec{x}$, p being the total pressure. A time averaged equation of the motion of fluid is used in this research for the Reynolds Averaged Navier Stokes (RANS) model. This enables to introduce the mean and fluctuating components of the flow.

Volume of fluid (VOF)

Due to wave breaking and reflection processes the flow is assumed to be highly nonlinear at the interface between waves and coastal structures. To account for the non-linearities a two-phase incompressible Navier-Stokes solver was incorporated in the RANS model, to address flow of water and air. The free surface waves are tracked with an extended VOF equation as explained in detail in Berberović et al. (2009). A non-diffusive solution is obtained, when solving transport type equations (see Equation (A.6) below), therefore the numerical model (OpenFoam) uses the MULES (multidimensional limiter scheme) technique.

$$\frac{\partial\alpha_1}{\partial t} + \frac{1}{n_p}[\nabla \cdot \vec{U}\alpha_1 + \nabla \cdot \vec{U_c}\alpha_1(1 - \alpha_1)] = 0 \tag{A.6}$$

Where $\frac{1}{n_p}$ ensures that only the pores of the material can be filled with water (n_p being the porosity of a permeable structure). u is the velocity and u_r the relative velocity between both fluids. Smearing of the interface between fluids is induced by using this two-phase approach. The last term on the lest side of the equation reduces the smearing effect. The term becomes active when α lies between 0 and 1, which is called an indicator function. This is a scalar function, found by solving Equation (A.6) in each control volume. Consequently, the volume fraction in each cell is obtained and is tracked for all cells. Empty cells are represented by an indicator function α equal to 0, whereas wet cells are indicated by α equal to 1. Next to that there are cells which contain some fluid that have values between 0 and 1. The value of α is then used to examine properties such as densities and viscosities in each grid cell, using Equations A.7 and A.8.

$$\rho = \alpha \cdot \rho_w + \rho_a(1 - \alpha) \tag{A.7}$$

$$\mu = \alpha \cdot \mu_w + \mu_a(1 - \alpha) \tag{A.8}$$

Where subscripts a and w represent air and water respectively. The time-averaged velocities in each grid cell are determined by the viscosities and densities within the RANS equations. For each time step the indicator function in each grid cell are than is re-evaluated with Equation (A.6) on the preceding page. The VOF method is a computational efficient way to track the free-surface by adding only one extra equation, to the advection equation (Moretto, 2020).

Relaxation

In this study the Wave generating and absorbing effects of the numerical model are accounted for by the Waves2-foam toolbox. The relaxation zone approach as boundary condition is used in this toolbox. Herein, the toolbox accounts for the reflection of the waves at boundaries and waves reflecting internally. Relaxation zones work by evaluating the computed velocity and indicator function solutions. The velocity and the indicator function are computed for each time step with Equations A.9 and A.10.

$$\phi = \alpha_R \cdot \phi_{computed} + (1 * \alpha_R) \cdot \phi_{target} \tag{A.9}$$

$$\alpha_R(\mathrm{X}_R) = 1 - \frac{exp(\mathrm{X}_R^3.5) - 1}{exp(1) - 1} \text{ for } \mathrm{X}_R \in [0; 1] \tag{A.10}$$

Where ϕ is either the velocity u or the indicator function α. Important to note is that α function and is not equal to α, the indicator function mentioned in previous paragraph. X_R is such that α_R is equal to 1 (X_R is equal to zero) at the interface between the non-relaxed part of the computational domain and the relaxation zone, thus only the target values remain Moretto (2020).

B

Design tool

B.1. Extended WBI assessment

In the WBI-2017 assessment of the strength of grass revetment the effect of the slope angle is not included (Verheij et al., 1998). Therefore, the effect of slope angle is substituted in the Equations B.1 and B.2.

$$t_{top} = \frac{tan(1/3)}{tan(\alpha)} \frac{1}{c_b} \ln\left(\frac{max((Hs - c);0)}{c_a}\right) \tag{B.1}$$

$$t_{sub} = \frac{tan(1/3)}{tan(\alpha)} \frac{max((d_{tot} - 0.2);0)}{c_d(1/3)^{1.5} max((H_s - 0.5);0)} \tag{B.2}$$

In which, d_{tot} is the layer thickness of the clay layer, including the top layer with grass roots, c_d is a constant depending on the sand fraction f_{sand} given by.

$$c_d = 1.1 + 8max(f_{sand} - 0.7;0) \tag{B.3}$$

The resistance duration is now determined by $t_{top} + t_{sub}$. The wave load duration $t_{load,eff}$ is expressed as the duration of the period in which the water level is between the peak still water level ζ and a distance of Δz below the peak water level. The wave impact zone is assumed to range between still water level and 0.5 times the significant wave height below still water level $(H_s/2)$. This is because the water level is only during a limited time in the specified range, the load duration of the section is smaller than if the grass slope is considered as a whole. An expression for $t_{load,eff}$ is given by.

$$t_{load,eff} = t_{load} min\left(\frac{H_s}{2\Delta z};1\right) \tag{B.4}$$

During a storm, the wave heights and water level vary. To asses the grass for wave impact, the failure fraction is calculated for different wave heights during the water level set-up. The failure fraction is calculated for a time step Δt in each section Δz of the dike slope. Whenever on section exceeds the failure fraction $F_{frac} = 1$, the clay erosion model starts calculating.

$$F_{frac} = \frac{\Delta t}{t_{load,eff}} \tag{B.5}$$

B.2. Clay erosion model

The formula by Mourik (2015) is given in Equation (B.6).

if $H_s > 0,4m$ than:

$$\frac{\partial V_e}{\partial t} = c_e \cdot \underbrace{\left(1,32 - 0,079\frac{V_{e0}}{H_s^2}\right)}_{\text{i}} \cdot \underbrace{(16,4(\tan\alpha^2))}_{\text{ii}} \cdot \underbrace{\left(min\left(3,6; \frac{0.0061}{s_{op}^{1,5}}\right)\right)}_{\text{iii}} \cdot \underbrace{(1,7(H_s - 0,4)^2)}_{\text{iv}} \quad \text{(B.6)}$$

Otherwise $H_s \leq 0,4m$:

$$\frac{\partial V_e}{\partial t} = 0$$

With, $\frac{\partial V_e}{\partial t}$ as the erosion velocity per time step $(m^3/m/h)$, c_e is the erosion coefficient for clay erosion (-) determined from clay erosion experiments. The following four terms are specified below:

i. The first term is the influence of the initial erosion volume V_{e0} (m^3/m)made dimensionless by the significant wave height $H_s(m)$. this shows that the erosion velocity decreases if the dimensionless volume becomes larger.

ii. The second term is the influence of the slope angle of the original profile$\tan(\alpha)$ (-). The trend shows that the erosion velocity decreases if the slope becomes more gentle.

iii. The third term accounts for the influence of the wave steepness $s_{op} = \frac{H_s}{1{,}56T_p^2}$ (-) with T_p as the wave period of the wave spectrum (s). This term shows roughly that the erosion velocity decreases if waves become steeper.

iv. The last term is the influence of the significant wave height. This rough relation that the erosion velocity increases with larger waves.

The schematisation profile of an erosion hole is presented in Figure B.1. with α_u = angle of the slope underneath the berm, α_t = angle of the slope of the erosion terrace, $hterrace$ = height of the erosion terrace, $hcliff$ = height of the erosion cliff, Ep = erosion depth perpendicular to the slope, dt = distance from still water level to the foot of the erosion terrace, dk = distance from still water level to the foot of the erosion cliff, Bt = width of the erosion terrace. For the depth of the foot of the erosion terrace d_t the following formula is used.

$$d_t = min\left(0.4\frac{V_e^0.25}{\sqrt{H_s}} + 0.7; 2H_s\right) \quad \text{(B.7)}$$

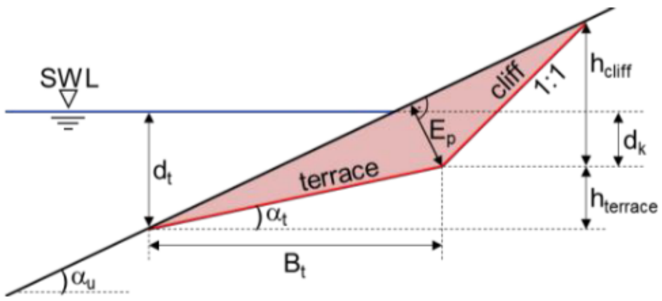

Figure B.1: Definition of the schematised erosion profile (adopted from (Kaste and Breteler, 2015))

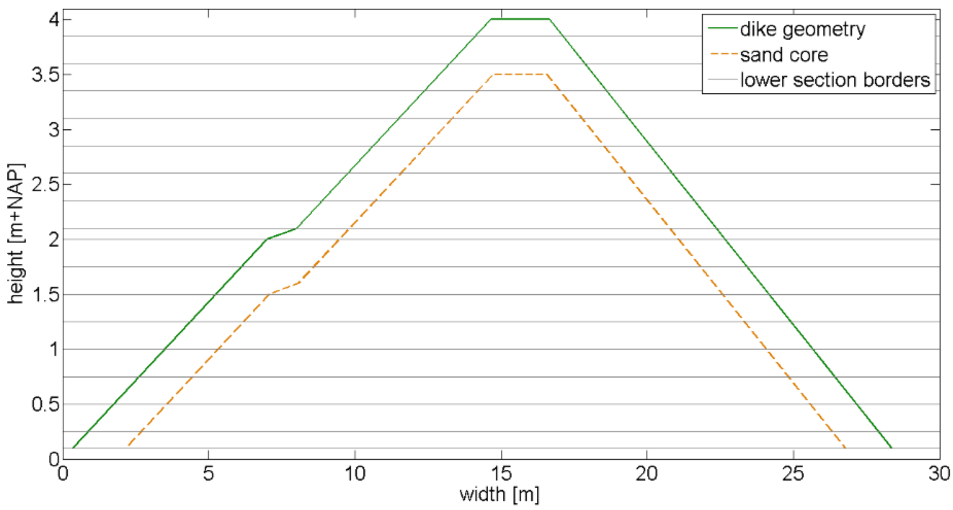

Figure B.2: Example of the dike split up into sections (adopted from (Kaste and Breteler, 2015))

B.2.1. Numerical erosion model

The numerical model for the erosion of a dike is set up in Matlab. The model operates in time steps of a certain length and calculates the erosion volume in each time step. The steps carried out in the model are described below. Herein, the main structure of the study of Kaste and Breteler (2015) is kept the same. For more elaboration on the numerical method refer to the study of Kaste and Breteler (2015). Before the model enters a loop over the time steps, the dike is split into sections. The following steps are repeated for every time step:

1. The hydraulic conditions of the specific time step are determined from the input
2. The zone, which is loaded by the waves, is determined
3. Determine the influence of the already present erosion underneath the loaded zone
4. Determine the already present erosion volume in the loaded zone V_{e0}
5. Calculate the erosion volume of the current time step ΔV_e
6. Determine the erosion profile of the erosion of the current time step
7. Split the erosion volume and distribute it over the sections of the dike

The steps are repeated until the time series of the hydraulic conditions is completed, or until failure is noticed, by breaking through of the clay layer.

1. input of the numerical model

As input for the numerical dike erosion model, a dike geometry can be used as is shown in Figure B.2. The clay layer is also needed. The first step in the numerical model is to split up the dike into horizontal sections. With this the erosion can be stored in those sections, according to where on the slope the erosion occurs. For the sections a favoured height is set to 0.25 m on default. Additionally, The hydraulic conditions are derived following the method in section 3.5.1, with the time series of a water level (h), the significant wave height H_s and the wave period T_p. For each time step, the hydraulic boundary conditions are read from the time series.

2. Define the loaded zone

The loaded zone is dependent on the water level and wave height, but also on the value of the already present erosion volume. The loaded zone defines the sections, which are considered in calculating the already present erosion volume, which is needed to calculate the erosion of the current time step.

The loaded zone is determined with an iteration with several steps. The first estimate only depends on the water level and wave conditions. The remaining estimates consider also the value of the already present erosion in those sections.

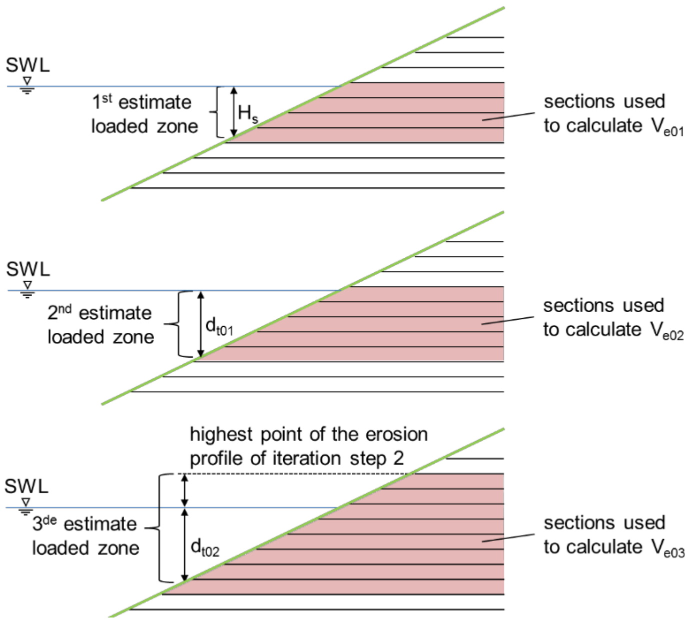

Figure B.3: Example for the iteration steps to determine the loaded zone (adopted from (Kaste and Breteler, 2015))

1. The first estimate of the loaded zone spans from the water level to H_s below the water level (see Figure B.3, above). With the erosion volume of the sections in the loaded zone, the first estimate of already present erosion V_{e0} is calculated, namely V_{e01}. With this value, the depth of the toe of the erosion profile is calculated: d_{t01}. see Figure B.1 on page 68 and Equation (B.7) on page 68.
2. In the second estimate of the loaded zone, it spans from the water level to d_{t01} below the water level (see Figure B.3, middle). With this, the second estimate of the present erosion volume is calculated: V_{e02}. With this value, a schematised erosion profile is determined, which can also reach above the water level. Also, a new value for dt is calculated: d_{t02}.
3. For the third estimate of the loaded zone, the erosion profile from the previous step is used. The loaded zone spans from the highest point of the erosion profile to the lowest (see Figure B.3, below). With this estimate, again the present erosion volume V_{e03} and the depth of the erosion toe d_{t03} are calculated. Also the erosion profile is determined.
4. The procedure of the third iteration step is then repeated three times to gain a more accurate result. This gives the final value for the already present erosion volume V_{e0}.

3. Determine the influence of the already present erosion underneath the loaded zone

The already present erosion underneath the loaded zone is checked and accounted for with the following formula.

$$V_{e,S,corr} = min(V_{e,S} - d_{e,mean} \cdot h_{sect}; 0) \tag{B.8}$$

$V_{e,S,corr}$ is the list of erosion volumes per section, corrected for the erosion underneath the loaded zone $[m^3/m]$. $V_{e,S}$ is the list of erosion volumes per section (uncorrected) $[m^3/m]$. $d_{e,mean}$ is the mean erosion depth in the zone underneath the loaded zone until a level of $h - 2H_s$ $[m]$. h_{sect} is the height of the sections $[m]$. This all is summarized in Figure B.4 on the next page.

Determine the already present erosion volume in the loaded zone The

The already present erosion volume is calculated with the sum of the corrected erosion volumes of the sections in the loaded zones:

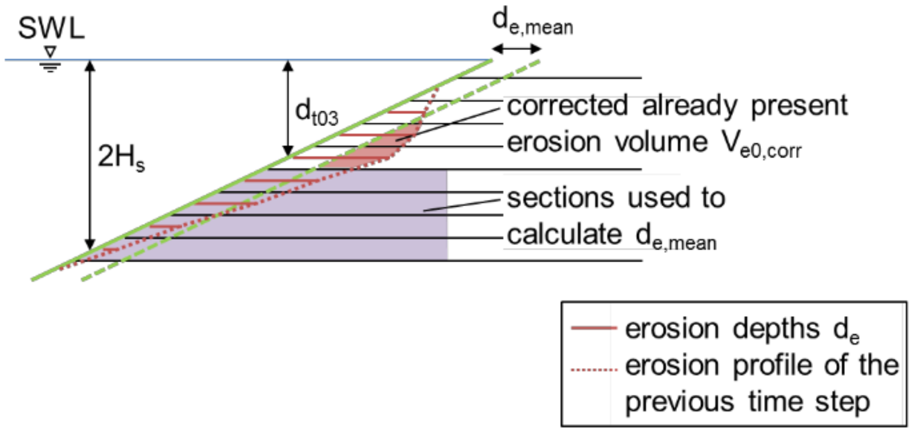

Figure B.4: Example of the correction of the erosion volume due to the parallel movement of the slope (adopted from (Kaste and Breteler, 2015))

$$V_{e0,corr} = \sum_{i}^{n_{sections}} V_{e,corr,i}; \text{ if section i lies in the loaded zone} \tag{B.9}$$

$V_{e,0,corr}$ is the already present corrected erosion volume in the loaded zone $[m^3/m]$. $n_{sections}$ is the number of sections and $V_{e,corr,i}$ is the corrected erosion volume of a certain section i $[m^3/m]$.

Calculate the erosion volume of the current time step

With the already present erosion volume $V_{e,0,corr}$ from the previous step, the additional erosion of the current time step ΔV_e can be calculated with Equation (B.6) on page 68

Determine the erosion profile of the erosion of the current time step

To determine the erosion profile of the current time step the uncorrected present erosion volume is used: V_{e0}. It is calculated according to Equation (B.9) with the uncorrected erosion volumes per section. The total erosion volume in the loaded zone of the current time step is thus:

$$V_e = V_{e0} + \Delta V_e \tag{B.10}$$

V_e is the erosion volume in the loaded zone in the current time step $[m^3/m]$. V_{e0} is the already (not-corrected) erosion volume in the loaded zone $[m^3/m]$. ΔV_e is the additional erosion of the current time step calculated with Equation (B.6) on page 68. With the erosion volume of the current time step the schematised erosion profile can be determined. First, the depth of the erosion toe can be calculated with Equation (B.7) on page 68. Then the geometry of the erosion profile can be calculated with the schematisation of Breteler (2012) Figure B.1 on page 68. Details of the determination of the erosion profile can be found in Kaste and Breteler (2015).

Distribute the erosion volume of the current time step over the relevant sections of the dike

The schematised erosion profile is split up by the sections into trapeziums such that the erosion volume per section can be determined with the geometry of those trapeziums. The height of the sections was determined as explained in the first step and stored to be used here. It is taken care that the added erosion volume is exactly the additional erosion volume of the current time step ΔV_e. This is described in more detail in Kaste and Breteler (2015). With the erosion volume distributed over the sections, the horizontal erosion depth can easily be calculated as the mean erosion depth per section: with:

$$d_{e,i} = \frac{V_{e,i}}{h_{sect}} \tag{B.11}$$

$d_{e,i}$ is the horizontal depth per section $[m]$. $V_{e,i}$ is the erosion per section $[m^3/m]$.

B.2.2. Wetland wave attenuation

The wetland wave attenuation is derived from Vuik et al. (2016). This study conducted a SWAN analysis based on long vegetation with $k_N = 0.090m$ and Wadden sea conditions. The long and short vegetation are directly derived from several studies described in Chapter 3. However, for the middle long vegetation this was less straight forward. van der Reijden (2019) has studied the wave attenuation at the same dike location 32.2km at the Koehool-Lauwersmeer dike trajectory. Herein, also a SWAN analysis was used with different k_N numbers shown in Figure B.5. By relating the $k_N = 0.09m$ of Vuik et al. (2016) with the k_N values of van der Reijden (2019) the wave attenuation of middle long vegetation is derived. The effect of middle long vegetation in Figure B.5 is approximately a factor 0.6 smaller compared to the long vegetation, reading out the k_N values. Therefore this factor is applied in the wave attenuation of middle long vegetation.

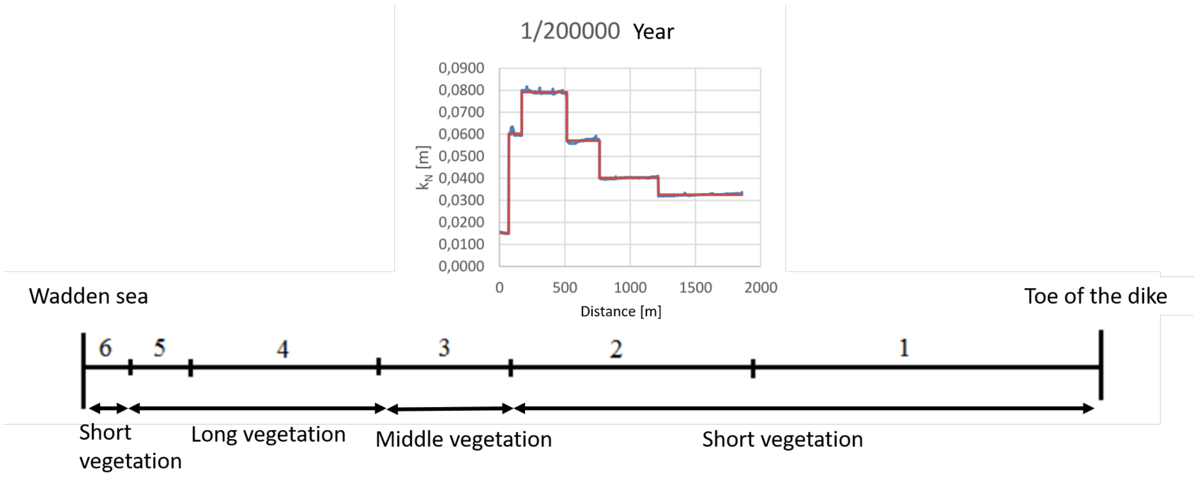

Figure B.5: percentage of wave attenuation by long vegetation ($k_N = 0.090m$) adopted from Vuik et al. (2016)